Spatiotemporal Distribution, Abundance, and Persistence of Kelp Forests in the Broughton Archipelago, British Columbia, Canada

By

Long Ching Man 文朗晴

B.Sc. University of California, Los Angeles, 2022

A Thesis Submitted in Partial Fulfilment of the Requirements for the

Degree of

MASTER OF SCIENCE

in the Department of Geography

We acknowledge and respect the lək^{w}əŋən peoples on whose traditional territory the university stands and the Songhees, Esquimalt and W̱SÁNEĆ peoples whose historical relationships with the land continue to this day.

Spatiotemporal Distribution, Abundance, and Persistence of Kelp Forests in the Broughton Archipelago, British Columbia, Canada

By

Long Ching Man 文朗晴

B.Sc. University of California, Los Angeles, 2022

Supervisory Committee:

Dr. M. Costa, Supervisor (Department of Geography)

Dr. A. Bates, Committee Member (Department of Biology)

Abstract

Kelp forests are highly productive coastal ecosystems on 25% of the world's coastlines, providing key biogenic habitats in nearshore ecosystems. These ecosystems are experiencing variable changes worldwide, ranging from detrimental impacts from climate change and pollution to trophic collapses. Still, in British Columbia (BC), Canada, the kelp distribution and drivers of kelp change remain largely unknown in many locations. Thus, local-scale studies are needed to understand kelp dynamics to inform marine spatial planning decisions for coastal practitioners. In particular, the Broughton Archipelago, BC, located in Kwakwaka'wakw territories, supports floating kelp forests of various species compositions and sizes in a spatially explicit environmental gradient across an outer archipelago subregion and an inner fjord subregion. The Mamalilikulla First Nation, ''Namgis First Nation, and the Kwikwasut'inuxw/Haxwa'mis First Nation, who formed the Broughton Aquaculture Transition Initiative (BATI), are interested in the status and trends of kelp forests due to their utility as juvenile salmon habitat. This research investigates kelp forests' spatiotemporal distribution, abundance, and persistence in the Broughton Archipelago. We first identify environmental and biotic variables that drive spatial differences in kelp forest distribution and abundance. We achieved this by mapping floating kelp abundance (giant kelp: *Macrocystis pyrifera*, bull kelp: *Nereocystis luetkeana)* at 31 focal sites across the environmental gradient using unmanned aerial vehicle and high-resolution satellite imagery, compiling environmental data from in-situ sources and environmental models, and characterizing grazer (sea urchins, *Strongylocentrus spp.* and *Mesocentrotus franciscanus)* and predator (sunflower sea stars, *Pycnopodia helianthoides)* abundances from remotely operated vehicle footage. Second, we investigate the spatiotemporal persistence and resilience of kelp forests in the face of climate change. This was achieved by creating long-term (1984 to 2023) and short-term (2016 to 2023) time series of floating kelp areas in association with environmental drivers of change using medium- (30 m) to high- (3 m) resolution satellite imagery, and spatially combining yearly kelp areas to identify spatial patterns of kelp persistence. Overall, we found that the lower sea-surface temperatures, flatter bottom slopes, and higher tidal current speeds typical of the archipelago subregion were positively associated with kelp abundance; whereas the warmer sea-surface temperatures, steeper bottom slopes, and lower tidal current speeds found in the fjord subregion were

negatively associated with kelp abundance, reinforcing the known spatial patterns of kelp distribution and abundance found in other studies across the BC coast. Biotically, sea urchin and *Pycnopodia* abundances did not significantly affect kelp abundance, likely due to low abundances of sea urchins. Kelp forests were temporally persistent, with most kelp areas displaying increases or no change in kelp areas, and kelps were more persistent in their centers than the edges of each kelp bed. These findings provide a baseline understanding of kelp distribution, abundance, persistence, and their associated environmental and biotic drivers in the Broughton Archipelago. Ultimately, this can inform kelp forest conservation and management decisions such as kelp harvesting and kelp restoration for by local communities and First Nations, and contribute to a broader regional understanding of the spatiotemporal patterns of kelp forests in the Northeast Pacific Ocean.

Table of Contents

Abstract iii

Table of Contents v

List of Tables vii

List of Figures viii

Acknowledgments xi

1.0 Introduction 1

1.1 Overview 1

1.2 Research Objectives 3

1.3 Thesis Structure 3

1.4 Personal Relation to the Research and Place 3

2.0 Spatial characterization of environmental and biotic drivers of kelp distribution and abundance across an archipelago-fjord system in British Columbia, Canada 5

2.1 Abstract 5

2.2 Introduction 6

2.3 Methods 9

2.3.1 Study area 9

2.3.2 Data collection & processing 11

2.3.3 Analysis 21

2.4 Results 24

2.4.1 Environmental drivers of spatial differences in kelp distribution and abundance 24

2.4.2 Effects of grazer and predator distribution and abundances on the distribution and abundance of kelp 29

2.5 Discussion 31

2.5.1 Environmental drivers of spatial differences in kelp distribution and abundance 32

2.5.2 Characterize the effects of grazer and predator abundances on the distribution and abundance of kelp 35

2.5.3 Limitations and Future Directions 39

2.6 Conclusions 41

3.0 Kelp forests display persistence in the dynamic region of the Broughton Archipelago, British Columbia, Canada 42

3.1 Abstract 42

3.2 Introduction 43

3.3 Methods 47

3.3.1 Study area 47

3.3.2 Data compilation and processing 50

3.3.3 Data analysis 58
3.4 Results 61
3.4.1 Environmental conditions 61
3.4.2 Long-term (1984 to 2023) and short-term (2016 to 2023) kelp response to environmental changes 70
3.4.3 Spatial patterns of kelp persistence 73
3.5 Discussion 77
3.5.1 Long-term (1984 to 2023) and short-term (2016 to 2023) kelp response to environmental changes 77
3.5.2 Spatial patterns of kelp persistence 82
3.6 Conclusion 85
4.0 Summary and Conclusion 86
4.1 Thesis overview 86
4.2 Limitations and Future Research 88
5.0 References 90
Appendix A - Supplementary material of Chapter 2 105
A1 UAV flight plan specifications 105
A2 Orthomosaicking methods of UAV imagery 105
A3 Imagery processing and classification methods 106
A4 Photosynthetically available radiation measurements 106
A5 Supplementary tables 108
A6 Supplementary figures 119
Appendix B - Supplementary material of Chapter 3 121
B1 *Macrocystis* site land mask creation 121
B2 Object-based image analysis classification methods 122
B3 Accuracy assessment methods 122
B4 Supplementary tables 123
B5 Supplementary figures 125

List of Tables

Table 1: Table showing the details about the two imagery types used, with their source, their spectral bands, their spatial resolutions, and the number of sites each method was used for. 13
Table 2: Table showing the methods used for collecting data about environmental and biotic conditions, including details about the instrument or data source used, the processing software, survey or measurement area for each method, and the variables extracted from each method..... 20
Table 3: The environmental variables from local, regional, and global scales..... 53
Table 4: Table detailing imagery used for the long-term and short-term analysis, as well as imagery validation 58
Table 5: Mann-Kendall's test results testing for significant increases, decreases, or lack thereof in environmental variables from 1984 to 2023, with cells colored in grey, and Kruskal-Wallis and Dunn's test results representing environmental differences between climate periods with cells colored in white (P1 = Period 1, P2 = Period 2, P3 = Period 3) at A) local, B) regional, and C) global scales. Bolded values represent statistical significance. 68

Table A. 1: Table showing each study site's environmental attributes..... 108
Table A. 2: Table showing all study sites' coordinates, subregions, kelp species (if present), and all kelp metrics and biotic metrics 111
Table A. 3: Table showing differences in each environmental variable between subregions. Bolded variables are the variables selected for the cluster analysis 111
Table A. 4: Table showing differences in environmental and biotic variables between the kelp and non-kelp sites in the fjord subregion. 112
Table A. 5: Results from linear models 1 and 2 showing significant (bold) environmental predictors that affected the kelp abundance index. Model 1 was significant ($p=8.17\times10^{-7}$) and explained 67.8% of the variation in the kelp abundance index, whereas model 2 was significant ($p=0.002$) and explained 58.0% of the variation. Bolded text indicates significant variables ($p<0.05$), italicized text indicates variables approaching significance ($p<0.1$), and normal text indicates variables that are not significant..... 113
Table A. 6: Results of the hotspot analysis: GI* statistic for urchin abundance..... 115
Table A. 7: Results of the hotspot analysis: GI* statistic for Pycnopodia abundance..... 116
Table A. 8: Results from generalized linear model 3 showing significant (bold) predictors that affected kelp density. This model explained 50.8% of the variation in kelp density..... 117
Table A. 9: Table showing differences in all absolute PAR measurements between subregion. 118

Table B. 1: Precision and recall of kelp classification of satellite imagery 123
Table B. 2: Table describing the results of the changepoint analysis. 123
Table B. 3: Table describing the climatological summer mean and standard deviation of local SST at each Nereocystis site. 124
Table B. 4: Table describing the results of the linear model used to identify potential environmental drivers of percent kelp area change. The combination of predictors listed below was decided using the lowest AIC, however, note that no combinations of predictors resulted in any significant relationship between environmental conditions and the percent kelp area. 124

List of Figures

Fig. 1: Map of the study area and the 31 survey sites. Purple dots denote Macrocystis sites, orange dots denote mixed Macrocystis and Nereocystis sites, green dots denote Nereocystis sites, and white dots denote sites with no kelp (as per observation from the surface during the 2023 summer field season). The inset map denotes the study area's location within BC. 11
Fig. 2: Flow chart showing the analysis pipeline from data acquisition to data analysis to achieve the specific objectives of this research..... 12
Fig. 3: Schematic showing the relationship between classified kelp area, kelp bed area, kelp density, and kelp abundance index. The schematic visually represents the classified kelp area in red and the kelp bed area in dark blue-grey of four different sites and lists the classified kelp area, kelp bed area, kelp bed density, and kelp abundance index of the associated sites. The scales of all site maps are all uniform at 1:1144. A) represents a site with high kelp abundance index, B) represents a site with a medium kelp abundance index with a smaller classified kelp area relative to its larger kelp bed area, C) also represents a site with a medium kelp abundance index, but with a higher classified kelp area relative to its smaller kelp bed area, and D) represents a site with a low kelp abundance index. Note that the kelp beds at the sites shown in panels A and B are not shown in their entirety in these panels due to the extensive size of these kelp beds. 16
Fig. 4: A) Map showing the spatial distribution of the sites belonging to the archipelago subregion ("A") in blue dots and the sites belonging to the fjord subregion ("F") in red dots. B) The PCA biplot shows the results of the k-means cluster analysis, with each point representing the selected environmental variables of each site, and the distance between each point representing the Euclidean distance between each site. Blue points and hulls represent the archipelago subregion, and red points and hulls represent the fjord subregion, with the distance between each hull representing the Euclidean distance between each subregion. C) Box plots show the differences in medians of the selected environmental variables for the cluster analysis between the two subregions, as well as their associated interquartile ranges and outliers (dots). The level of significant difference for each environmental variable between each subregion is indicated by asterisks (* = $p<0.05$, ** = $p<0.01$, *** = $p<0.001$)..... 27
Fig. 5: Linear model results, with the black lines showing marginal effects (i.e. considering every other predictor variable used in each model as constant) of each significant environmental predictor variable (site-level mean)on the kelp abundance index at each site, the grey shading behind the black line showing the confidence interval of each marginal effect plot, and the grey dots showing the raw data. (A) shows the results of linear model 1, which includes all the sites (n=31), and (B) shows the results of linear model 2, which only includes sites where kelp was present (n=22). 29
Fig. 6: Map showing the kelp abundance index, and the hotspots of urchins and Pycnopodia across sites as determined by the GI* statistic. Hotspots are visually indicated as ellipses drawn over sites identified as hotspots ("concentric hotspots") with >95% confidence ($p<0.05$) and with >90% confidence ($p>0.1$). There are two concentric hotspot ellipses for urchins, with pale green denoting sites with 90% confidence ($p<0.1$), and dark green denoting sites with >95% confidence ($p<0.05$). There is only one concentric hotspot for Pycnopodia, which has >99% confidence. 31
Fig. 7: A schematic showing the environmental and biotic conditions at the archipelago subregion (left panel) and fjord subregion (right panel). The archipelago subregion had cooler waters (represented by symbol Temp ↓), higher salinities (Sal ↑), lower stratification (Strat ↓), flatter slopes (Slope ↓), higher tidal current speeds (Currents ↑), higher PAR (PAR ↑), higher fetch (Fetch ↑), and higher abundances of urchins, although the urchins are not prevalent throughout the entire subregion. The fjord subregion had warmer temperatures (Temp ↑), lower salinities (Sal ↓), higher stratification (Strat ↑), steeper slopes (Slope ↑), lower tidal current speeds (Currents ↓), lower PAR (PAR ↓), lower

fetch (Fetch ↓), and higher abundances of Pycnopodia, although the Pycnopodia were not commonplace throughout the whole fjord subregion. All Nereocystis, sea urchins, and Pycnopodia graphics were taken from phylopic.org, and the Nereocystis graphic was further edited (CC0 1.0 Universal Public Domain Dedication license.) 38
Fig. 8: The main map shows the study area (the dynamic subregion of the Broughton Archipelago), with the Macrocystis site on the north shore of Malcolm Island marked in grey and the eight Nereocystis sites marked in black. The Nereocystis sites include kelp beds at Nimpkish River (NR), Alert Bay Lighthouse (ABL), Alert Bay East (ABE), Pearse Islands (PI), Bold Head (BH), Wedge Island (WI), and South Leading Islet (SLI). The background of the main map is the Landsat-derived SST from Aug 4, 2023. The left inset map shows the location of the study area (marked by a red rectangle) at a provincial scale relative to Vancouver Island (VI) and mainland BC (BC). The right inset map shows the study area (marked by the red rectangle) situated within the Queen Charlotte Strait region, relative to the location of the Pine Island Lighthouse (PIL), from which the regional SST and MHW metrics were derived (see 3.3.2). 50
Fig. 9: A flow chart representing the data compilation and processing, as well as the spatial and temporal dimensions of the study, and how satellite-derived kelp classifications and environmental data are combined to achieve the objectives of the study. 51
Fig. 10: A) Mean regional spring SST, and B) mean regional summer SST from 1984 to 2023. All data was derived from the Pine Island Lighthouse daily SST climatology (1984 to 2023), with error bars representing the standard deviations. The vertical black lines depict the transitions between the climate periods. 63
Fig. 11: A) Scatterplot showing the mean local summer SST for the Macrocystis site ("Malcolm Island") and each Nereocystis site (as denoted by the abbreviated site names) from 1984 to 2023, with the error bars around each point representing the standard deviation for each year. The vertical black lines in 1999 and 2014 represent the boundaries between climate periods. The Mann-Kendall's τ and p-value are reported in the top left corner for sites with significant monotonic trends. The green shaded areas of each site's panel represent the length of the kelp time series analyzed for each site. B) The differences in mean local summer SST between each period. Sites with an asterisk (*) are sites with significant differences in local SST across periods. Different letters above each boxplot denote significant pairwise differences. 65
Fig. 12: Regional and global conditions across the three climatic periods identified (Period 1, Period 2, and Period 3). For both panels, the black lines represent the transitions between climate periods. A) MHWs and their associated duration and category level. The x-axis shows the date of each MHW's maximum intensity peak, and the y-axis shows the maximum intensity of each MHW. B) Pacific Decadal Oscillation (PDO) and Oceanic Niño Index (ONI) from 1984 to 2023. 67
Fig. 13: Kelp area changes in the Macrocystis site (Malcolm Island). A) The temporal changes in the yearly kelp area from 1984 to 2023. Vertical lines in A) indicate the boundaries between periods. The τ is the Kendall rank correlation coefficient, representing the direction of monotonic change as determined by the Mann-Kendall's test, ranging from -1 (representing negative change) to +1 (positive change). The p represents the p-value. There is no data available for 1992. B) Boxplots showing the differences in the median kelp area and their associated interquartile ranges among climate periods. Identical letters above the boxes represent no significant differences in median kelp area between the pair of periods as determined by the Kruskal-Wallis test, whereas different letters above the boxes represent significant differences in median kelp area between the respective periods. 71
Fig. 14: **A)** Changes in percent kelp area in the 8 Nereocystis sites from 2016 to 2023. Sites with "N" under the site name are sites with no significant temporal trends, and the site with "I" had a significantly increasing trend, as per the Mann-Kendall test results. The significant Mann-Kendall test

result is shown for the associated site. **B)** Boxplot showing median kelp area and their associated interquartile ranges from 2016 to 2023 at each site. The mean percent kelp area for the Macrocystis site ("Malcolm Island") from 2016 to 2023 is also included for reference, although it is not part of the short-term time series. 73
Fig. 15: Maps showing the spatial patterns of kelp persistence at the Macrocystis site: the north shore of Malcolm Island. A) shows the number of years of kelp presence, which was used to determine the areas of kelp persistence. The yellow-red scale indicates the number of years of kelp presence. B) shows the persistent area in pink and the maximum kelp area in green. The total percentage area of the maximum kelp area that is persistent is indicated in B. For both panels, the frame around the kelp beds shows the area considered for the analysis. Refer to Fig. 8 for the location of the Macrocystis site. 75
Fig. 16: Maps showing the spatial patterns of kelp persistence at each Nereocystis site. A) shows the number of years of kelp presence, which was used to determine the areas of kelp persistence. The yellow-red scale indicates the number of years of kelp presence. B) shows the persistent area in pink and the maximum kelp area in green. The total percentage area of the maximum kelp area that is persistent is indicated in B. Refer to Fig. 8 for the location of each Nereocystis site. 76
Fig. 17: Map showing the location of historic kelp forests (1850s to 1950s) as documented in the British Admiralty nautical charts (red) and the maximum kelp area as derived from 'present-day' (Macrocystis site: aggregate from 1984 to 2023, 8 Nereocystis sites: aggregate from 2016 to 2023) satellite imagery (green). Note that the historic kelp polygons are only evidence of kelp presence, not kelp absence, and their shapes and sizes may not be related to the size of the actual kelp beds present during that time (Costa et al., 2020). Refer to Fig 8 for the location of each Macrocystis and Nereocystis site. 82

Fig. A 1: Assessing the fit of linear model 1 (for all 31 sites: kelp abundance index ~ SST + tidal current speeds + slope): Plots of the model's fitted values vs residuals, residuals' quantile-quantile plots, residuals with observation number, and a histogram of the models' residuals. 119
Fig. A 2: Assessing the fit of linear model 2 (for sites with kelp: kelp abundance index ~ SST + tidal current speeds + slope): Plots of the model's fitted values vs residuals, residuals' quantile-quantile plots, residuals with observation number, and a histogram of the models' residuals. 120
Fig. A 3: Assessing the fit of the Tweedie generalized linear model (kelp density ~ subregion + urchin abundance + Pycnopodia abundance + subregion*urchin abundance + subregion*Pycnopodia abundance + urchin abundance * Pycnopodia abundance): Plots of the model's fitted values vs residuals, residuals' quantile-quantile plots, residuals with observation number, and a histogram of the models' residuals. 121

Fig. B 1: A) Mean regional spring SST anomaly, and B) mean regional summer SST anomaly, derived from the yearly seasonal mean subtracting the climatological mean calculated with daily values from 1984 to 2023. All data was derived from the Pine Island Lighthouse daily SST climatology (1984 to 2023), with error bars representing the standard deviations. The vertical black lines depict the transitions between the climate periods. 125
Fig. B 2: A) Cumulative intensity of pre-summer MHWs (September of the previous year to June of the current year) from 1984 to 2023. B) Cumulative intensity of summer MHWs (July to August of the current year) 127

Acknowledgments

I acknowledge the Kwakwaka'wakw people, whose unceded traditional territories this research was conducted. Thank you to the Mamalilikulla First Nation, 'Nam̱gis First Nation, and Kwikwasut'inuxw/Haxwa'mis First Nation for allowing me to work with the Broughton Aquaculture Transition Initiative on their beautiful waters, which they continue to protect and steward since time immemorial.

I thank my supervisor, Dr. Maycira Costa, for all the wisdom, guidance, and laughs. Thank you so much to my mentor, labmate, and friend, Dr. Romina Barbosa, for all the tireless feedback and edits on my analysis and thesis, the fun in the field, and many adventures around Victoria. Thanks to my committee member, Dr. Amanda Bates, and my external examiner, Dr. Kylee Pawluk, for your kind and thoughtful advice on my thesis. Many thanks to the folks at BATI–Andrew Wadhams, Daniel Wadhams, Dennis Johnson, Gerald Alfred, Jack Alfred, Joey Webber, Jonah Johnson (especially for the ROV monitoring), Scott Rufus, Tre Alfred, Peter Mountain, Nic Dedeluk, Una Kim, Emily Wisden-Seaweed, Kieran Pinder, Patricia Alfred, and Elysanne Durand for all the tireless administration, fieldwork, the study design help, the stories and observations about your beautiful territories, the salmon snacks, and all the good times on the boat. Thank you to Hereditary Chief Robert Mountain for sharing your lived knowledge about the status and changes of kelp in the past that no satellite can capture, and many thanks to the folks at Salmon Coast Field Station for the support and insight in the field. I would like to extend my thanks to Luba Reshitnyk for the provision of one of the kelp temporal datasets, and the rest of the Hakai Geospatial Team for all the guidance and spatial analysis ideas during my summer internship. Thank you, Dr. Alyssa Gehman, for sharing your *Pycnopodia* insights with me. Thank you to Tyler Cowdrey and Danielle Claar at WADNR, and Markus Thompson for sharing your tips and tricks on drone-based kelp mapping. Thank you so much to Lianna Gendall for the initial conception of this project and for conducting the initial fieldwork, the grad school advice, and the satellite processing advice, thanks so much to Alena Wachmann for figuring out fieldwork with me, and thanks to Dr. Alejandra Mora-Soto for the statistics help, grad school advice, and kelp forest snorkels! Thank you to my research assistant, Amelia Gray, for tirelessly counting all the urchins and *Pycnopodia* in the ROV videos. Thank you to all of my other

wonderful labmates–Marta, Jordanna, Sarah, Alyssa, Aidan, Loic, Piper, Lucian, Shawn, and Nicola for all the fun hangouts, advice, and moral support! Last of all, thank you to my family and friends for the emotional support throughout this journey.

Funding for this research was provided through the Broughton Aquaculture Transition Initiative and the BC Kelp Resilience Project.

1.0 Introduction

1.1 Overview

Kelp forests (Order Laminariales) are found on 25% of the world's temperate coastlines and provide vital biogenic habitat in nearshore rocky reef systems (Druehl & Clarkston, 2016; Krumhansl et al., 2016). As the largest vegetated coastal ecosystem on the planet, globally, kelp forests are a significant source of net primary productivity (NPP) and have high carbon sequestration potential (Pessarrodona et al., 2022; Krause-Jensen et al., 2016; Bayley et al., 2021; Filbee-Dexter et al., 2024). Due to their height and structural complexity, kelp forests can provide refuge and nursery habitat for many species (Miller et al., 2018; Lamy et al., 2020), including Pacific salmon, rockfish, herring, and abalone, as well as predators such as sea otters *(Enhydra lutris)* and sunflower sea stars *(Pycnopodia helianthoides)* (DFO, 2015; Watson & Estes, 2011; Burt et al., 2018; Shaffer et al., 2023). Kelp is also highly valued in Northwest Pacific Indigenous cultures, with uses in woodworking, fishing, trade, and traditional medicines (Turner, 2001; Reid et al., 2022).

Currently, kelp forests are threatened by a myriad of stressors, such as climate change (Krumhansl et al., 2016; Wernberg et al., 2019; Smale et al., 2020; Filbee-Dexter et al., 2024), industrial pollution (Wernberg et al., 2019; Filbee-Dexter & Wernberg., 2018), and ecosystem changes (Rogers-Bennett & Catton, 2019; Eisaguirre et al., 2020; Gregr et al., 2020), leading to a 2% decrease in kelp populations worldwide (Krumhansl et al., 2016). Notable losses have occurred around the world, including in Western Australia, where *Ecklonia radiata* experienced a 100 km range contraction due to climatic changes (Wernberg et al., 2013, 2016); Northern California, where *Nereocystis luetkeana* was decimated by marine heatwaves and the subsequent overgrazing by sea urchins after 2014 (Rogers-Bennett & Catton, 2019); and in Northern Europe, where *Saccharina latissima* forests experienced regime shifts to turfs due to anthropogenic eutrophication (Filbee-Dexter & Wernberg, 2018).

Despite decreases on a global scale, kelp persistence and resilience to stressors often vary on regional and local scales due to spatially explicit patterns of environmental and biotic variation

(Starko et al., 2022, 2024; Jayathilake & Costello, 2021; Gendall et al., 2023; Gonzalez-Aragon et al., 2024). This spatial variation in kelp responses is particularly present in British Columbia (BC), which presents a long, complex coastline with different exposures, temperatures, and community compositions (Nijland et al., 2019; Schroeder et al., 2019a; Starko et al., 2022, 2024; Mora-Soto et al., 2024a, 2024b; Gendall et al., submitted). For instance, kelps have increased on the northwest coast of Vancouver Island where keystone predators (sea otters) have returned (Watson & Etses, 2011). On the other hand, kelps have displayed no significant change in the cooler waters of the Strait of Juan de Fuca (Mora-Soto et al., 2024a) and the cooler Cumshewa Inlet of Haida Gwaii (Gendall et al., submitted). Conversely, decreases have occurred in the warmer waters of the central Gulf Islands (Mora-Soto et al., 2024a, 2024b), inner Barkley Sound (Starko et al., 2022, 2024), and the warmer Gray Bay subregion in Haida Gwaii (Gendall et al., submitted). As such, kelp change and its associated drivers cannot be determined without a quantitative understanding of kelp distribution and abundance, and the environmental and biotic conditions associated with the kelp ecosystems in a specific location.

Remote sensing and other remotely operated technologies offer the ability to monitor kelp forests' distribution, abundance, and changes across various spatial and temporal scales. Researchers and practitioners alike have used unmanned aerial vehicle (UAV) and satellite imagery to map floating kelp areas from the air, which can be used to investigate the spatial distribution and abundance of kelp, as well as characterize the changes in kelp area through time (Cavanaugh et al., 2011, 2013, 2021; Bell et al., 2020, 2023; Saccomanno et al., 2023; Schroeder et al., 2019b; Cavanaugh et al., 2022; Gendall et al., 2023, submitted; Mora-Soto et al., 2024a, 2024b). Under the kelp canopy, remotely operated vehicles (ROVs) offer a less costly and labor-intensive way to investigate sub-canopy biotic conditions (Buscher et al., 2020; Gendall et al., submitted; Randell et al., 2023). When combined with in-situ data, satellite-derived and modeled environmental data allow for characterizing the distribution, abundance, and changes of kelp forests, as well as the associated environmental and biotic drivers, at various spatiotemporal scales.

1.2 Research Objectives

The main goal of this thesis is to investigate the spatiotemporal distribution, abundance, and persistence of kelp forests in the Broughton Archipelago. We address this goal with the following objectives:

1. Identify environmental and biotic variables that drive spatial differences in kelp forest distribution and abundance;
2. Investigate spatiotemporal persistence and resilience of kelp forests in the face of environmental change.

1.3 Thesis Structure

This thesis is separated into two papers to address the research objectives. The first paper (Chapter 2) provides a spatial characterization of the environmental and biotic drivers of kelp distribution and abundance in the present day (2023). The second paper (Chapter 3) uses a long-term and a short-term time series of floating kelp areas combined with environmental drivers to understand kelp's spatiotemporal persistence and resilience in the face of environmental change. Each paper was developed as an independent publication for scientific journals, and consequently, some information is repeated. The first paper's characterization of the study area is used to inform the study design of the second paper; thus, the second paper cites the first paper as a source of this information. Finally, the conclusion (Chapter 4), summarizes the two papers and discusses the broader implications of the results.

1.4 Personal Relation to the Research and Place

As an international student from Hong Kong conducting research in Canada, it is important to acknowledge my positionality while working within a Western academic institution. I am a guest on the Kwakwaka'wakw territories and the Songhees, W̱SÁNEĆ, and Esquimalt Nations on which this research was conducted, and I aim to do my utmost to uphold Indigenous sovereignty. This work was requested by and aims to provide data to the Mamalilikulla First Nation, 'Na̱mgis First Nation, and the

Kwikwasut'inuxw/Haxwa'mis First Nations, who form the Broughton Aquaculture Transition Initiative, for stewarding the kelp forests of the region. The initiative was formed to bring back wild salmon to their territories, and kelp forests serve as important habitats for migrating juvenile salmon. I must emphasize that many local observations have been made of varying kelp forest trends from increases, and stability, to decreases around various parts of the Broughton Archipelago, and that this specific research is not the first to document kelp persistence in Chapter 2.

2.0 Spatial characterization of environmental and biotic drivers of kelp distribution and abundance across an archipelago-fjord system in British Columbia, Canada

2.1 Abstract

Kelp forest distribution and abundance are driven by variations in environmental and topographic characteristics, including ocean temperature and seafloor slopes, as well as biotic factors such as grazer and predator abundances. Here, we investigate the effects of environmental and biotic drivers on kelp distribution and abundance across an archipelago-fjord environmental gradient in the Broughton Archipelago, BC, Canada, using field surveys, unmanned aerial vehicle and satellite imagery from the summer of 2023, and environmental model data. We identified two environmentally distinct subregions within the Broughton Archipelago: a cooler, more dynamic archipelago subregion to the west and a warmer, more sheltered fjord subregion to the east and north. We found that lower sea-surface temperatures, flatter bottom slopes, and higher tidal current speeds, typical of the archipelago subregion, were positively associated with kelp abundance, whereas the fjord subregion, with higher sea-surface temperatures, steeper bottom slopes, and lower tidal current speeds, had lower kelp abundance. By contrast, sea urchin and *Pycnopodia* abundance did not affect kelp abundance; however, spatial patterns of sea urchin and *Pycnopodia* abundances were present, with sea urchin abundance being relatively higher within the archipelago subregion, and *Pycnopodia* abundance being higher within the fjord subregion. Despite sea urchin abundances being relatively higher in the archipelago subregion, they were likely lower than in urchin barrens elsewhere on the BC coast. This study reinforces known findings on the interactions between the environment and kelp distribution and provides additional insight into how environmental gradients may potentially interact with kelp-urchin-*Pycnopodia* dynamics.

2.2 Introduction

Kelp forests (Order Laminariales) are found on 25% of the world's temperate coastlines and provide vital biogenic habitat in nearshore rocky reef systems (Druehl & Clarkston, 2016; Krumhansl et al., 2016; Lamy et al., 2020). As the largest vegetated coastal ecosystem on the planet, globally, kelp forests are a significant source of net primary productivity (NPP) and have high carbon sequestration potential (Pessarrodona et al., 2022; Krause-Jensen et al., 2016; Bayley et al., 2021; Filbee-Dexter et al., 2024). In the Northeast Pacific, the dominant surface canopy-forming kelp species are the giant kelp (*Macrocystis pyrifera, "Macrocystis"* hereafter) and bull kelp (*Nereocystis luetkeana, "Nereocystis"* hereafter) (Raffaelli & Hawkins, 1996), which are the focus of this research ('kelp' refers to these two species hereafter). Due to their height and structural complexity, kelp forests provide refuge and nursery habitat for many species (Miller et al., 2018; Lamy et al., 2020), including Pacific salmon, rockfish, herring, and abalone, as well as predators such as sea otters *(Enhydra lutris)* and sunflower sea stars *(Pycnopodia helianthoides)* (DFO, 2015; Watson & Estes, 2011; Burt et al., 2018; Shaffer et al., 2023). Additionally, kelp is highly valued in Indigenous cultures, with uses in woodworking, fisheries, trade, and traditional medicines (Turner, 2001; Reid et al., 2022). However, ocean warming and anthropogenic activities are causing decreases in kelp forests worldwide, threatening their ecosystem service provision (Wernberg et al., 2019; 2024; Smith et al., 2024). Consequently, many local communities, including those in British Columbia (BC), Canada, are prioritizing kelp conservation and management (Hamilton et al., 2022).

Variations in environmental and topographic characteristics drive the presence and abundance of kelp (Jayathilake & Costello, 2021; Gendall et al., 2023; Gonzalez-Aragon et al., 2024; Mora-Soto et al., 2024a). For instance, ocean temperature is one of the key factors driving kelp distribution and abundance across the global ocean (e.g. Gonzalez-Aragon et al., 2024) and within regions (e.g., Starko et al., 2022; Mora-Soto et al., 2024a). Along many temperate coastlines across the globe, cool, nutrient-rich water is brought to the nearshore environment with upwelling currents, tidal currents, and wave action**,** which can stimulate kelp growth (Krumhansl et al., 2016; Bekkby et al., 2019; Bell et al., 2020). Thus, larger kelp forests have generally been documented in cooler, oceanic waters with

high exposure and flow compared to warmer, more protected waters in the same region (Springer et al., 2010; Pfister et al., 2017; Starko et al., 2022; Mora-Soto et al., 2024a). Glacial influence in coastal fjord systems can also affect kelp distribution and abundance, with glacial meltwater contributing to decreasing water salinity and increasing turbidity, as observed in the Chilean Patagonia (Traiger & Konar., 2018; Huovinen et al., 2019). For instance, in Southern Chilean Patagonia, Huovinen et al. (2019) found the lowest kelp abundance near the mouth of a glacially fed river with high turbidity, with kelp abundance increasing towards the ocean. Nutrients can also drive kelp distribution and abundance, but this relationship can be quite complex (Hollarsmith et al., 2022). An increase in nutrient levels can enhance kelp canopy and holdfast growth but may also increase competition between kelp and other opportunistic fast-growing species of algae, ultimately decreasing kelp abundance (Dayton et al., 1999; Hollarsmith et al., 2022; Karez et al., 2004). Seafloor depth and slope also shape the size of kelp beds, with larger kelp beds generally occurring in shallow areas of low to mid-slope and fringing kelp beds in areas of high slope that drop quickly to euphotic depths, such as fjords (Mora-Soto et al., 2021; Gendall et al., 2023). In BC, the rocky coastline is complex and contains many fjords, islands, and shorelines of varying exposure levels, leading to various environmental and topographic conditions. Thus, the main environmental conditions driving the distribution and abundance of kelp forests vary throughout the coastline (Nijland et al., 2019; Starko et al., 2024a; Mora Soto et al., 2024a, 2024b)

Other than environmental variation and topographic characteristics, the effects of herbivore grazers and top-down control by grazers' predators may also affect kelp distribution and abundance (Burt et al., 2018; Rogers-Bennett & Catton, 2019; Eisaguirre et al., 2020; Hamilton et al., 2021). Key grazers in kelp forest ecosystems include sea urchins *(Strongylocentrotus spp.* and *Mesocentrotus franciscanus*, "sea urchins" hereafter*)* (Campbell & Harbo, 1991; Rogers-Bennett & Okamoto, 2020), which generally feed on drift kelp but graze on standing kelp when there is insufficient drift kelp (Kriegisch et al., 2019). An important sea urchin predator in the Northeast Pacific kelp forests is the sunflower sea star *(Pycnopodia helianthoides, "Pycnopodia"* hereafter*)* (Duggins, 1983). Recently, *Pycnopodia* populations crashed across the Northeast Pacific due to sea star wasting disease (SSWD), a disease that has been associated with sea-surface temperature (SST) increase (Burt et al., 2018;

Hamilton et al., 2021). *Pycnopodia* populations experienced more than 87.8% decline from the Salish Sea to the Gulf of Alaska, with the BC population crashing in 2017 (Hamilton et al., 2021). A population decline below a minimal threshold of *Pycnopodia* can reduce the top-down control of sea urchins, which, in turn, can lead to an increase in sea urchin populations (Eisaguirre et al., 2020). Once urchin densities increase above ~8.2–14 urchins m^{-2}**,** kelp forests can rapidly shift phases into urchin barrens, characterized by fronts of sea urchins that can span 10-100s m^2 to hundreds of kilometers (Filbee-Dexter & Scheibling, 2014). Such urchin barrens have been observed in Southern and Northern California (Eisaguirre et al., 2020; Rogers-Bennett & Catton., 2019) and the Central Coast and Barkley Sound in BC (Burt et al., 2018; Starko et al., 2022).

Climate change and anthropogenic activities can affect these environmental and biotic factors, and in turn, influence kelp distribution and population dynamics with impacts that vary at different spatial scales **(**Krumhansl et al., 2016; Wernberg et al., 2019; Smale et al., 2020). Specifically in BC, kelp forests have experienced variable patterns of change across the past few decades, with areas with warmer waters displaying loss and areas with cooler waters displaying persistence, and this variation can be seen even on fine spatial scales (e.g., a few kilometers or less) (Schroeder et al., 2019a; Gendall et al., submitted*;* Mora-Soto et al., 2024a, 2024b; Starko et al., 2022; 2024a). As such, a better understanding of the drivers of kelp change at a local scale requires a quantitative understanding of kelp distribution and abundance and the environmental and biotic conditions associated with the kelp ecosystem.

Here, we investigate the effects of environmental and biotic drivers on kelp distribution and abundance across an archipelago-fjord environmental gradient in the Broughton Archipelago (BC). Specifically, this study addresses two objectives: 1) Identify the environmental drivers of kelp distribution (presence/absence) and abundance (floating kelp area and kelp bed area); and 2) Characterize the effects of grazer and predator distribution and abundances on kelp distribution and abundance. These objectives were achieved by conducting fieldwork during the summer of 2023 to characterize underwater environmental and biotic conditions, and surface kelp distribution and abundance. Data from environmental models were also incorporated to better characterize the environmental conditions of the area. The dataset consisted of underwater profiles of temperature,

salinity, and photosynthetically available radiation (PAR), underwater video footage, unmanned aerial vehicle (UAV) and very-high-resolution satellite imagery ("satellite imagery" in this chapter), and environmental models of tidal current speeds, bathymetry, and shoreline fetch across 31 study sites. These sites were selected based on their importance to the Mamalilikulla, 'Namgis, and Kwikwaxuitinuxw/Haxwa'mis First Nations, which formed the Broughton Aquaculture Transition Initiative (BATI), a coalition that emphasized the need to continue monitoring and protecting the Archipelago's kelp forests, which provide habitat for out-migrating juvenile salmon (BATI, 2020). Our research allowed us to map the relationships between environmental conditions, key grazers and predators, and kelp distribution and abundance, potentially providing insights for the kelp monitoring and marine spatial planning efforts in the Broughton Archipelago. At a broader spatial scale, this study also contributes to regional and global efforts to understand the distribution and abundance of kelp forests during an era of unprecedented climate change.

2.3 Methods

2.3.1 Study area

The study area, the Broughton Archipelago, is located on Kwakwaka'wakw territories (Umista Cultural Society, n.d.), at the interface of two major bodies of water, the Johnstone Strait and Queen Charlotte Strait, near Northeast Vancouver Island, BC. It encompasses the fjords of Kingcome Inlet to the north, the mouth of Knight Inlet to the east, and Malcolm Island to the west, across an area of ~5,000 km^2 (BC Parks, 2003; BATI, 2021) *(Fig. 1)*. Due to past glacial ice loading and retreat, the geomorphology of this region is characterized by many channels, islands, bays, and deep fjords with sloping walls (Shugar et al., 2014). The water transport mechanisms within the archipelago include tidal currents, estuarine flows from watersheds fed by rain and glacial/snow freshets, and wind-driven currents (Foreman et al., 2006; Brewer-Dalton et al., 2014; Giesbrecht et al., 2022; Lin & Bianucci, 2023). Spring sea-surface temperatures range from 8.3°C to 11.0°C, according to a model by Foreman et al. (2006), and summer sea-surface temperatures range from 8.0°C to 16.0°C (Chapter 3; Lin &

Bianucci, 2023). Biologically, one of the key biogenic marine habitats in the region is kelp forests (BC Parks, 2003; BATI, 2021). Sutherland's (1990) Malcolm Island kelp inventory, comprising only part of the region, describes 4.67 million m^2 of *Macrocystis* and 2.72 million m^2 of *Nereocystis.* Shorezone's 1995 helicopter surveys identified the presence of *Nereocystis* beds along the majority of the coastlines throughout the region, and *Macrocystis* beds along the north coast of Malcolm Island *(Fig. 1)* (Shorezone, n.d.). Historical data from the 1850s based on the British Admiralty nautical charts indicated that kelp (not differentiated by species) has been present throughout the region since at least the 1850s to 1950s (Costa et al., 2020). More recently, the Mamalilikulla Guardian Watchman Program and local community members have reported kelp decline and loss in various parts of the archipelago (BATI, 2021; SCFS, 2023a).

Within the Broughton Archipelago, 31 sites were selected to represent the environmental gradient across the region. These sites include areas with and without kelp from the more exposed, cooler shorelines in the Broughton Strait, Fife Sound, and Johnstone Strait to the protected, warmer Knight Inlet, Tribune Channel, and Kingcome Inlet, which directly receive estuarine outflows *(Fig. 1)*. These sites were selected based on the BATI crew's lived knowledge during an exploratory field survey to identify focal areas of study in 2022, preliminary assessments from satellite imagery, and the aforementioned kelp distribution data sources. 21 sites had kelp (2 of the 21 kelp sites had *Macrocystis* present, 18 had *Nereocystis* present, 1 had a mixed *Macrocystis* and *Nereocystis* bed), and 10 sites had no kelp. These sites were surveyed in the summer of 2023, the season of peak above-water kelp biomass (Springer et al., 2010).

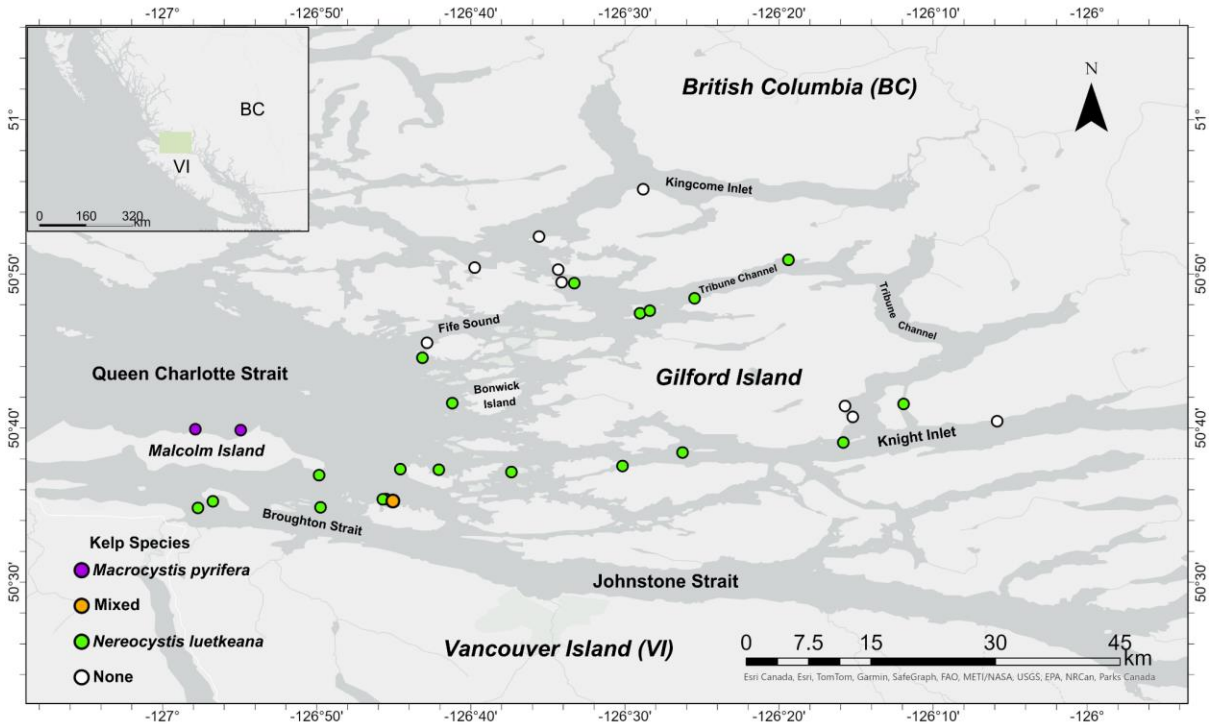

Fig. 1: Map of the study area and the 31 survey sites. Purple dots denote Macrocystis *sites, orange dots denote mixed* Macrocystis *and* Nereocystis *sites, green dots denote* Nereocystis *sites, and white dots denote sites with no kelp (as per observation from the surface during the 2023 summer field season). The inset map denotes the study area's location within BC.*

2.3.2 Data collection & processing

The following data was collected for each site: (1) imagery was acquired with an unmanned aerial vehicle (UAV) or satellite to obtain the surface kelp distribution and abundance; (2) environmental conditions, including water temperature, salinity, and PAR were measured with a CTD and an optical profiler, and tidal current, slope, and fetch from available environmental models. This dataset was used to group sites into environmental subregions and to identify the environmental drivers of kelp distribution and abundance *(Fig. 2)*. (3) Sub-surface substrate and biotic conditions were derived from underwater remotely operated vehicle (ROV) surveys to identify spatial abundance hotspots for kelp grazers and their predators and investigate how these biotic factors may interact with environmental conditions to drive kelp distribution and abundance (objective 2) *(Fig. 2)*.

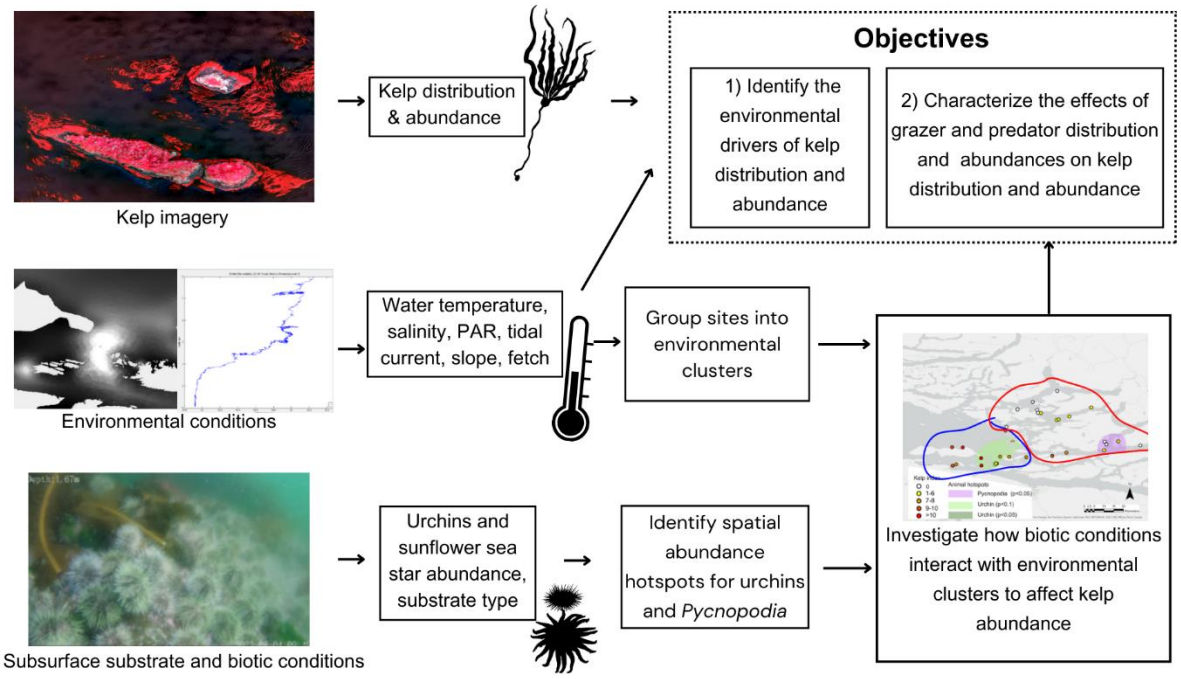

Fig. 2: Flow chart showing the analysis pipeline from data acquisition to data analysis to achieve the specific objectives of this research.

Kelp imagery

Imagery collection and processing

UAV surveys were conducted at sites where kelp was present to map the floating kelp area and quantify kelp distribution and abundance. All surveys were conducted below 2.70 m tidal height to control for the effect of tidal height on the detectable floating kelp area (Timmer et al., 2022, 2024). To ensure most of the floating kelp present at the sites would be covered in the flight plan, we ensured that the flight plan boundaries covered all suitable kelp habitats (i.e. areas shallower than 20 m in depth and with rocky substrate) by assessing the local bathymetry (Davies et al., 2018) and bottom substrate type (Haggarty et al., 2020). For the sites without clear suitable kelp habitat boundaries delineated by the bathymetry and the bottom substrate type, we deployed manual UAV flights on-site to identify the edges of the kelp bed before setting the site's flight plan (refer to supplementary material A1 for flight plan specifications). However, due to their large extent, kelp beds in 3 of the 31 sites were not surveyed in their entirety during the low tide window. For the six sites with UAV flight

zone restrictions or challenges with the orthomosaicking process, satellite imagery (GeoEye-1 and Worldview-3) was used to derive kelp distribution and abundance metrics *(Table 1).*

Table 1: Table showing the details about the two imagery types used, with their source, their spectral bands, their spatial resolutions, and the number of sites each method was used for.

Imagery type	Source	Spectral bands (central wavelength)	Spatial resolution (cm)	Sites covered
UAV imagery	Images from a DJI Mavic 3M (acquired during July-August 2023) (DJI, Shenzhen, Guangdong, China)	Green: 560 nm Red: 650 nm Red-edge (RE): 730 nm Near-infrared (NIR): 860 nm	2.30-5.50	16/31
Satellite imagery	Worldview-3 (acquired August 4, 2023) and GeoEye-1 (acquired August 6, 2023) (Maxar Technologies, Colorado, United States)	Green: 545 nm Red: 660 nm RE: 725 nm NIR: 833 nm	46.0	6/31

UAV images were orthomosaicked in Agisoft Metashape (version 2.0.2, Agisoft Metashape Professional, St. Petersburg, Russia) (refer to Appendix A2 for orthomosaicking methods). Satellite imagery (with multispectral and panchromatic bands) was pan-sharpened using the Gram-Schmidt method (Laben & Bower, 2000) in ArcGIS Pro (ESRI, Redlands, United States), resulting in a spatial resolution of 50.0 cm. Both UAV and satellite imagery were georeferenced using a single-order polynomial transformation against the ArcGIS Pro base map, and masked for land and rocks, following the methods of Gendall et al. (2023). Linear enhancements were applied to enhance the spectral separability between water and kelp pixels in ENVI (NV5 Geospatial Solutions, Broomfield, Colorado, United States) (Schroeder et al., 2019b; Gendall et al., 2023). Then, all images were segmented and classified as either “kelp”, “water”, or “mask” using an object-based image analysis (OBIA) approach in ECognition (Trimble Geospatial Imaging, Munich, Germany) (Blaschke, 2010; Gendall et al., 2023), producing polygons of floating kelp area – “classified kelp area” (refer to Appendix A3 for details about the segmentation and classification methods).

Computation of kelp abundance metrics

The following four metrics of kelp abundance were computed to assess the variation in the area and density of the kelp beds *(Fig. 3):* classified kelp area, kelp bed area, kelp bed density, and kelp abundance index. Only kelp bed density and kelp abundance index were used in the statistical models (see 2.3.3), however, these metrics were generated from the first two metrics of classified kelp area and kelp bed area. The metrics were defined as:

1) Classified kelp area (m^2): this metric corresponds to the area classified as "kelp" during the OBIA process. It primarily includes the area of floating kelp blades and bulbs at the water surface; however, pixel mixing (pixels consisting of spectral signals from both kelp and water) may have incorporated small areas of water in the classified kelp area metric *(Fig. 3)*.

2) Kelp bed area (m^2): this metric corresponds to a contiguous kelp bed area, including the classified kelp area (defined above) and the water area between adjacent kelp blades and bulbs *(Fig. 3)*. This metric follows the definition of a "kelp bed" established by the North Pacific Ocean Marine Plan Partnership (MaPP) protocols: any cluster of kelp plants at least 3 m long in any direction, with less than 10 m between each plant (Thompson, 2021). Furthermore, this metric complements the classified kelp area metric because it helps reduce the variation of classified kelp area from sampling design (e.g., tidal height during image acquisition) and current-induced kelp movement. The kelp bed area was calculated using the Buffer Analysis tool in ArcGIS Pro with a buffer radius of 4.99 m to link all classified kelp area features within 10 m of each other *(Fig. 3).*

3) Kelp bed density (%): this metric refers to the percentage of the kelp bed area covered by the classified kelp area, representing how densely packed the kelp blades and bulbs are in a kelp bed. This metric allows the comparison of kelp bed density between sites, as there are some sites where kelp beds span large areas but are formed with only a few blades and bulbs, i.e., low density, and some sites where kelp beds span a large area, with the blades and bulbs closely packed together, i.e. high density *(Fig. 3)*.

4) Kelp abundance index (unitless): This index is derived from the product of the classified kelp area by the kelp bed area, thus creating a unified metric for kelp abundance**.** The kelp abundance index was calculated as:

$$\text{Kelp abundance index} = log\ (classified\ kelp\ area\ \times\ kelp\ bed\ area) + 1) \quad (1)$$

The log transformation used in the kelp abundance index resulted in the linearization of index values, allowing for easier comparison for sites with extreme kelp abundance values. As illustrated in *Fig. 3*, sites with the highest kelp abundance index have a larger classified kelp area, kelp bed area, and density (i.e., high density over a large area) (*Fig. 3A*). In contrast, sites with a medium kelp abundance index either have a smaller classified kelp area relative to its larger kelp bed area, i.e. sparse kelp spread over a large area (*Fig. 3B*), or a larger classified kelp area relative to its smaller kelp bed area, i.e., dense kelp bed that spread over a small area (*Fig. 3C*). Finally, sites with a low kelp abundance index have smaller classified kelp areas and kelp bed areas, i.e., sparse kelp beds over a small area (*Fig. 3D*).

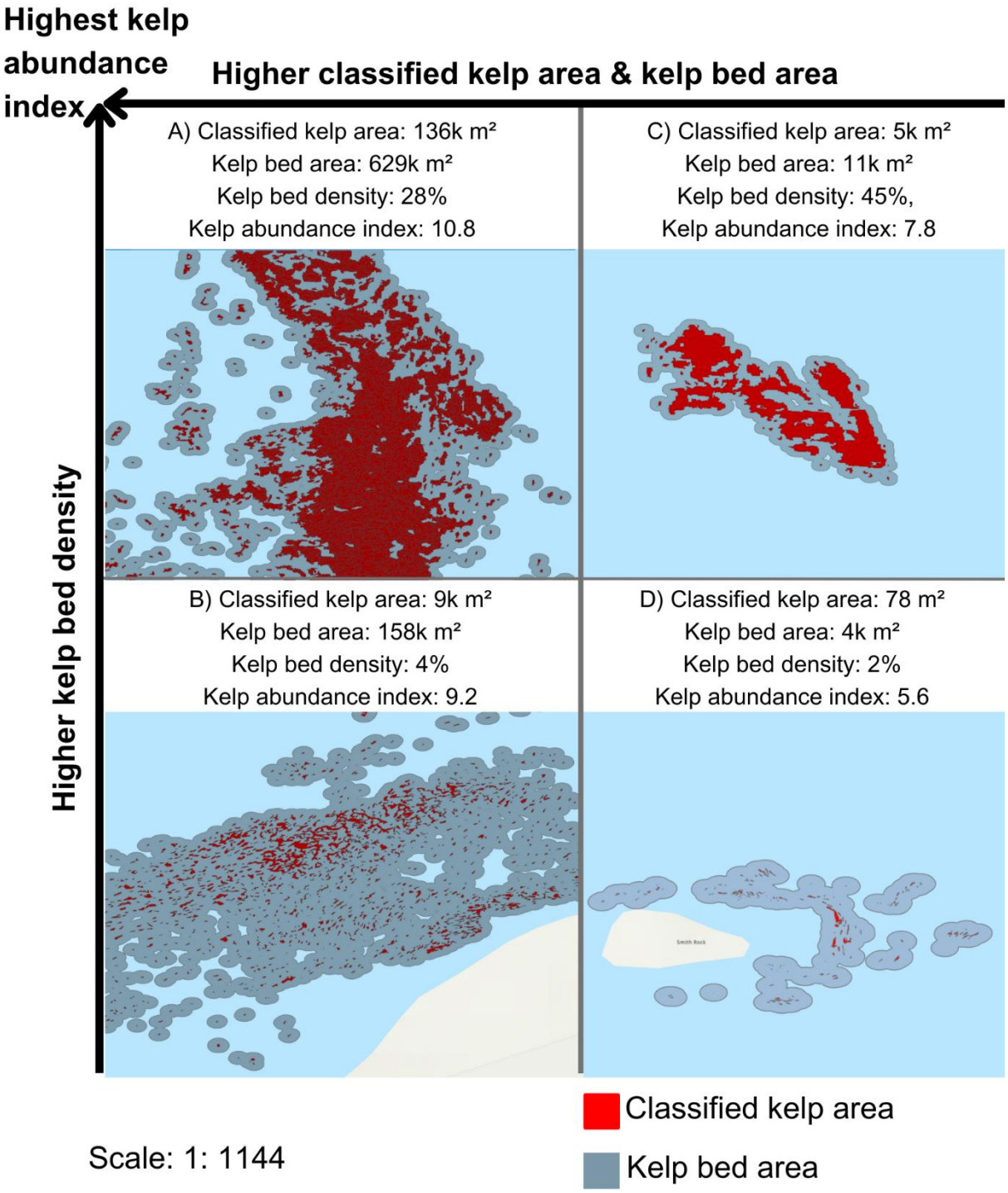

Fig. 3: Schematic showing the relationship between classified kelp area, kelp bed area, kelp density, and kelp abundance index. The schematic visually represents the classified kelp area in red and the kelp bed area in dark blue-grey of four different sites and lists the classified kelp area, kelp bed area, kelp bed density, and kelp abundance index of the associated sites. The scales of all site maps are all uniform at 1:1144. A) represents a site with high kelp abundance index, B) represents a site with a medium kelp abundance index with a smaller classified kelp area relative to its larger kelp bed area, C) also represents a site with a medium kelp abundance index, but with a higher classified kelp area relative to its smaller kelp bed area, and D) represents a site with a low kelp abundance index. Note

that the kelp beds at the sites shown in panels A and B are not shown in their entirety in these panels due to the extensive size of these kelp beds.

Tests for confounding effects of tides and imagery source on classified kelp area

Kendall's correlation test (Kendall, 1948) was used to ensure that various tidal heights (between 0.200 and 2.70 m) at the time of image acquisition and the imagery source (UAV or satellite imagery) did not significantly affect the kelp metrics derived from the imagery classification, and subsequently confound the subsequent statistical analysis. Tidal height did not significantly relate to classified kelp area *(Kendall's correlation test $R=0.240$, $p=0.0623$).* Next, we tested for the effect of imagery source by classifying both UAV and satellite imagery acquired three days apart from each other for the same area (tidal height – UAV: 2.60 m, satellite imagery: 1.80 m), separately considering dense and sparse sections within the same kelp bed. The satellite-derived area was 18.6% higher than the UAV-derived area for the dense section and 15.3% lower for the sparse section. From a visual examination of UAV and satellite imagery, in the dense area, the satellite-derived area was higher than the UAV-derived area likely because of pixel mixing due to the satellite imagery having a lower spatial resolution where small areas of water adjacent to the kelp falsely classified as kelp. Conversely, in the sparse kelp area, the satellite-derived area was lower than the UAV-derived area, likely because of environmental and radiometric factors, such as submersion by tidal currents and the effects of the pan-sharpening procedures. Nonetheless, we expect these adjacent areas to contribute negligible differences to the measured kelp area as the highest classified kelp area was ~9,000 times higher than the lowest classified kelp area (see section 2.4.1), i.e., magnitudes higher than that observed in the test. Moreover, these kelp area classifications were used to investigate spatial patterns of kelp abundance, rather than to construct a time series for one specific site, where very small differences in the detected kelp area could affect the detection of temporal trends. Based on a presumed negligible influence of any misclassified areas, we decided that the kelp metrics were suitable for subsequent statistical analysis (see section 2.3.3).

Environmental conditions

In situ mean surface, midwater, and benthic temperatures (°C), conductivity (mmho/cm), and underwater downwelling irradiance ($Ed(z,\lambda)$, m^{-1}) measurements were collected to identify potential environmental drivers of kelp distribution and abundance *(equipment and survey methods in Table 2)*. Conductivity measurements were converted to practical salinity units (PSU) using the ec2pss function (wql package, Jassby & Cloern, 2015) in R (R Core Team, 2022)**.** A stratification index, $\Delta\sigma t$ ($kg\ m^{-3}$) was used to quantify water column stratification at each site. The index was initially created to characterize stratification across a wider range of depths (surface to 50 m+ depth; Drinkwater & Johes, 1987; Suchy et al., 2016), but we adapted it for use in the shallower waters where our measurements were conducted. This parameter was calculated as the difference in density between the surface water and mid-water (Drinkwater & Jones, 1987; Suchy et al., 2016, 2019), with a stratification index above 1.00 $kg\ m^{-3}$ indicating a more stratified water column (Drinkwater & Jones, 1987). The midwater temperature/salinity measurements were used instead of the bottom measurements because not all sites had benthic measurements. Percent PAR (PAR available at a given depth divided by PAR at the surface) measurements were calculated from downwelling plane irradiance measurements with the Prosoft processing software. This metric was used for the statistical analysis instead of absolute PAR (mol photons $m^{-2}\ day^{-1}$) as it normalized PAR measurements by the variable illumination conditions at the water surface, however, this provided a relative measure of light availability that is related to light attenuation and turbidity of the water column, rather than the actual amount of light available for kelps' photosynthesis (*Table 2*, see Appendix A4 for PAR processing methods)**.**

For each site, fetch was derived from the model by Gregr et al. (2018) as a proxy for exposure to wind and waves (Gregr et al., 2018, 2019). In addition, mean tidal current speeds and mean depths and slope were derived from the models by Foreman et al. (2009) and Davies et al. (2018), respectively *(Table 2).* To retrieve the corresponding values representing mean fetch, tidal current, depth, and slope, while accounting for outliers and spatial variability, zonal statistics at a 100 m buffer around each site location were used.

Subsurface substrate and biotic conditions

An ROV was used to collect videos to obtain sea urchin and *Pycnopodia* abundance metrics and qualitative assessments of the bottom substrate type at each study site *(Table 2)*. 2-3 transects were conducted at each site: one towards the shore and two parallel to the shore in opposing directions. At the sites with kelp beds, the toward-shore transect was conducted as far as possible inside the kelp bed, avoiding entanglement in the kelp stipes, and the along-shore transects followed the edges of the kelp beds. The ROV was kept at approximately -45° angle view to the bottom substrate, ~1 m above the seafloor, and at a constant speed along the transect. Transect video lengths (minutes) and transect distances (m) varied due to challenging survey conditions, including strong currents, dense kelp, and the different bathymetry at each site.

The analysis of the ROV videos to derive standardized sea urchin and *Pycnopodia* abundances was based on still images extracted from the videos to reduce analysis time, while still yielding the same results as video analysis (Cabaitan et al., 2007). First, the number of seconds needed for the field of view in the videos to change ("change rate" hereafter) was determined, following the methods of Buscher et al. (2020). To do so, we used ten ROV transect videos from different sites to calculate the minimum "change rate", which was determined to be 4 seconds per field of view. Still images were then extracted from each ROV video every 4 seconds using ImageGrab (VideoHelp)**.** Once all the images were extracted, quality checks were done to exclude stills with the same field of view and/or where the benthos were not visible. From the selected images, the number of sea urchins (any species) and *Pycnopodia*, as well as a final metric of normalized abundance (counts/image), were counted for each site to account for variations in survey length between sites. This abundance metric is analogous to urchin and *Pycnopodia* density metrics typical of quadrat surveys (e.g. Starko et al., 2022). Based on the ROV survey protocol and a visual quality control of images, we assumed that each usable image covered a similar area of the benthos, allowing a quantitative assessment of species abundance.

The bottom substrate type was qualitatively assessed directly from the ROV survey videos and visually classified into: 'rocky', 'mixed', and 'sandy', based on the classifications included in the substrate model for all BC coastal areas by Haggarty et al. (2020). 'Rocky' was assigned to video

transects where more than half of the video showed a bottom substrate size larger than pebbles (4-64 mm diameter) (Greene et al., 1999). 'Mixed' was assigned to transects with a mixture of rocky and sandy bottom substrates, as well as sites with primarily sandy bottom substrate and some kelp growing on small chunks of an unknown substrate–presumed rocks, as kelps only attach their holdfasts to rock (Springer et al., 2010). Finally, 'sandy' was assigned to transects of completely sandy flats with no kelp growth.

Table 2: Table showing the methods used for collecting data about environmental and biotic conditions, including details about the instrument or data source used, the processing software, survey or measurement area for each method, and the variables extracted from each method

Method	**Data acquisition instrument or data source**	**Processing software**	**Survey or measurement area**	**Variables**
Environmental conditions				
Profiler (1.00-7.00 m depth)	Satlantic Minispec OCR-3000 sensor (400–800 nm; 1 nm spectral resolution), Seabird CTD instrument	ProSoft (v7.4, Satlantic, Halifax, NS, Canada).	The profiler was deployed in triplicates at 31/31 sites. If a kelp bed was present, it was deployed outside the kelp bed at >7.00 m depth. If a kelp bed was not present, it was deployed at any point around the site > 7.00 m depth.	Mean surface (0.00-1.00 m), midwater (4.00-5.00 m), and benthic (6.00-7.00 m) temperature (°C) and salinity (PSU) Mean percent PAR (percent of PAR at each depth relative to the PAR available at the surface) at every depth between 1.00 and 5.00 m
Bathymetry model (all depths)	Davies et al. (2018)	ArcGIS Pro (ESRI, Redlands, United States)	The bathymetry layer was provided from a 20 m resolution coastal digital elevation model made for marine ecological analyses in Pacific Canadian waters. The slope raster was calculated using the Slope Geoprocessing tool in ArcGIS	Mean slope (°) calculated using zonal statistics in a 100 m buffer polygon buffer.
Tidal current speeds (all depths)	Foreman et al. (2009)	ArcGIS Pro (ESRI, Redlands, United States)	Finite volume circulation model for tidal harmonics, run for the period March 13 to April 3, 2008	Mean tidal current (m/s) calculated using zonal statistics in a 100 m buffer polygon buffer.
Fetch model (nearshore points located at 50 m intervals)	Gregr et al., 2018	ArcGIS Pro (ESRI, Redlands, United States)	Each point represents the sum of linear distances at every 5 degrees ("total fetch").	Mean fetch (km) calculated using zonal statistics in a 100 m buffer polygon buffer.
Subsurface substrate and biotic conditions				
ROV (~1-17 m depth)	FiFish V6 (Qysea, Shenzhen, Guangdong, China)	ImageGrab (VideoHelp, https://www.videohelp.com/software/ImageGrab)	The ROV was deployed 3 times at each of the 31 sites, with 2 transects parallel to the coast in opposite directions, and 1 perpendicular to the coast. If a kelp bed was present at the site, the perpendicular transect would go into the kelp bed	Urchin and *Pycnopodia* abundance (counts/image), bottom substrate type

2.3.3 Analysis

The spatial patterns of kelp distribution and abundance were examined by first dividing the Broughton Archipelago region into distinct environmental subregions. To define the subregional-scale relationships between environmental and biotic variables and kelp, the kelp, urchin, and *Pycnopodia* abundances were compared between these subregions. Next, the spatial patterns of grazer (urchins) and predator *(Pycnopodia)* abundances were identified using a hotspot analysis. Finally, the site-level effects of environmental and biotic drivers on kelp distribution and abundance were defined using linear and generalized linear models.

Identify the environmental drivers of kelp distribution and abundance

Environmental subregions

We selected environmental variables for the spatial grouping of sites into environmental subregions following the methods in Mora-Soto et al. (2024a) and Gendall et al. (submitted). First, all the environmental variables *(Table 2, Table A1)* were tested for collinearity by generating a correlation matrix using Kendall's correlation test (Kendall, 1948), and highly correlated variables (i.e. significant variables with an $R > 0.5$) were excluded to prevent overfitting the statistical model (Hawkins, 2004). The selected variables (i.e. non-highly correlated variables) were SST, midwater salinity, percent PAR at 1.00 m depth, tidal current speed, slope, and fetch. In contrast, midwater and benthic sea temperatures, surface and benthic salinity, and all percent PAR measurements from 2-5 m were excluded from the analysis due to high correlation with the selected variables. The bottom substrate type was excluded because it was observed that both rocky and mixed substrates equally supported kelp presence, and only 3/31 sites had sandy substrate that could not support kelp presence.

Next, the selected environmental variables were used in a k-means clustering analysis (Hartigan & Wong, 1979) using the "kmeans" function in R (stats package, R Core Team, 2022). First, the environmental variables were rescaled using Z-scores to ensure equal distance consideration by the clustering algorithm (Mohamad & Usman, 2014). The optimal number of subregions (clusters) was chosen using the "NbClust" function (NbClust package, Charrad et al., 2014), systematically

comparing 30 different cluster-choosing indices. A Principal Component Analysis (PCA) (Abdi & Williams, 2010) biplot was also considered to visualize the Euclidean distance between the subregions and the main variables driving the differentiation between the subregions. The final environmental subregions defined areas of contrasting SST, midwater salinity, surface PAR, tidal current speed, slope, and fetch. Kruskal-Wallis tests were conducted to test for significant differences for each of the selected variables between the subregions (Kruskal & Wallis, 1952). In addition, the Kruskal-Wallis tests were also conducted for the excluded environmental variables, i.e., midwater and benthic sea temperatures, surface and benthic salinity, and sub-surface percent PAR (2-5 m depths), to define if they also differed between subregions.

Relationship between environmental variables and kelp:

To understand subregional relationships between the environmental variables and kelp, we conducted Kruskal-Wallis tests to test for differences in the classified kelp area, kelp bed area, kelp density, and kelp abundance index among environmental subregions (Kruskal & Wallis, 1952). Moreover, as we found that only one subregion contained sites with no kelp (see 2.4.1), we also conducted Kruskal-Wallis tests to compare the differences in the environmental variables at the sites with and without kelp within that subregion.

We further fitted two linear models to identify the potential environmental drivers of the kelp abundance index on a site level (R Core Team, 2022). For this, the kelp abundance index was chosen as the dependent variable as it integrated both the classified kelp area and kelp bed area and linearized the kelp abundance values (eq. (1)). Linear model 1 included all 31 sites (regardless of whether the sites had kelp or not) to test what environmental variables drove kelp presence and abundance. Linear model 2 included sites with kelp beds (22 sites) to test what environmental variables drove the kelp abundance index, given that a site already had kelp. For both models, first, univariate relationships between each environmental variable selected for use in the clustering analysis and kelp abundance index were tested, followed by the creation of multivariate models incorporating significant variables. Second, the lowest Akaike Information Criterion (AIC) was used to define the best combination of predictor variables for each significant multivariate model (Akaike, 1974). Once the final models

were selected with the lowest AIC, the marginal effect of each significant predictor variable on the kelp abundance index was represented graphically by predicting the response variable over the in-situ ranges of the environmental variables (Fox & Weisberg, 2019).

The assumptions of both linear models were visually evaluated with histograms of the model residuals, residuals' quantile-quantile plots, plots of the fitted values vs residuals, and statistically evaluated for the normality assumption using Shapiro-Wilk tests (Shapiro & Wilk, 1995). A plot of the residuals vs the observed site numbers was used to identify patterns in the order of the data, which tests for the assumption of the independence of observations, whereas a plot of the models' fitted vs residuals values was used to test for the linearity and constant variance assumptions. All visualizations were consistent with the assumptions required by the models *(Figs. A1-A2),* and the results of the Shapiro-Wilk tests confirmed that the residuals of both models were normal (Model 1: W = 0.984, p-value = 0.908, Model 2: W: 0.979, p=0.906).

Characterize the effects of grazer and predator distributions and abundances on the distribution and abundance of kelp.

First, we tested for differences in urchin and *Pycnopodia* abundances between environmental subregions with Kruskal-Wallis tests (Kruskal & Wallis, 1952). Moreover, since only one subregion contained sites with no kelp (see 2.4.1), we conducted Kruskal-Wallis tests of the biotic variables at the sites with and without kelp within that subregion. This was followed by a spatial hotspot analysis, which identified locations where urchin and *Pycnopodia* abundances were higher than the other sites. The hotspot analysis was conducted in ArcGIS Pro 3.0 (ESRI, Redlands, United States) using the Getis-Ord GI* (GI*) statistic with a fixed distance band, which identified confidence interval (CI) categories at 99% ($p<0.01$), 95% ($p<0.05$), and 90% ($p<0.1$) based on the p-values to identify the significance levels of the hotspots (Getis & Ord, 1992).

In addition, on a site level, we investigated if the presence of *Pycnopodia,* a known urchin predator (Duggins, 1983), significantly affected urchin abundance. This was conducted using a Kruskal-Wallis test among sites with either urchins, *Pycnopodia,* or both urchins and *Pycnopodia*

present (18 sites). Urchin abundance was the dependent variable, and the presence-absence of *Pycnopodia* was the independent variable.

Finally, we fitted a Tweedie generalized linear model (GLM) with a compound Poisson distribution to determine if urchin and *Pycnopodia* abundances had significant interactions with environmental subregions to affect kelp bed density (R "tweedie" package, Dunn, 2022). Here, the dependent variable was kelp bed density as it normalized kelp abundance to a fixed area, just as urchin and *Pycnopodia* abundances were calculated relative to a fixed area (counts of each animal / ROV still image) (see section 2.2.3). The predictor variables included urchin abundance, *Pycnopodia* abundance, subregion, and all interactions between these three variables. Univariate relationships between each variable and kelp density were tested for significance, followed by the creation of multivariate models incorporating significant variables. The assumptions of the GLM were verified with histograms of the model residuals, residuals' quantile-quantile plots, and plots of the models' fitted values vs residuals, as detailed in 2.3.1 *(Fig. 3)*. A Shapiro-Wilk test was not conducted for the GLM residuals as the Tweedie GLM did not assume a normal distribution.

2.4 Results

2.4.1 Environmental drivers of spatial differences in kelp distribution and abundance

Environmental subregions

The clustering analysis spatially separated the Broughton Archipelago into two distinct environmental subregions representing: a more dynamic area (the "archipelago subregion") and a more sheltered area (the "fjord subregion") *(Fig. 4A).* These subregions were primarily distinguished by differences in SST, slope, tidal current speeds, and midwater salinity (*Fig. 4B, Fig. 4C)*. The Euclidean distance between the two subregions is visually represented in the PCA biplot by the separation of the subregions along PC1, the principal component that explains the most variation (41.78%) *(Fig. 4B).* Among the selected environmental variables, the archipelago subregion had

significantly colder SST than the fjord subregion (archipelago subregion = “A”, fjord subregion = “F”; A: 9.95±0.583°C, F: 14.3±2.48°C), lower slopes (A: 4.83±3.47°, F: 17.5±9.57°), higher tidal current speeds (A: 0.218±0.171 m/s, F: 0.0917±0.0397 m/s), higher percent PAR at 1 m depth (A: 68.0±8.99%, F: 60.5±6.47%), higher fetch (A: 462±539 km, F: 139±168 km), and higher midwater salinity (A: 31.2±0.818 PSU, F: 25.5±3.18 PSU**)** *(Fig. 4B-4C, Table A1)*.

Notably, the Kruskal-Wallis tests confirmed that all the environmental variables measured were significantly different between environmental subregions, regardless of whether they were selected or excluded from the clustering analysis *(Fig. 4C, Table A1)*. Regarding the variables that were excluded from the clustering analysis due to high autocorrelation with the included variables, the archipelago subregion was characterized by lower temperatures, higher salinities, and higher PAR regardless of depth, and lower stratification indices than the fjord subregion *(Table A1)*.

A

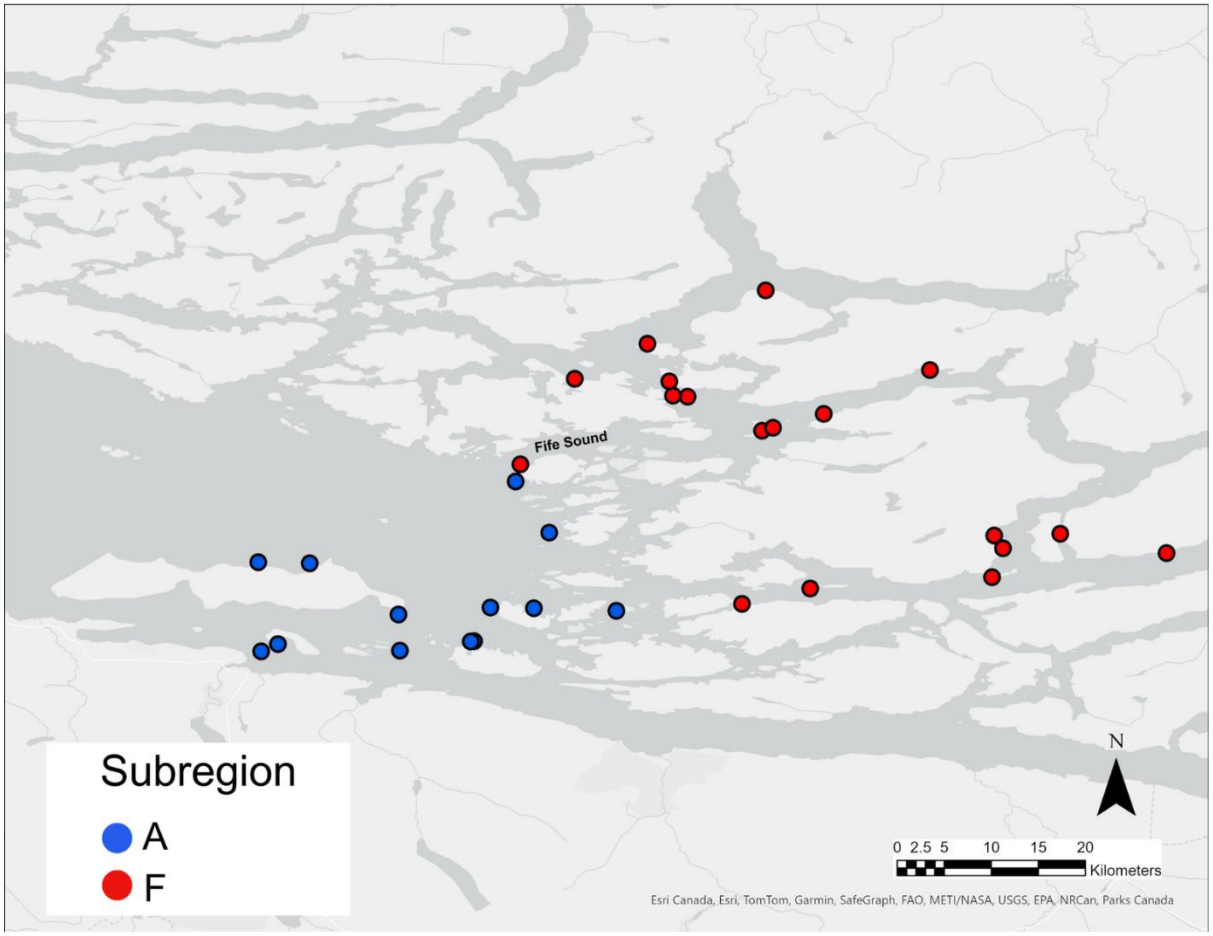
Fife Sound
Subregion
A
F
N
0 2.5 5 10 15 20
Kilometers
Esri Canada, Esri, TomTom, Garmin, SafeGraph, FAO, METI/NASA, USGS, EPA, NRCan, Parks Canada

B

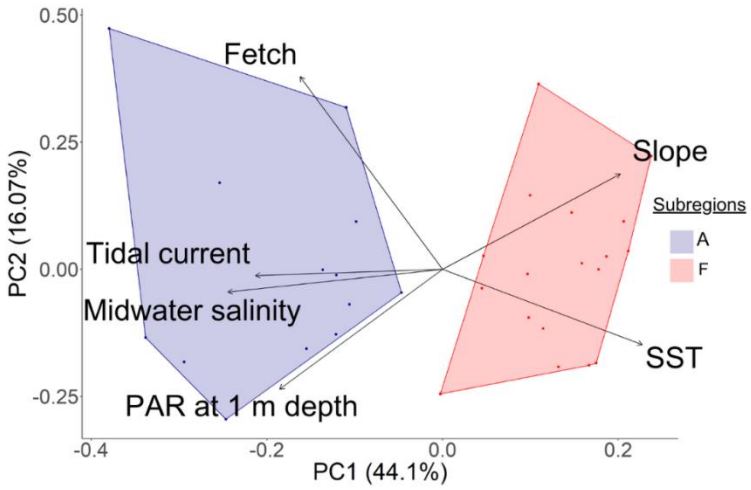
Fetch
Slope
Tidal current
Midwater salinity
SST
PAR at 1 m depth
Subregions
A
F
PC2 (16.07%)
PC1 (44.1%)
0.50
0.25
0.00
-0.25
-0.4
-0.2
0.0
0.2

C

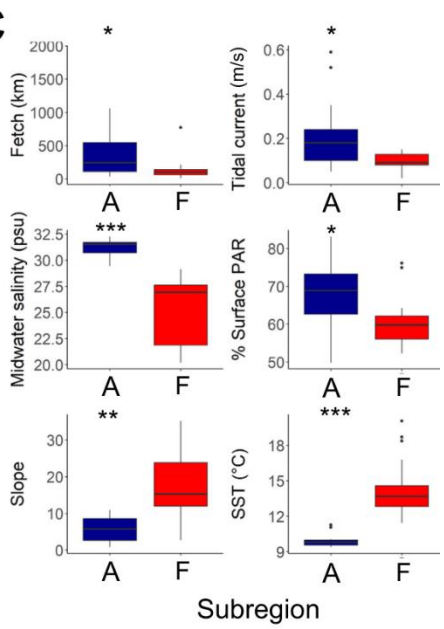
Fetch (km)
Tidal current (m/s)
Midwater salinity (psu)
% Surface PAR
Slope
SST (°C)
A
F
Subregion

Fig. 4: A) Map showing the spatial distribution of the sites belonging to the archipelago subregion ("A") in blue dots and the sites belonging to the fjord subregion ("F") in red dots. B) The PCA biplot shows the results of the k-means cluster analysis, with each point representing the selected environmental variables of each site, and the distance between each point representing the Euclidean distance between each site. Blue points and hulls represent the archipelago subregion, and red points and hulls represent the fjord subregion, with the distance between each hull representing the Euclidean distance between each subregion. C) Box plots show the differences in medians of the selected environmental variables for the cluster analysis between the two subregions, as well as their associated interquartile ranges and outliers (dots). The level of significant difference for each environmental variable between each subregion is indicated by asterisks (= p<0.05, ** = p<0.01, *** = p<0.001)*

A noteworthy spatial pattern was observed in the boundaries of the environmental subregions, specifically, the two sites near the mouth of Fife Sound were separated into distinct environmental subregions despite being adjacent to each other *(Fig. 3A).* A closer examination revealed that the environmental conditions between these two sites differed significantly, with the site belonging to the archipelago subregion having lower SST (A: 9.95°C, F: 11.7°C), slopes (A: 10.7°, F: 28.1°), higher percent PAR (A: 66.0%, F: 58.7%), and fetch (A: 545 km, F: 182 km) compared to the site associated with the fjord subregion *(Table A2)*

Relationship between environmental variables and kelp indices

High variability in the classified kelp area, kelp bed area, kelp density, and kelp abundance index were observed across the Broughton Archipelago *(Table A3)*. At sites where kelp was present (n=22), classified kelp area ranged from 13.6 m^2 to 136,000 m^2, with an average of 13,200 m^2, whereas kelp bed area ranged from 589 m^2 to 484,000 m^2, with an average of 67,300 m^2. Kelp bed density ranged from 0.52% to 56.1%, with an average of 12.4%, and kelp abundance index ranged from 3.90 to 10.8, with an average of 7.37. All kelp metrics, including classified kelp area (A: 21,500 ± 37,900 m^2, F: 638 ± 2,210 m^2), kelp bed area (A: 95,800 ±140,000 m^2, F: 13,100±37,100 m^2), kelp bed density (A: 19.4±16.5%, F: 1.08±1.46%) and kelp abundance index (A: 8.27±1.55, F: 3.04±3.31) were significantly higher in the archipelago subregion than the fjord subregion (respective Kruskal-Wallis tests: $\chi2=17.1$, $p=3.57\times10^{-5}$; $\chi2=13.6$, $p=2.26\times10^{-4}$; $\chi2=21.0$, $p=4.66\times10^{-6}$; $\chi2=16.1$, $p=6.02\times10^{-5}$).

All the sites that did not have kelp present (n=9) were in the fjord subregion (18 sites total). Note that this is a result of the sampling design, and there were also parts of the archipelago subregion not sampled in this study that had no kelp. The fjord subregion kelp sites (n=9) had significantly higher stratification indices than the non-kelp sites (Kruskal-Wallis test: $\chi 2=4.68$, p=0.0305, kelp sites: 2.11±1.56 kg m^{-3}, non-kelp sites: 6.74±5.23kg m^{-3}) *(Table A4).* Furthermore, the only sites with sandy substrate (n=3) across all 31 study sites were the non-kelp sites *(Table A4).*

The variability in the kelp abundance index was affected by spatial differences in environmental conditions across the Broughton Archipelago, with SST, slope, and tidal current tested as predictors in statistical models. Specifically, the linear model 1 (which included all 31 sites regardless of whether the sites had kelp or not) showed that the kelp abundance index was negatively related to SST and slope, but was not significatively related to tidal current, with a 40% SST increase and a 97% slope increase corresponding to a 50% decrease in the kelp abundance index *(Fig. 5A, Table A5, n=31,* R^2 =0.678, model: $p=8.17\times10^{-7}$**,** slope: p=0.00949, SST: p=0.00118). Linear model 2, which only included sites where kelp beds were present (n=22), showed that the kelp abundance index presented a significant positive relationship with only tidal current speed, but was not significantly related to SST or slope, with a 96% increase in tidal current speeds corresponding to a doubling in the kelp abundance index *(Fig. 5B, Table A5, n=22,* R^2 =0.579, model: p=0.00376, tidal current: p=0.00880). Note that as the kelp abundance index is a log-transformed value, an increase in this index actually represents exponential increases in classified kelp area or kelp density (see examples in *Fig 3).*

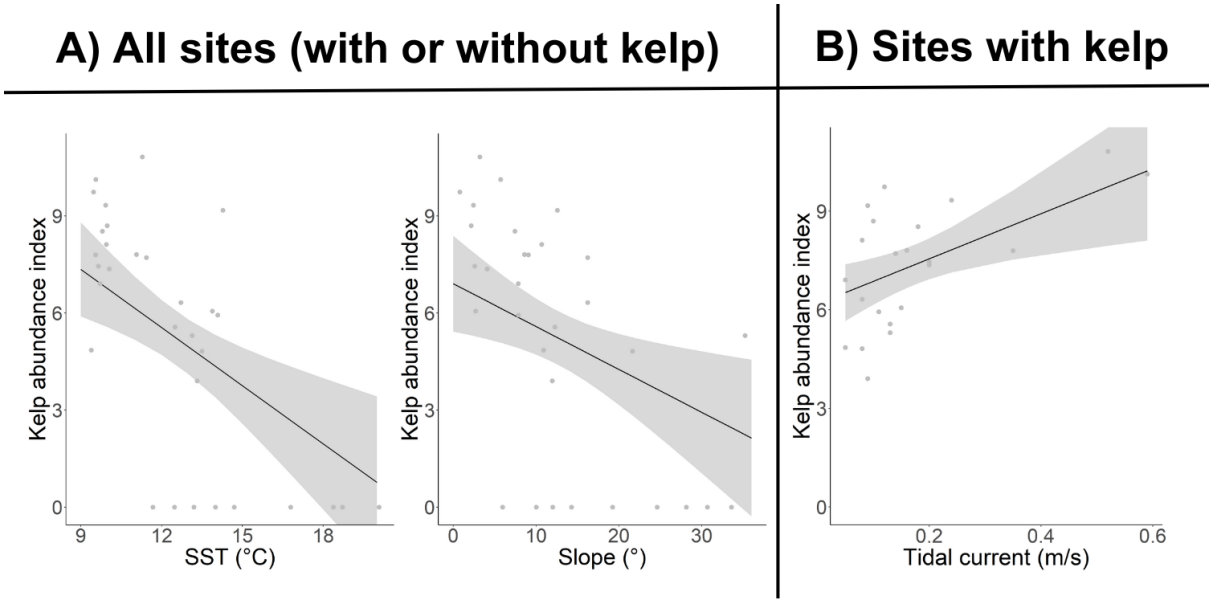

Fig. 5: Linear model results, with the black lines showing marginal effects (i.e. considering every other predictor variable used in each model as constant) of each significant environmental predictor variable (site-level mean)on the kelp abundance index at each site, the grey shading behind the black line showing the confidence interval of each marginal effect plot, and the grey dots showing the raw data. (A) shows the results of linear model 1, which includes all the sites (n=31), and (B) shows the results of linear model 2, which only includes sites where kelp was present (n=22).

2.4.2 Effects of grazer and predator distribution and abundances on the distribution and abundance of kelp

Urchin and *Pycnopodia* abundances varied greatly across the archipelago. Urchins were present in 16 sites, with mean site abundance ranging from 0.00362/image to 15.2/image and an overall average of 4.31/image. In contrast, *Pycnopodia* were only present in 6 sites, with mean site abundance ranging from 0.00450/image to 0.377/image with an overall average of 0.0989/image. Spatially, the GI* statistic showed two hotspots with varying levels of significance of urchin abundance (urchin hotspot 1: 4 sites >90% CI, urchin hotspot 2: 2 sites > 95% CI, *Table A6*) within the archipelago subregion to the west, specifically, from Broughton Strait to Bonwick Island. There was one *Pycnopodia* abundance hotspot (a group of 4 sites > 99% CI) within the fjord subregion, around Knight Inlet and the southeastern shore of Gilford Island *(Fig. 6, Table A7).* The urchin and *Pycnopodia* abundance hotspots did not overlap, and urchin abundance was significantly lower when *Pycnopodia* was present (Kruskal-Wallis $\chi 2=5.94$, $p=0.0148$). Although the urchin abundance hotspot

was located within the archipelago subregion, and the *Pycnopodia* abundance hotspot in the fjord subregion, neither hotspot spanned the entirety of the respective subregions, and ultimately, there were no significant differences in urchin (Kruskal-Wallis $\chi 2 = 0.406$, $p=0.524$; A: 3.09±5.46 counts/image, F: 1.59±3.51 counts/image) or *Pycnopodia* abundances (Kruskal-Wallis $\chi 2 = 0.485$, $p=0.486$, A: 0.000892±0.00224 counts/image, F: 0.0323±0.0910 counts/image) between the archipelago and fjord subregions.

From the Tweedie GLM analysis, sea urchin and *Pycnopodia* abundance did not significantly relate to kelp bed density, whereas the subregions significantly related to differences in kelp bed density, with kelp bed density being significantly higher in the archipelago subregion than the fjord subregion, corroborating the findings in Section 2.4.1 (model: $R^2 = 0.508$, urchin: $p=0.179$, *Pycnopodia*: $p=0.709$, subregion: $p=0.00168$). Note that sea urchin and *Pycnopodia* abundances did not significantly relate to kelp bed density even if subregion was excluded as a predictor variable. Additionally, none of the variable interactions (sea urchin × *Pycnopodia*, sea urchin × subregion, *Pycnopodia* × subregion) significantly affected kelp bed density *(Table A8)*.

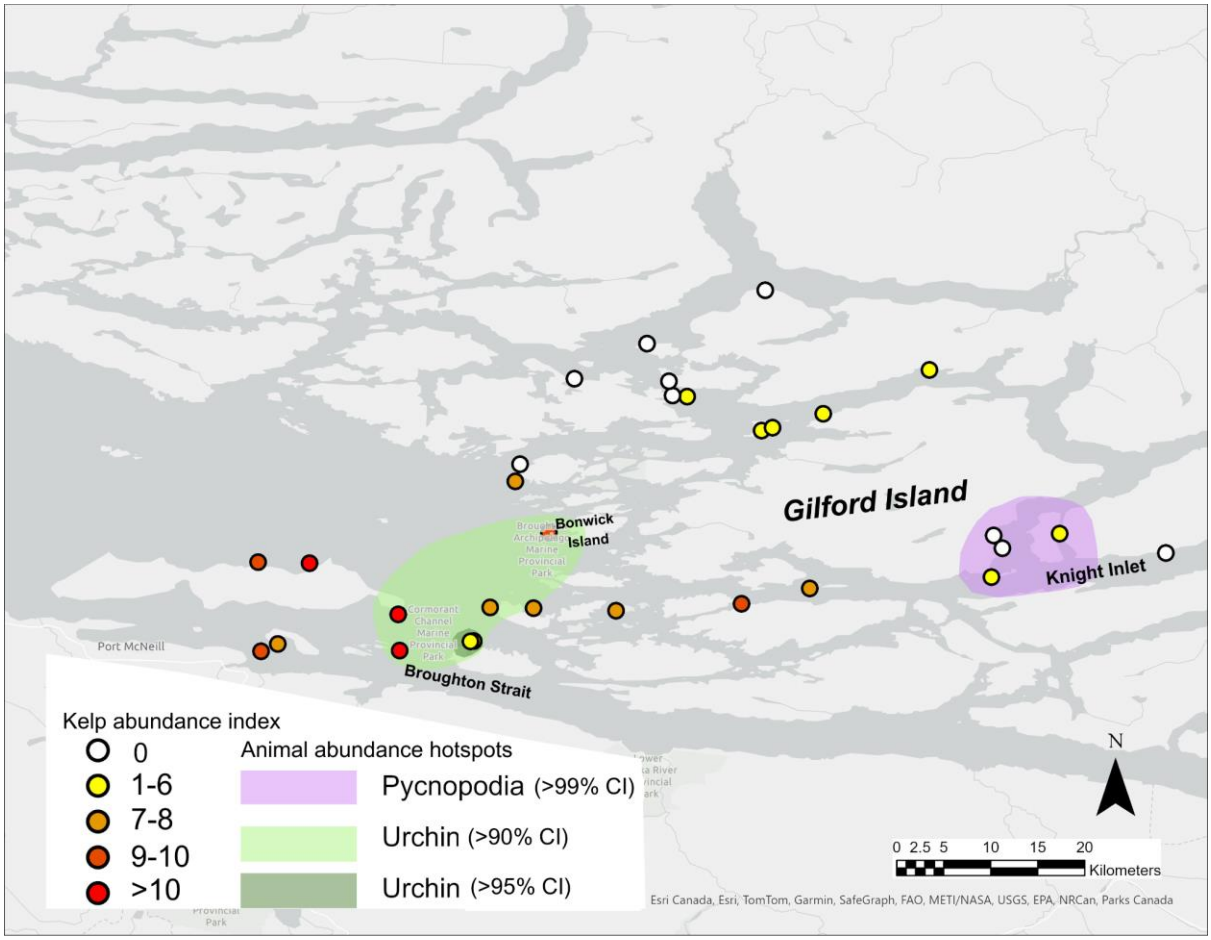

Fig. 6: Map showing the kelp abundance index, and the hotspots of urchins and Pycnopodia *across sites as determined by the GI* statistic. Hotspots are visually indicated as ellipses drawn over sites identified as hotspots ("concentric hotspots") with >95% confidence ($p<0.05$) and with >90% confidence ($p>0.1$). There are two concentric hotspot ellipses for urchins, with pale green denoting sites with 90% confidence ($p<0.1$), and dark green denoting sites with >95% confidence ($p<0.05$). There is only one concentric hotspot for* Pycnopodia*, which has >99% confidence.*

2.5 Discussion

This study characterized kelp distribution and abundance across the Broughton Archipelago, a ~5,000 km^2 archipelago-fjord system with a large environmental gradient, including differences in SST, salinity, bottom slope, and tidal current speeds, and differences in sea urchin and *Pycnopodia* abundance. This was achieved with a survey of 31 sites, where we mapped the floating kelp with UAV and satellite imagery, obtained environmental data with a CTD, an optical profiler, and environmental models, and investigated biotic conditions with an underwater ROV. A clustering analysis was conducted to identify two distinct environmental subregions. Next, two linear models

and one GLM were fitted to identify the relationships between environmental and biotic variables with kelp distribution and abundance. Additionally, hotspot analyses were conducted to identify spatial patterns of urchin and *Pycnopodia* abundances. We found an environmental gradient represented by two contrasting subregions, the archipelago subregion and the fjord subregion. The archipelago subregion was characterized by lower SST, higher tidal current speeds, and flatter bottom slopes than the fjord subregion, providing more favorable conditions for widespread kelp distribution and higher kelp abundance. Due to the sampling design, only the fjord subregion had non-kelp sites, and the non-kelp sites had higher stratification indices than the fjord kelp sites. There were no significant differences in urchin and *Pycnopodia* abundances between the two subregions, and urchin and *Pycnopodia* abundance did not significantly relate to kelp distribution or abundance. However, the spatial hotspot analyses revealed urchin abundance hotspots within the archipelago subregion and a *Pycnopodia* hotspot within the fjord subregion, though neither hotspot spanned the entirety of their respective subregions. These results and their implications are discussed below.

2.5.1 Environmental drivers of spatial differences in kelp distribution and abundance

Significantly higher kelp abundance (including all kelp metrics: classified kelp area, kelp bed area, kelp bed density, and kelp abundance index) was observed in the archipelago subregion than the fjord subregion, associated with lower SST, higher tidal current speeds, and flatter slopes *(Fig. 4A).* These environmental conditions likely benefited kelp physiology and growth (Supratya et al., 2020; Dean & Jacobsen, 1984). Kelps generally prefer cooler waters, with *Nereocystis* experiencing maximum growth at 12°C (Supratya et al., 2020; Pontier et al., 2024), and temperatures exceeding ~12.0°C-18.0°C can be detrimental to *Nereocystis* sporophyte growth (Korabik et al., 2023) and kelp gametophyte survival (Weigel et al., 2023). Note that these thermal limit ranges are wide, as these physiological limits differ between kelp species, life stages, and specific populations. For example, *Macrocystis* has a thermal optimum of ~12.0-17.0°C (Lüning & Neushul, 1978), and *Nereocystis* has a lower thermal limit in Central BC (~12.0°C) than in California (~16°C) (Pontier et al., 2024;

Korabik et al., 2023; Weigel et al., 2023). Regardless, the cooler waters of the archipelago subregion (mean SST: 9.95±0.583°C) may act as a thermal refuge for kelps, and the warmer waters of the fjord subregion (mean SST: 14.3±2.48 °C, four sites with SST between 16.8°C and 20.1°C) may hinder kelp growth, development, and survival (Supratya et al., 2020; Korabik et al., 2023; Weigel et al., 2023). High flow conditions (e.g. high tidal current speeds) found in the archipelago subregion can increase kelps' thermal tolerance and plasticity (Supratya et al., 2020) and are typically associated with higher nutrient levels and encourage kelps' nutrient uptake, a key factor benefiting kelp growth (Berry et al., 2021; Dean & Jacobsen, 1984). Besides presenting more optimal ocean temperature conditions for kelp development, the archipelago subregion also had flatter slopes (4.83±3.47°) spanning shallower depths (6.90±4.04 m) where kelp could grow across larger areas of relatively shallow photic zones and reach higher abundances compared with the fjord subregion (mean slope: 17.5±9.57°, depths: 23.4±18.2 m). The mean depth of the sites in the fjord subregion was deeper than 20 m, a depth threshold beyond which kelps are unlikely to grow in BC (Nijland et al., 2019; Gendall et al., 2023). Gendall et al. (2023) found that areas with steeper slopes (> 11.3%/6.45°) could only support smaller kelp beds (<17,000 m^2), an observation that our findings in the fjord subregion reinforce (mean kelp bed area of ~13,100 m^2).

Salinity, fetch, percent PAR, and stratification index were excluded from the linear model during the AIC-based model selection process but may also drive kelp distribution and abundance. The fjord subregion had lower salinity, fetch, percent PAR, and higher stratification indices than the archipelago subregion (values in *Table A3)*. Lower salinity can reduce kelps' growth rates and induce blistering or bleaching (Li et al., 2020; Vettori et al., 2020), with salinities <26.0 PSU being detrimental to *Nereocystis* spore settlement (Lind & Konar, 2017). Higher water column stratification reduces nutrient distribution throughout the water column, negatively affecting kelps' nutrient uptake (Hollarsmith et al., 2022). Thus, the lower salinity and higher stratification in the fjord subregion may be detrimental for kelps. Conversely, lower fetch, which served as a proxy for shoreline exposure (Gregr et al., 2018, 2019), may not inherently be unfavorable to kelp, as *Nereocystis* can be found anywhere on protected to exposed shorelines (Springer et al., 2010). Indeed, high fetch may be detrimental to kelps, as high wave exposure can lead to kelp blade breakage (Simonson et al., 2015).

Rather, low fetch in the fjord subregion may be associated with lower kelp abundance primarily because of its negative correlation with temperatures and slope, and the positive correlation with salinity in this region.

Similarly, the percent PAR in the fjord subregion, despite being lower than that in the archipelago subregion, may not necessarily have been limiting for kelps. An ancillary examination of the absolute PAR values revealed no significant differences in absolute PAR values between the subregions regardless of depth *(Table A9)*. Furthermore, our measured absolute PAR only occasionally dropped below the optimal PAR threshold for *Nereocystis* (2.13 mol photons m^{-2} day^{-1}) defined in lab experiments (Vadas, 1972). In our measurements, at 5 m depth, only six *Nereocystis* sites in the archipelago subregion (1.29±0.48 mol photons m^{-2} day^{-1}, *Table A9)* and five *Nereocystis* sites in the fjord subregion **(**1.11±0.57 mol photons m^{-2} day^{-1}**,** *Table A9***)** had absolute PAR below *Nereocystis'* optimal PAR threshold (<2.13 mol photons m^{-2} day^{-1}). We did not find any *Macrocystis* sites where absolute PAR at 5 m (3.88±3.08 mol photons m^{-2} day^{-1}) dropped below the optimal PAR threshold for *Macrocystis* (1.00 mol photons m^{-2} day^{-1}) (Dean & Jacobsen, 1984; Tait et al., 2019). Note that these absolute PAR values are instantaneous measurements of the light field that likely varied depending on different illumination conditions and water turbidity, whereas the kelp PAR thresholds identified in the literature were derived from long-term averages. Due to the variable nature of absolute PAR measurements, we only used percent PAR values in the analyses, which were less sensitive to variation in illumination conditions and served mainly as a metric of light attenuation and water turbidity (Loos et al., 2017). High water turbidity in the fjord subregion is likely due to variables not measured in this study such as the high sedimentation rate from glacial runoff (Hodson et al., 2004) in this subregion (Giesbrecht et al., 2022). Physical disruption by sediments can be disadvantageous for kelp growth (Lind & Konar, 2017; Tait et al., 2019), potentially explaining the significantly lower kelp abundance in the fjord subregion when compared to the archipelago subregion.

The observed spatial pattern of lower kelp abundances in the fjord subregion than in the archipelago subregion corroborates those observed in other temperate coastal fjords in Alaska (Traiger & Konar, 2018), BC (Starko et al., 2022, 2024a; Mora-Soto et al., 2024b; Gendall et al. 2023,

submitted), southern Chile (Dayton, 1985; Huovinen et al., 2019; Mora-Soto et al., 2021), and the Nordic region (Kvile et al., 2022)**.** For example, Mora-Soto et al. (2024b) found relatively small kelp areas in the warmer, more sheltered Saanich Inlet, a non-glacially-fed coastal fjord in coastal BC, but documented higher kelp abundance in the cooler, more exposed coastlines adjacent to the inlet. Similarly, Huovinen et al. (2019) found the lowest kelp abundance near the turbid river mouth of the Yendegaia Fjord in Southern Chilean Patagonia, increasing towards the more oceanic Beagle Channel. This is due to the spatially distinct environmental and bathymetric gradients that are typical of these coastal fjord systems, with warmer, less saline, and more protected waters being less favorable for kelp, and the cooler, more saline, and more dynamic waters in the more oceanic areas (the archipelago subregion in our case) being more favorable for kelp.

2.5.2 Characterize the effects of grazer and predator abundances on the distribution and abundance of kelp

The distribution and abundance of grazer (sea urchins) and predator (*Pycnopodia*) populations did not significantly relate to kelp distribution and abundance (Tweedie GLM: R^2 =0.508, urchin = p=0.178, *Pycnopodia*: p=0.709); nonetheless, there were spatial patterns of urchin and *Pycnopodia* abundances identified in the hotspot analysis that coincided with the spatial patterns of kelp abundance. Interestingly, sea urchin abundance hotspots were located within the archipelago subregion where kelp was more abundant, and the *Pycnopodia* abundance hotspot was located within the fjord subregion *(Fig. 6)*. This pattern of higher sea urchin and kelp abundances, and lower *Pycnopodia* abundance in the archipelago subregion is noteworthy, as other coastal regions of the Northeast Pacific (Monterey Bay, California, and Barkley Sound and Central Coast of BC) have experienced the proliferation of urchin barrens in the absence of *Pycnopodia* predation, ultimately leading to the extirpation of kelp forests (Selgrath et al., 2024; Starko et al., 2022; Burt et al., 2018).

We hypothesize that kelps and urchins coexisted in the archipelago subregion because the urchin density observed in our study may be lower than the threshold urchin densities needed to initiate a phase shift from kelp forest to urchin barren (~8.2–14.0 urchins m^{-2}) (Filbee-Dexter &

Scheibling, 2014; Ling et al., 2015; Rogers-Bennett & Catton, 2019). This lower urchin abundance likely resulted in lower grazing pressure on kelp. However, we can only hypothesize and not definitively conclude that the urchin abundances in the archipelago subregion (3.09±5.46 urchins/image) were lower than those found in other regions' urchin barrens, as it is challenging to directly compare urchin numbers derived from our ROV methods with urchin numbers derived from the fixed diver transects often used in other studies such as Eisaguirre et al. (2020) and Starko et al. (2022).

Assuming that the urchin abundances in our archipelago subregion were indeed below the urchin density threshold needed to cause a phase shift from kelp forest to urchin barren, there are many potential reasons that a relatively higher abundance of urchins was found in the archipelago subregion than the fjord subregion. Kelps serve as a food source for urchins, who consume drift kelp instead of standing kelp when there is a sufficient supply of drift kelp to sustain the urchins (Kriegisch et al., 2019), allowing urchins and kelp to exist in a stable state (Kriegisch et al., 2019). As the archipelago subregion had a higher abundance of kelps than the fjord subregion, it likely can sustain the present abundance of urchins. Since urchin herbivory rates were not high enough to decimate the kelps, there may be other forms of population control for the urchins, even in the absence of *Pycnopodia*, such as physical disturbance and other predators not accounted for in this study (Cowen et al., 1982; Steneck & Johnson, 2013; Watson & Estes, 2011). Winter storms, waves, and the sweeping motion of kelp blades can cause sea urchins to retreat, easing the grazing pressure on kelps (Konar & Estes, 2003). Moreover, sea otters are slowly returning to the archipelago subregion (SCFS, 2023a), however, their potential population control of sea urchins in the region has not yet been documented. Furthermore, *Nereocystis'* opportunistic quality and ability to thrive under disturbance (Dayton et al., 1984; Springer et al., 2010) may be another reason for kelp-urchin coexistence. In a nearly 200-year time series of kelp forests in Monterey Bay, California, Selgrath et al. (2024) found that *Nereocystis* could persist even in high urchin densities, contrasting with perennial species (e.g. *Macrocystis*), which only reached high kelp abundances when urchin densities were low. Indeed, the patterns found in the archipelago subregion corroborate this, with the three sites with *Macrocystis* having no urchins and the ten *Nereocystis* sites having 4.02 ± 5.97 urchins/image.

In contrast, *Pycnopodia* abundance was higher in the fjord subregion, where both kelp and urchin abundances were lower than in the archipelago subregion. *Pycnopodia's* negative association with urchin abundance (Kruskal-Wallis test: $\chi 2 = 5.94$, $p=0.0148$) may be associated with *Pycnopodia's* predation of urchins (Burt et al., 2018; Galloway et al., 2023). Interestingly, the location of the *Pycnopodia* abundance hotspot in the warmer fjord subregion was unexpected, as *Pycnopodia* mortality tends to increase in warmer waters (Harvell et al., 2019; Hamilton et al., 2021) due to a higher likelihood of sea-star wasting disease (SSWD) spreading through the population (Harvell et al., 2019; Hamilton et al., 2021). However, our observed spatial pattern of *Pycnopodia* abundance is not completely novel, as Hamilton et al. (2021) and Gehman et al. (submitted) also documented higher abundances of *Pycnopodia* in BC Central Coast fjords when compared to the more oceanic islands nearby. Coastal fjords connected to the BC mainland can experience Arctic outflow wind events that can create a cooler, salty, and high-oxygen water mass under the stratifying freshet layer (Bianucci et al., 2023; Gehman et al., submitted; MacNeill, 1974). As *Pycnopodia* and other sea stars generally prefer higher salinities (>15.0 PSU) (Hemery et al., 2016; Held & Harley, 2009), the surface freshet layer drives *Pycnopodia* into cooler, more saline, and more oxygenated waters in the deep (Gehman et al., submitted). Gehman et al. (submitted) hypothesized that these cooler waters below the *Pycnopodia* thermal threshold of 14°C (Bonaviri et al., 2017) slow the rate at which SSWD spreads through the *Pycnopodia* population, increasing their chances of survival, whereas *Pycnopodia* experienced higher mortality in the nearby outer islands, where there was no surface freshet layer.

As expected, we found higher water column stratification (A: 0.414±0.848 kg m^{-3}, F: 5.10±4.37 kg m^{-3}) in the fjord subregion than the archipelago subregion of the Broughton. In the fjord subregion, benthic water temperature was lower (10.4±0.762°C), and benthic salinity was higher (27.2±2.78 PSU) than surface measurements (temperature: 14.3±2.47°C, salinity: 19.6±5.12 PSU). These benthic measurements were also below the *Pycnopodia* upper thermal limit (14°C, Bonaviri et al., 2017) and above sea stars' lower salinity limit (~15.0 PSU, Held & Harley, 2009). Therefore, an alternate explanation for the *Pycnopodia* abundance hotspot's location in the fjord subregion may be that the fjord subregion serves as a better refuge from SSWD for *Pycnopodia* than the archipelago

subregion, corroborating Gehman et al.'s (submitted) hypothesis. Moreover, we can postulate that the negative association between urchins and *Pycnopodia* abundance may not solely be due to *Pycnopodia* predation on sea urchins. Rather, *Pycnopodia* may be unable to get to the archipelago subregion where the sea urchins are abundant due to SSWD-imposed limits and are instead subsisting on other invertebrates in the fjord subregion *(Fig. 7)*. *Pycnopodia* also feed on other invertebrates including but not limited to gastropods, mussels, and bivalves (Duggins, 1983) that were not included in this study, warranting more investigation in future studies.

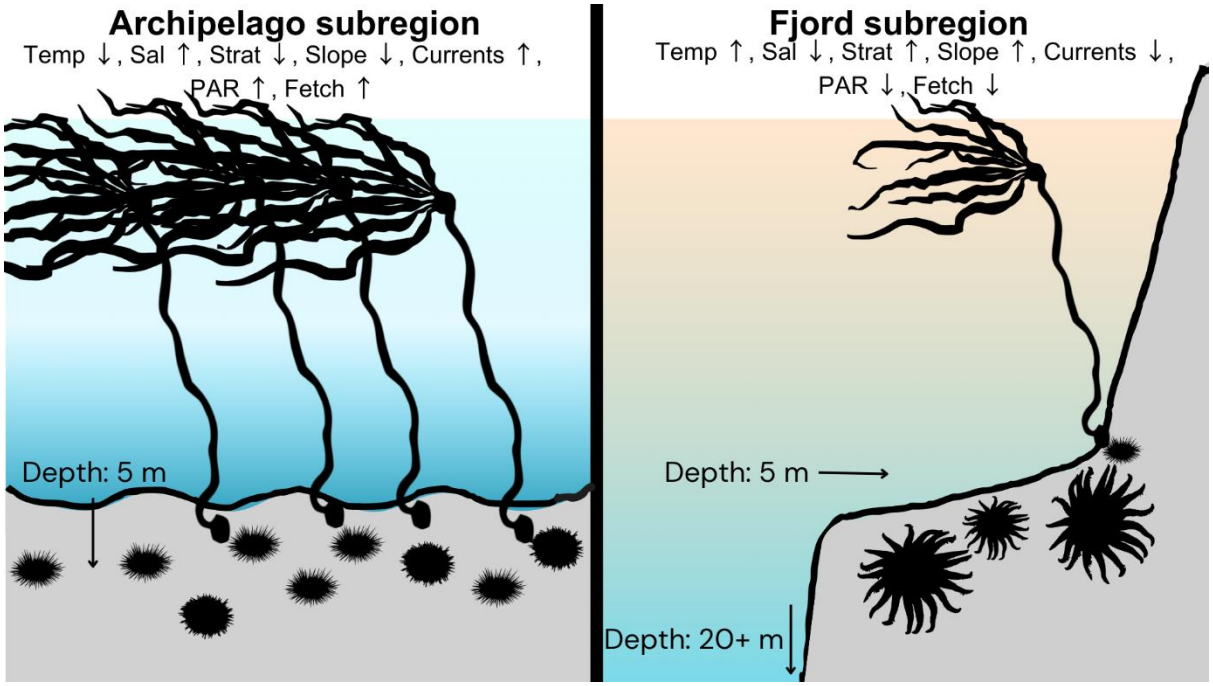

Fig. 7: A schematic showing the environmental and biotic conditions at the archipelago subregion (left panel) and fjord subregion (right panel). The archipelago subregion had cooler waters (represented by symbol Temp ↓), higher salinities (Sal ↑), lower stratification (Strat ↓), flatter slopes (Slope ↓), higher tidal current speeds (Currents ↑), higher PAR (PAR ↑), higher fetch (Fetch ↑), and higher abundances of urchins, although the urchins are not prevalent throughout the entire subregion. The fjord subregion had warmer temperatures (Temp ↑), lower salinities (Sal ↓), higher stratification (Strat ↑), steeper slopes (Slope ↑), lower tidal current speeds (Currents ↓), lower PAR (PAR ↓), lower fetch (Fetch ↓), and higher abundances of Pycnopodia*, although the* Pycnopodia *were not commonplace throughout the whole fjord subregion. All* Nereocystis*, sea urchins, and* Pycnopodia *graphics were taken from phylopic.org, and the* Nereocystis *graphic was further edited (CC0 1.0 Universal Public Domain Dedication license.)*

2.5.3 Limitations and Future Directions

The limitations of this study include the short duration of the field sampling efforts and the methodological trade-offs of using a UAV and ROV instead of more traditional kayak or diver-based methods. Kelp forests are dynamic ecosystems (Steneck & Johnson, 2013)**,** and this study solely characterized kelp distribution, abundance, and the associated environmental and biotic conditions during the summer of 2023. Thus, our observed results and patterns may not be representative of conditions during other seasons or years. However, our study's summer timing captured kelp at peak canopy height (Springer et al., 2010), similar to the timing of other studies on kelp dynamics from BC (e.g. Schroeder et al., 2019; Starko et al., 2022; Mora-Soto et al., 2024a, 2024b; Gendall et al., submitted)**,** ensuring comparability between the findings**.** Future work should include long-term monitoring of kelp and an expanded suite of environmental and biotic conditions, such as nutrient content (Hollarsmith et al., 2022), which may further elucidate the temporal dynamics of kelp forest communities in the Broughton Archipelago.

Moreover, potential limitations or biases lie in the methods for deriving kelp abundance, mainly due to technical limitations. For instance, in this study, we attempted to map all the kelp present at each site after defining the boundaries of suitable kelp habitat from bathymetry and substrate type. However, in some sites, it was challenging to map the entire extent of the large kelp beds during the limited low tide window, resulting in some variation in the survey limits, possibly affecting the values of the classified kelp area metric. This was mitigated by creating the kelp abundance index, which considered both the classified kelp area and the kelp bed area, with the linearization from the log transformation lessening the impact of extreme values. This index and the kelp bed density metric were used in statistical models instead of the classified kelp area, which would have been more affected by the variable survey area limits.

Furthermore, the multispectral imagery used in this survey can only detect canopy-forming kelps *(Nereocystis* and *Macrocystis)* that reach the water surface, missing the subsurface kelps that may still provide habitat for kelp forest biota. Although other spectral bands available on UAV and satellite imagery can detect kelps slightly underneath the surface (such as RGB true-color combinations or spectral indices involving the red-edge band), their detection abilities vary based on

the water turbidity and the bottom depth (Timmer et al., 2022). These spectral bands may also detect understory kelps such as *Pterygophora californica*, which may be misclassified as *Nereocystis* and *Macrocystis* (Timmer et al., 2024). Thus, the limitation of only detecting surface kelps can be viewed as a trade-off for the benefit of kelp detection consistency. Moreover, the use of UAVs and satellite imagery allowed us to define kelp bed areas over relatively large spatial scales, which may not have been feasible with kayak or diver-based surveys. Ultimately, the use of multispectral UAV and satellite imagery in defining floating kelp areas has been well-established in many places, including BC (e.g. Nijland et al., 2019; Timmer et al., 2022, 2024; Thompson, 2021; Gendall et al., 2023, submitted; Mora-Soto et al., 2024a, 2024b), Oregon (Hamilton et al., 2020), Washington (Cowdrey, 2021; Cowdrey & Claar, 2024), and California (Saccomanno et al., 2023).

Similarly, there are trade-offs to using ROVs to derive biotic data compared to more traditional and standardized methods like quadrats and SCUBA surveys. ROVs, like other underwater video methods, miss organisms that may be hidden under understory macroalgae (Buscher et al., 2020). However, our survey targets (sea urchins and *Pycnopodia)* are large and conspicuous, making them easy to detect from the ROV video still images. Our ROV also occasionally faced navigational difficulties in kelp forests, leading to a few ROV surveys being cut short and resulting in variability in survey lengths. Potential variation stemming from different survey lengths was accounted for by splitting each ROV survey into still images and dividing the total counts of each organism by the number of images in each survey to provide a metric of abundance. Moreover, the ROV had no geolocation capabilities, and therefore, it was challenging to acquire measurements of distance or area from the images. This could have led to potential biases associated with the variability of the seafloor area covered in each image. The accuracy of the species abundance information derived from the ROV surveys could be improved in the future by incorporating ROV-tracking capabilities, which would allow the calculation of the area surveyed (Randell et al., 2023). To minimize variability in the seafloor covered in each image, we conducted a visual verification to confirm similar variability in the area covered in each image among the sites. Thus, a more accurate quantification of the area covered by each image would improve the accuracy of sea urchin and *Pycnopodia* abundance calculations but would not necessarily change the patterns described.

2.6 Conclusions

This study presented the first spatial characterization of kelp distribution and abundance and its associated environmental and biotic drivers across an environmental gradient in the Broughton Archipelago, BC, Canada. Kelp distribution and abundance spatially varied across this environmental gradient, with cool waters, flat seafloors, and high tidal current speeds related to higher kelp abundances in the archipelago subregion, and warmer waters, steep seafloors, and lower tidal current speed related to lower kelp abundance in the fjord subregion. Biotic conditions, specifically urchin and *Pycnopodia* distribution and abundance, also displayed distinct spatial distribution patterns but were not directly related to kelp distribution and abundance. These results reinforce other research on the interactions between the environment and kelps and provide additional insight into kelp-urchin-*Pycnopodia* relationships.

With climate change and its effects on the ocean (Krumhansl et al., 2016; Wernberg et al., 2019; Smale et al., 2020; Filbee-Dexter et al., 2024), *Pycnopodia* declines (Rogers-Bennett & Catton, 2019; Gregr et al., 2020), and the proliferation of urchin barrens (Rogers-Bennett & Catton, 2019; Eisaguirre et al., 2020) being associated with the declines of kelp forests, a nuanced understanding of the environmental and biotic drivers of kelp distribution and abundance is of paramount importance. Moreover, with complex, fjord-laden coastlines representing a large proportion of global kelp habitat (Jayathilake & Costello, 2021), a fine-scale understanding of kelp distribution and abundance across coastal fjord systems is crucial. Ultimately, our study indicates the environmental and biotic drivers of kelp distribution and abundance across a coastal archipelago-fjord system, the results of which can inform biomonitoring and ecosystem-based management efforts (e.g. kelp harvest and restoration) in kelp forest systems on local and regional scales.

3.0 Kelp forests display persistence in the dynamic region of the Broughton Archipelago, British Columbia, Canada

3.1 Abstract

Canopy-forming kelp forests act as foundation species that provide a wide range of ecosystem services along temperate coastlines. With climate change, these ecosystems are experiencing changing environmental and biotic conditions; however, the kelp distribution and drivers of change in British Columbia remain largely unexplored. This research aims to use satellite imagery and environmental data to investigate the spatiotemporal persistence and resilience of kelp forests in a dynamic subregion of cool ocean temperatures and high kelp abundance in the Broughton Archipelago, British Columbia. The specific objectives were to identify: 1) long-term (1984 to 2023) and short-term (2016 to 2023) kelp responses to environmental changes; and 2) spatial patterns of kelp persistence. The long-term time series was divided into three climate periods: 1984 to 1998, 1999 to 2014, and 2014 to 2023. The first transition between these periods represented a shift into cooler regional sea-surface temperatures and a negative Pacific Decadal Oscillation in 1999. The second transition represented a change into warmer temperatures (with more marine heatwaves and El Niño conditions) after 2014. In the long-term time series (1984 to 2023), which covered a site with *Macrocystis pyrifera* beds, kelp area increased slightly after the start of the second climate period in 1999. For the short-term time series (2016 to 2023), which focused on eight sites with *Nereocystis luetkeana* beds, most sites either did not change significantly or expanded in kelp area. This suggests that kelp areas remained persistent across these periods despite showing interannual variability. Thus, the dynamic subregion of the Broughton Archipelago may be a climate refuge for kelps, likely due to cool water temperatures that remain below both species' upper thermal limits. Spatially, on a bed level, both species were more persistent in the center of the kelp beds, but across the subregion, *Macrocystis* had more persistent areas than *Nereocystis*, suggesting life history and/or other factors may be impacting these kelp beds differently. These findings demonstrate the spatiotemporal persistence of kelp forests in the dynamic subregion of the Broughton Archipelago, informing the management of kelp forest ecosystems by First Nations and local communities.

3.2 Introduction

Canopy-forming kelp forests (order Laminariales) are key habitats in temperate marine regions globally (Jayathilake & Costello, 2021) and are vulnerable to climate change impacts (Reed et al., 2016; Smale, 2020; Wernberg et al., 2024), which can potentially disrupt ecosystem functions, such as habitat provision, fisheries production, nutrient cycling, carbon sequestration, and cultural value (Lamy et al., 2020; Eger et al., 2023; Turner, 2001). Kelp distribution and extent are affected by changes in environmental and biotic conditions, including ocean temperature, salinity, exposure, light, nutrient availability, and the abundance of kelp grazers and predators (Jayathilake & Costello, 2021; Springer et al., 2010; Druehl, 1977; Traiger & Konar, 2018; Hollarsmith et al., 2022; Starko et al., 2024a). These conditions are often closely related to temperature in region-specific ways; for example, in the Northeast Pacific Ocean, warmer waters can correlate with lower salinities (Druehl, 1977), poor nutrient availability (Lowman et al., 2022), and ecological regime shifts (Burt et al., 2018; Hamilton et al., 2021). Furthermore, studies have shown how ocean temperatures directly or indirectly drive kelp dynamics (e.g. Jayathilake & Costello, 2021; Gonzalez-Aragon et al., 2024; Hamilton et al., 2020; Bell et al., 2020; Starko et al., 2022; Mora-Soto et al., 2024a, 2024b; Gendall et al., submitted).

In the Northeast Pacific Ocean, temperature changes can occur at variable time scales, from steady long-term trends or cyclic changes spanning decades or years to short-term marine heatwaves, affecting the kelp dynamics differently (Cavanaugh et al., 2011; Krumhansl et al., 2016; Levitus et al., 2000; Mora-Soto et al., 2024a; Smith et al., 2024; Wernberg et al., 2024). Long-term increases in ocean temperatures are primarily driven by anthropogenic climate change (Cheng et al., 2022) and can drive changes in kelp distribution and area (Beas-Luna et al., 2020; Berry et al., 2021; Mora-Soto et al., 2024a). For instance, Berry et al. (2021) documented a shift in kelp distribution and a 63% decrease in its area alongside a 0.7°C sea-surface temperature (SST) increase throughout the 20th century in Puget Sound, Washington. Additionally, ocean temperatures are influenced by cyclic climatic oscillations (Di Lorenzo et al., 2008), such as the El Niño Southern Oscillation (ENSO)

(quantified with the Oceanic Niño Index, ONI) and the Pacific Decadal Oscillation (PDO), which are multi-year and decadal modes of climate variability (Di Lorenzo et al., 2008). These oscillations often lead to warming in the Northeast Pacific Ocean when in a positive phase (Di Lorenzo & Mantua, 2016), with consequent changes in kelp responses. For instance, kelp areas decreased after shifting to positive PDO and ONI but rebounded after the oscillations shifted to negative phases in the Strait of Juan de Fuca (Pfister et al., 2018) and the Strait of Georgia (Mora-Soto et al., 2024a); conversely, kelp disappeared after a positive PDO shift in the 1970s and did not rebound afterward in Gray Bay, Haida Gwaii (Gendall et al., submitted).

Furthermore, ocean temperature change can also manifest in the form of short-term marine heat waves (MHWs), which are anomalously warm events (>5 days) with temperatures more than 90th percentile based on a 30-year climatological baseline (Hobday et al., 2016). A higher frequency and magnitude of MHWs have been observed due to climate change (Frölicher et al., 2018) and are generally associated with positive PDO and ONI years (Di Lorenzo & Mantua, 2016), resulting in prolonged, anomalously warm conditions (Bond et al., 2015). Such conditions were present during the Blob of 2014 to 2016, a prolonged MHW (Bond et al., 2015) that devastated kelp forests across the Northeast Pacific Ocean (Bell et al., 2023; Arafeh-Dalmau et al., 2019; Starko et al., 2022, 2024a; Mora-Soto et al., 2024a, 2024b; Gendall et al., submitted). Kelp was reduced after the Blob to 60% of its pre-Blob distribution in Barkley Sound (Starko et al., 2022), to 21% of its pre-Blob distribution in the Northern Salish Sea (Mora-Soto et al. 2024b), and to 13% of its historical area in Haida Gwaii (Gendall et al., submitted).

Kelp forest persistence and resilience to ocean warming and climatic oscillations can be characterized in temporal and spatial domains. In this context, persistence refers to the continued existence of kelp forests through time (Connell & Sousa, 1983), and resilience refers to kelps returning to a reference state after a disturbance, such as thermal stress periods (Holling, 1973). Some studies consider kelp persistence and resilience in the temporal domain, including increasing, decreasing, or no change in kelp areas within a specific study site or region (e.g. Cavanaugh et al., 2019; Mora-Soto et al., 2024a, 2024b; Gendall et al., submitted, etc.). Other studies investigate kelp persistence and resilience in the spatial domain, i.e., identifying areas where kelp is often present.

(e.g. Schroeder et al., 2020; Hamilton et al., 2020; Cavanaugh et al., 2023; Arafeh-Dalmau et al., 2023). Currently, kelp forests are declining globally (Krumhansl et al., 2016), however, their persistence and resilience to climate change have been spatially variable, with decreases in 38% of the regions, increases in 27% of regions, and no change in 35% of regions (Krumhansl et al., 2016). This variability in persistence and resilience is often due to spatially explicit patterns in environmental and biotic conditions (Smale, 2020; Bell et al., 2023; Starko et al.,2024a), which can influence the amount of stress the kelps directly experience, as well as have implications for adaptation and ecosystem-scale responses to stressors (Starko et al., 2024b). For instance, kelp areas are expanding in the Arctic due to the increase in ice-free areas (Filbee-Dexter et al., 2019), and conversely, are diminishing in subtropical latitudes such as in Baja California due to the increase in ocean temperatures (Cavanaugh et al., 2019; Beas-Luna et al., 2020; Bell et al., 2023). Beyond global-scale variability, this spatially driven variation in kelp persistence and resilience can be observed at a regional scale in British Columbia (BC), Canada. Kelp areas are increasing on the northwest coast of Vancouver Island where keystone predators (sea otters) have returned (Watson & Estes, 2011; Starko et al. 2024a), and displaying no change in area in the cooler waters of the Strait of Juan de Fuca (Mora-Soto et al., 2024a). Conversely, kelp areas decreased in the warmer waters of the central Gulf Islands and Northern Salish Sea (Mora-Soto et al., 2024a, 2024b). This spatial variation in kelp responses can also be found on local scales (a few kilometers or less), with kelps persisting on the cooler outer coasts and displaying loss in the warmer inlets, for instance, in Barkley Sound and around the Gray Bay and Cumshewa Inlet region of Haida Gwaii (Starko et al., 2022; Gendall et al., submitted). As such, local-scale studies are needed to understand the response of kelp to environmental conditions.

Canopy-forming kelp species such as *Macrocystis pyrifera* and *Nereocystis luetkeana* can be present at the ocean surface and have biomass that is detectable by optical remote sensing tools, equipping researchers with the ability to survey kelp across large spatial and temporal scales (Stekoll et al., 2006; Cavanaugh et al., 2011, 2019; Bell et al., 2015; Schroeder et al., 2019, 2020; Nijland et al., 2019; Mora-Soto et al., 2020, 2024a, 2024b; Gendall et al., 2023, submitted). Mid-resolution satellite imagery such as Landsat (spatial resolution: 30 to 80 m), available since 1972 (NASA, n.d.), allows for creating a longer time series of large kelp beds (Cavanaugh et al., 2011; Bell et al., 2020;

Gendall et al., 2023). This enables researchers to differentiate kelps' interannual variability from monotonic trends (Reed et al., 2015; Wernberg et al., 2019) and establish a more historical and accurate baseline of kelp areas (Bell et al., 2023; Gendall et al., submitted; Mora Soto et al., 2024a). On the other hand, high-resolution satellite imagery such as Rapideye (5 m), Planetscope (3 m), and Quickbird-2 (1.84 m), allows for better accuracy when mapping fringing and smaller kelp beds (e.g., Gendall et al., 2023; Mora-Soto et al., 2024a), although their temporal coverage and resolution are more limited (Rapideye: 2009 to 2020, Planetscope: 2016 to present, Quickbird-2: 2001 to 2015) (Planet, 2024 ; ESA, n.d, a .; ESA, n.d., b). This difference in data sources results in a trade-off between spatial resolution, the ability to detect smaller kelp beds (Gendall et al., 2023), and the length of the time series. Due to the range of kelp bed sizes present on the BC coast, from large offshore beds to small fringing beds, utilizing satellite imagery of different spatial and temporal resolutions improves our ability to uncover temporal trends and identify areas of persistence and/or resilience in kelp beds of various sizes and distribution (e.g., Gendall et al., 2023, Mora-Soto et al., 2024a).

Here, we use satellite imagery to define the persistence and resilience of kelp forests to environmental changes in the dynamic subregion of the Broughton Archipelago, BC, Canada. The dynamic subregion is characterized by cool water temperatures, relatively flat bottom slopes, high seawater salinity, exposure, and tidal current speeds (Ch. 2; Foreman et al., 2009; Brewer-Dalton et al., 2014; Lin & Bianucci, 2023). Specifically, this study addresses the following two objectives: 1) to identify the temporal responses of *Macrocystis pyrifera* and *Nereocystis luetkeana*, respectively, to changes in temperature and climatic oscillations, and 2) to identify spatial patterns of kelp persistence. We achieved these objectives by first characterizing environmental conditions in the Broughton Archipelago across various spatial scales with 1) local SST climatologies from temporally discontinuous Landsat data, 2) regional SST and MHW climatologies from temporally continuous in-situ measurements, and 3) global ONI and PDO indices. Next, we identified kelp persistence and resilience at one *Macrocystis* site (time series length: 1984 to 2023) and eight *Nereocystis* sites (time series length: 2016 to 2023) and compared them to the environmental changes. In this study, kelp persistence is quantified in two domains: (1) temporal persistence corresponding to an increase or no

significant change in kelp area at the site level throughout the studied time series, and (2) spatial persistence corresponding to the existence of persistent areas inside each site where kelp was present >50% of the time series. Conversely, non-persistence is defined as (1) a temporal decrease in kelp and/or (2) spatially, the lack of any persistent area. Synthesizing both spatial and temporal domains, a kelp forest would be deemed resilient if the system experienced a disturbance and yet still displayed both temporal and spatial persistence. If the kelp forest displayed both spatial and temporal persistence but did not experience any disturbance, evaluating its resilience would not be possible. This study synthesizes both spatial and temporal domains to provide valuable information about the status of the kelp forests and their responses to environmental variability to the local First Nations and their monitoring efforts. At a broader spatial scale, this study also contributes to regional and global endeavors to understand the status and responses of kelp forests during an era of unprecedented climate change.

3.3 Methods

3.3.1 Study area

This study was conducted on the traditional and unceded territories of the Kwakwa̱ka̱'wakw peoples (Umista Cultural Society, n.d.) within the Broughton Archipelago. This region sits at the interface of two major bodies of water: the Johnstone Strait and Queen Charlotte Strait, near the northeast of Vancouver Island, BC, Canada *(Fig. 8)*. The Broughton Archipelago features many islands in the west and glacially carved fjords in the east (Shugar et al., 2014; Davies et al., 2018). Due to its strong environmental gradient in seawater temperature and clear differences in bathymetry, this region can be distinctly divided into two subregions: the cooler, dynamic western archipelago, and the warmer, sheltered, eastern fjords (Ch. 2; Foreman et al., 2009; Brewer-Dalton et al., 2014; Lin & Bianucci, 2023). This environmental gradient and spatial differences in bathymetry drives kelp abundance, with the larger and denser kelp beds that can be detected with satellite imagery only located in the dynamic subregion, whereas the smaller, fringing beds that are challenging to detect

with satellite imagery are in the fjord subregion (Ch. 2). We focused on the dynamic subregion due to the limited availability of high-resolution satellite imagery in the fjord subregion *(Fig. 8)*. This subregion is dominated by *Nereocystis* beds, except for on the north shore of Malcolm Island, which is lined with large, dense beds primarily composed of *Macrocystis* (Ch. 2; Sutherland, 1990). *Macrocystis* and *Nereocystis* are the only canopy-forming kelp species in the subregion, and "kelp" hereafter collectively refers to both species. *Nereocystis*, as an annual species, tends to display more interannual variability than *Macrocystis*, a perennial species (Dayton, 1984; Springer et al., 2010).

Local community members, including First Nations, have revealed that, generally, the kelp forests have declined in density and coverage in their territories (Broughton Aquaculture Transition Initiative (BATI), unpublished, 2021; Salmon Coast Field Station (SCFS), unpublished, 2023). Community members have also reported specific locations of kelp change in the region, including an increase around Malcolm Island, and decreases at an offshore kelp bed at the mouth of the Nimpkish River ("NR"), at a nearshore kelp bed off the shore of the Alert Bay Lighthouse ("ABL"), and along the salmon migration routes in the fjords near now-decommissioned open-net salmon farms (SCFS, 2023; Mountain, pers comm, 2023).

One *Macrocystis* site and eight smaller *Nereocystis* sites were selected to represent the temporal dynamics of kelp beds of different species and sizes exposed to different environmental conditions. The *Macrocystis* site encompasses the entire north shore of Malcolm Island (spanning 11.6 km^2) and the eight smaller *Nereocystis* sites (ranging from 0.03-1.45 km^2 per site) represent the portion of the eastern shore of Malcolm Island with high kelp abundance and the smaller islands east of Malcolm Island *(Fig. 8)*. The smaller site approach was chosen for the *Nereocystis* sites rather than mapping all of their coastlines due to the geomorphological complexity of the area, which imposed a challenge for the satellite remote sensing of kelp because of the increased land adjacency effects (Cavanaugh et al., 2021). The *Nereocystis* sites included the offshore kelp beds at the mouth of the Nimpkish River (NR), the nearshore kelp beds off the shore of the Alert Bay Lighthouse (ABL), the eastern coastline of Alert Bay (ABE), the eastern tip of Malcolm Island (MIE), Pearse Islands (PI), Bold Head (BH), Wedge Island (WI), and South Leading Islet (SLI) *(Fig. 8)*. The locations of the *Macrocystis* and *Nereocystis* sites were selected opportunistically during a field visit and based on

their importance to the Mamalilikulla First Nation, 'Nam̱gis First Nation, and Kwikwasut'inuxw/Haxwa'mis First Nation. These three Nations formed the Broughton Aquaculture Transition Initiative (BATI), a coalition that emphasized the need to continue monitoring and protecting the Archipelago's kelp forests due to their importance as nearshore salmon habitat (BATI, unpublished, 2021). The *Macrocystis* and the *Nereocystis* sites experience slightly different environmental and topographical conditions from each other, with the *Macrocystis* site having flatter slopes and lower tidal current speeds than the *Nereocystis* sites (Ch. 2; Davies et al., 2018; Foreman et al., 2009).

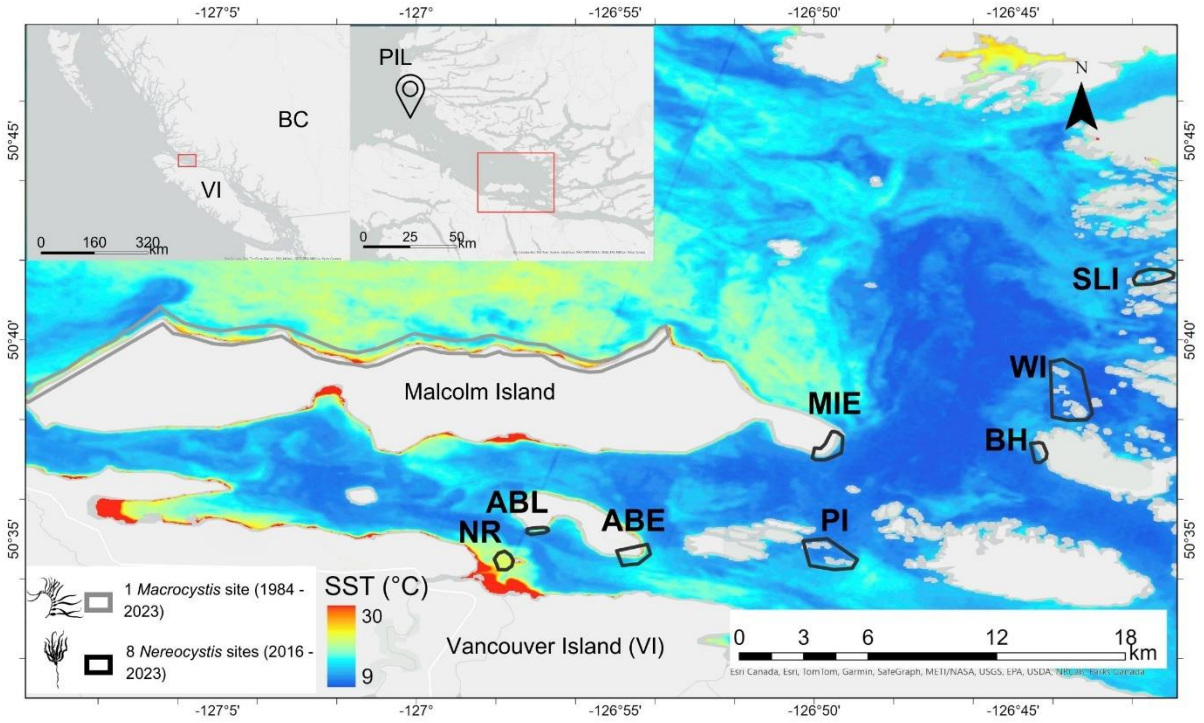

Fig. 8: The main map shows the study area (the dynamic subregion of the Broughton Archipelago), with the Macrocystis *site on the north shore of Malcolm Island marked in grey and the eight* Nereocystis *sites marked in black. The* Nereocystis *sites include kelp beds at Nimpkish River (NR), Alert Bay Lighthouse (ABL), Alert Bay East (ABE), Pearse Islands (PI), Bold Head (BH), Wedge Island (WI), and South Leading Islet (SLI). The background of the main map is the Landsat-derived SST from Aug 4, 2023. The left inset map shows the location of the study area (marked by a red rectangle) at a provincial scale relative to Vancouver Island (VI) and mainland BC (BC). The right inset map shows the study area (marked by the red rectangle) situated within the Queen Charlotte Strait region, relative to the location of the Pine Island Lighthouse (PIL), from which the regional SST and MHW metrics were derived (see 3.3.2).*

3.3.2 Data compilation and processing

The following data were compiled: (1) local, regional, and global-scale environmental conditions, (2) Landsat-derived canopy kelp area (1984 to 2023) at the *Macrocystis* site, and (3) Planetscope-derived kelp area (2016 to 2023) at the *Nereocystis* sites (both "kelp area" hereafter) *(Fig. 9)*. In addition, very high-resolution Worldview-2 and GeoEye-1 imagery was used to validate kelp classifications derived from Landsat and Planetscope imagery *(Fig. 9)*. The environmental variables were used to define climate periods (years with similar environmental conditions) *(Fig. 9)*. Objective 1 (identify the temporal responses of *Macrocystis pyrifera* and *Nereocystis luetkeana*, respectively, to changes in temperature and climatic oscillations) was achieved by analyzing both long-term and short-term kelp time series alongside environmental changes at local, regional, and global scales *(Fig. 9)*. Objective 2 (identifying spatial patterns of kelp persistence) was achieved by spatially combining yearly kelp areas *(Fig. 9)*.

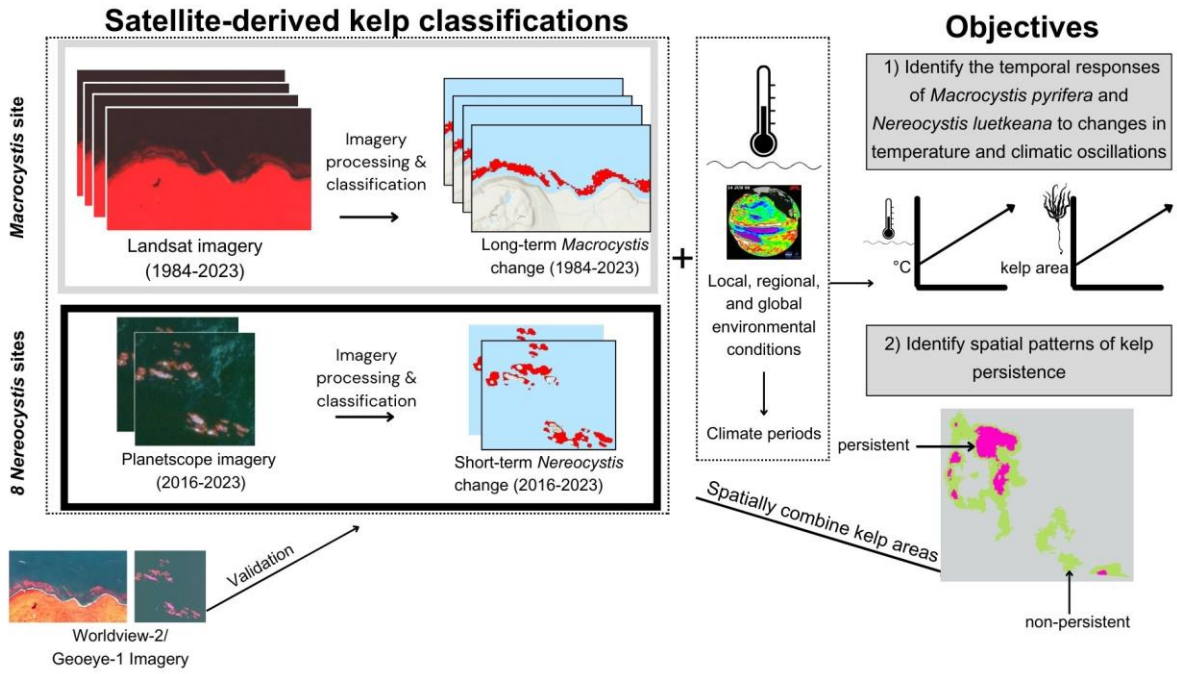

Fig. 9: A flow chart representing the data compilation and processing, as well as the spatial and temporal dimensions of the study, and how satellite-derived kelp classifications and environmental data are combined to achieve the objectives of the study.

Environmental conditions

The environmental conditions from the past four decades (1984 to 2023) were compiled to evaluate their roles as drivers of kelp area change. Environmental data was acquired to represent three different spatial scales: 1) Local: Summer climatologies compiled from temporally discontinuous Landsat-derived SST from the *Macrocystis* and *Nereocystis* sites; 2) Regional: spring and summer climatologies derived from temporally continuous (daily) in-situ SST measurements collected at Pine Island Lighthouse about 57 km north of the study area *(Fig. 8)*, representative of the Queen Charlotte Strait region; and 3) Global: annual ONI and PDO indices representing the climatic conditions of the broader Northeast Pacific Ocean.

Local SST

We characterized local SST changes in the study area by deriving mean summer (July-August) SST climatologies from the thermal infrared band of Landsat 5, 7, 8, and 9 imagery ("local SST" hereafter, spatial resolution: 30 m) for each year; note that this dataset was temporally discontinuous due to low availability of imagery related to frequent cloud cover. To create the SST

climatologies, we first compiled all cloud-free Landsat images captured during the summer months from 1984 to 2023, excluding years with only one cloud-free image to prevent skewing the summer mean with short-term extremes. As a result, only 13 years out of the 40 years analyzed of local SST data was available for the *Macrocystis* site *(Table 3)*. For each of the 13 years, mean local SST was calculated using zonal statistics in a polygon spanning the entirety of the *Macrocystis* site *(Fig. 8)*, buffered 300 m away from the shoreline. This reduced the interference of land temperature on the water pixels, producing accurate nearshore SST data (Wachmann et al., 2024). Mean local Landsat SST data for the *Nereocystis* sites were available for 26 out of the 39 years analyzed *(Table 3)*. For each of these 26 years, local SST was calculated using zonal statistics in a 200-m radius buffer 300 m from any land (Wachmann et al., 2024). These annual mean summer SST measurements were then compiled into site-specific climatologies. Note that although local SST measurements for the *Nereocystis* sites were acquired between 1984 and 2023, their kelp time series only ranged from 2016 to 2023 due to the limited availability of Planetscope imagery.

Regional SST and MHWs

We characterized the regional SST based on daily in-situ SST measurements collected at Pine Island Lighthouse ("regional SST" hereafter), compiled from 1982 to 2023 (Fisheries & Oceans Canada, 2024) *(Fig. 8)*. Pine Island Lighthouse is 57 km away from Malcolm Island, thus representing the general environmental conditions of the Queen Charlotte Strait region rather than the local conditions at the sites. However, its high temporal resolution allowed us to calculate MHW frequencies and magnitudes (Hobday et al., 2016).

The following metrics were calculated from the daily regional SST measurements: (i) mean yearly spring (May-June) and summer (July-August) SST climatologies, (ii) mean yearly spring and summer SST anomalies, and (iii) two- and three-year mean climatologies of regional spring and summer SST. The two- and three-year SST means were computed to evaluate the potential lagged effects of temperature changes on kelp (Pfister et al., 2018; Gendall et al., submitted.) *(Table 3)*. Beyond the SST metrics above, MHWs were identified from the regional daily SST measurements, with an MHW defined as when the maximum observed day temperature surpasses the day's seasonal

climatology and 90th percentile temperature threshold for more than five days, sensu Hobday et al. (2016). Following Hobday et al., (2016), we calculated four MHW categories (I - IV), corresponding to the number of times (one to four, respectively) the maximum intensity has surpassed the seasonal climatology. After identifying the MHWs, the cumulative intensity of each MHW was calculated as the MHW's temperature anomaly (°C) multiplied by the number of heatwave days. For each year n, the following metrics were noted: (i) total pre-summer MHW cumulative intensity, which is the cumulative intensity of all MHWs that occurred from September 1st of year n-1 to June 30th of year n, and (ii) total summer MHW cumulative intensity, which is the combined cumulative intensity of all MHWs between July and August of year n. The total pre-summer MHW cumulative intensity would represent the MHWs occurring in the fall and winter of year n-1, and in the spring of year n, which may affect the kelp spores and gametophytes that will eventually reach canopy height as sporophytes in year n (Springer et al., 2010), thus affecting the kelp area detected in year n.

Global: Climatic oscillations

The global environmental conditions were characterized by the mean yearly ONI and PDO (NOAA, 2024a, 2024b). Mean yearly ONI and PDO were calculated from spring and summer (May to August) values and were then rescaled using Z-scores to identify when each index was above or below their 40-year climatological mean, following the methods of Mora-Soto et al. (2024a). This resulted in an ONI and PDO Z-score for each year (Table 1), with positive values indicating warmer years with less optimal conditions for kelp (Mora-Soto et al., 2024a)

Table 3: The environmental variables from local, regional, and global scales

Variable	**Temporal availability**	**Temporal resolution**	**Explanation**
Local (from the Macrocystis *and* Nereocystis *sites, all derived from Landsat thermal bands)*			
Local summer SST (°C)	*Macrocystis* site: 1985, 1990, 1995, 2003, 2005, 2006, 2008, 2009, 2010, 2013 to 2017, 2020, and 2023 *Nereocystis* site: 1984, 1985, 1990, 1993, 1995, 1997, 2003 to 2011, 2014 to 2018, and 2020 to 2023	Discontinuous	July & August mean calculated from available cloud-free Landsat images

Regional (all derived from the Pine Island Lighthouse in-situ daily measurements)			
Regional summer SST (°C)	July & August, 1984 to 2023	Continuous	July & August mean calculated from daily data
Regional spring SST (°C)	May & June, 1984 to 2023	Continuous	May & June mean calculated from daily data
Regional summer SST anomaly (°C)	July & August, 1984 to 2023	Continuous	The difference between the yearly summer mean (July-August) and the total summer (July-August) climatological mean calculated from daily values
Regional spring SST anomaly(°C)	May & June, 1984 to 2023	Continuous	The difference between the yearly spring (May-June) SST for that year and the total spring (May-June) climatological mean calculated from daily values
The 2-year mean of regional summer SST (°C)	July & August, 1984 to 2023	Continuous	For a year *n*, this is a 2-year moving mean of summer SST measurements from years n-2 to n
The 2-year mean of regional spring SST (°C)	May & June, 1984 to 2023	Continuous	For a year *n*, this is a 2-year moving mean of spring SST measurements from years n-2 to n
The 3-year mean of regional summer SST (°C)	July & August, 1984 to 2023	Continuous	For a year *n*, this is a 3-year moving mean of summer SST measurements from years n-3 to n
The 3-year mean of regional spring SST (°C)	May & June, 1984 to 2023	Continuous	For a year *n*, this is a 3-year moving mean of spring SST measurements from years n-3 to n
Pre-summer MHW (°C days)	September - June, 1983 to 2023	Continuous	For a year *n*, the sum of the total cumulative intensity of all MHWs from September of year n-1 to June of year n
Summer MHW (°C days)	July-August, 1984 to 2023	Continuous	For a year *n*, the sum of the total cumulative intensity of all MHWs from July to August.
Global (all derived from NOAA, 2024a, 2024b)			
ONI	May-August, 1984 to 2023	Continuous	Z-scored spring and summer ONI calculated from the mean spring and summer ONI for that year
PDO	May-August, 1984 to 2023	Continuous	Z-scored spring and summer PDO calculated from the mean spring and summer PDO for that year.

Mapping floating kelp area

Kelp area was quantified by classifying satellite imagery spanning 1984 to 2023. Higher-resolution satellite imagery was selected to map the floating kelp area in the *Nereocystis* sites than the *Macrocystis* sites, as higher-resolution imagery is more appropriate for mapping the fringing *Nereocystis* beds typical of this region (Cavanaugh et al., 2021; Gendall et al., 2023). Landsat imagery

(spatial resolution: 30.0 m, 1984 to 2023) was selected to map the large kelp beds at the *Macrocystis* site, creating a longer time series. Planetscope imagery (spatial resolution: 3.00 m, 2016 to 2023) was used to represent kelp changes at the smaller *Nereocystis* sites after the Blob (Bond et al., 2015). Then, very-high-resolution Worldview-2 and Geo-eye-1 imagery (spatial resolution: 0.460 and 1.84 m, respectively) obtained from 2017 and 2023 were used to validate the satellite-derived kelp area classifications.

Long-term Macrocystis *time series*

For the *Macrocystis* site, the kelp area was derived from Landsat imagery using two different classification approaches: Multiple Endmember Spectral Mixture Analysis (MESMA) (Cavanaugh et al., 2011, Bell et al., 2020) and Object-Based Image Analysis (OBIA) (e.g. Gendall et al., 2023; Mora Soto et al., 2024a). The mixture of approaches was used due to the availability of a pre-existing dataset from 1984 to 2020 (Reshitnyk, unpublished data, 2024) classified using MESMA. Additional classifications of kelp area using OBIA allowed us to expand the time series to include 2021 to 2023. For the 1984-2020 Landsat dataset, atmospherically corrected surface reflectance products (Landsat Collection 1 Level-2 reflectance data) were downloaded from the United States Geological Survey Earth Explorer website for the sites for Landsat sensors TM, ETM+, and OLI for each year. To mask out intertidal areas, a land mask was derived for the region using a single Landsat scene collection at a 0.2 m tide (Mean Lower Low Water) to remove all land and intertidal pixels (mask creation details in supplementary material S1). Classification of the kelp area followed methods described by Bell et al., 2020. Following cloud and land masking, for each scene, a binary classification decision tree was used to classify each pixel into one of four classes: seawater, cloud, land, and kelp. A Multiple Endmember Spectral Mixture Analysis (MESMA) (Bell et al., 2020, Roberts et al., 1998) was used to determine the kelp fraction contained in each kelp pixel. We converted the fractional cover dataset to a binary time series based on a fractional kelp cover threshold of 13% (Houskeeper et al, 2022, Cavanaugh et al., 2011). The final dataset represents the maximum kelp area for a given year. 1992 was excluded from this analysis as there was no available cloud-free imagery for the study area.

For the 2021-2023 Landsat dataset, we used one yearly cloud-free Landsat image acquired during low tide between spring and summer, thus representing the kelp area captured at peak biomass (Springer et al., 2010). For each image, the land was masked out, and a Normalized Difference Vegetation Index (NDVI) and linear enhancements were applied to increase the spectral separability between kelp and water, following the protocols in Gendall et al. (2023). Each image was classified using an OBIA approach (OBIA classification methods in supplementary material S2). For the entire time series (1984 to 2023), kelp area was normalized as a percentage of the maximum kelp area, i.e. aggregated area of all kelp detected for the entire time series.

Short-term Nereocystis *time series*

Planetscope imagery was used to derive kelp areas for the short-term time series (2016 to 2023) covering the eight *Nereocystis* sites *(Table 4)*. One cloud-free summer image acquired at a tidal height less than 2.50 m above the chart datum was used to derive each site's yearly kelp area. The processing and classification of the short-term time series followed the methods delineated in Gendall et al. (2023). Imagery from 2016 required atmospheric correction as only top-of-atmosphere reflectance products were available. Atmospheric correction was performed using a Rayleigh correction, with dark targets selected using the darkest pixel histogram adjustment method described in Hadjimitsis et al. (2004). Atmospheric correction was not conducted on imagery from 2017 to 2023, as surface reflectance products were available. In terms of geometry, visual assessments of the satellite imagery's alignment were conducted relative to the ArcGIS base map, and all images used were confirmed to be georeferenced. Next, areas where kelp cannot grow (i.e. land, deep water (>20 m), and sandy and mud substrate) were masked from imagery to avoid false positives in kelp area classifications following the methods outlined in Gendall et al. (2023). The land mask was manually delineated based on the lowest tide Planetscope image (tidal height: 0.716 m) in this kelp time series, acquired on August 4, 2023; the sandy and mud substrate mask was created using the BC bottom patch model (Haggarty et al., 2020); and the deep water mask (depths >20.0 m) was created using a coastal digital elevation model for Pacific Canadian waters (Davies et al., 2018). Following the masking step, a Near-Infrared/Green (NIR/G) band ratio and linear enhancements were applied to the

imagery before classification (Gendall et al., 2023). The images were subsequently classified using the aforementioned OBIA methods (see details in the classification methods in Appendix S2), resulting in yearly kelp area products from 2016 to 2023 for each *Nereocystis* site. Finally, yearly kelp areas were normalized into percent kelp area.

Methods comparison and validation of kelp area products

We ensured that the MESMA-based yearly kelp aggregate area classification method (as used in 1984 to 2020 *Macrocystis* site classifications) and OBIA-based non-aggregate kelp area classification method (as used in 2021 to 2023 *Macrocystis* site classifications and 2016 to 2023 *Nereocystis* site classifications) created comparable results by conducting a sensitivity analysis. Two Landsat summer images, from 1986 and 2015, covering part of the *Macrocystis* site already classified using MESMA, were additionally classified using OBIA. The percent kelp area derived from the OBIA classification was within a 1% difference from that of the MESMA classification; thus, the two classification methods were deemed comparable.

Moreover, we confirmed that there were no confounding effects of tidal height on the percent kelp area by fitting a linear mixed model for the short-term time series (tidal height range: 0.716-2.500 m), with percent kelp area as the dependent variable, tidal height as a fixed effect, and site as a random effect (R package "lme4", Bates et al., 2015). This analysis confirmed that the percent kelp area was not significantly affected by tidal height ($p=0.320$) and, therefore, suitable for use in subsequent data analysis. This test was not conducted for the long-term time series as the kelp area for each year was derived from multiple images of various tidal heights, minimizing the tidal height-induced variability associated with this dataset.

The satellite-derived kelp area products were validated by comparing the spatial overlap between the kelp classifications and very high-resolution satellite images (spatial resolution: 0.460-1.84 m). The very high-resolution satellite images provided more accurate representations of the kelp beds due to the reduced pixel mixing between kelp and water (Cavanaugh et al., 2021; Gendall et al., 2023). As the validation of all the yearly kelp classifications is challenging due to the lack of historical in-situ data and very high-resolution imagery, we selected one year to validate the kelp

classification approach of each of the time series and assumed this validation would be representative of the other years. For the long-term *Macrocystis* time series, a Worldview-2 image (spatial resolution: 1.84 m, acquired on August 1, 2017), was used to validate the Landsat-based classification of the *Macrocystis* site kelp beds from 2017. For the short-term *Nereocystis* time series, we validated the 2023 Planetscope-derived classifications of six *Nereocystis* sites' kelp beds by using a pan-sharpened Worldview-2 image (spatial resolution: 0.460 m, acquired on August 4, 2023) and a pan-sharpened GeoEye-1 image (spatial resolution: 0.460 m, acquired on August 6, 2023) *(Table 4)*. Overall accuracies of 89.7% and 89.1% were found for the long-term and the short-term time series, respectively (Details on validation methods and results in supplementary material B3, *Table B1*).

Table 4: Table detailing imagery used for the long-term and short-term analysis, as well as imagery validation

Spatial coverage	Temporal coverage	Data source	Classification method	Purpose
Macrocystis site	1984 to 2023	Landsat 5, 7, 8 9 (30.0 m)	1984 to 2020 (MESMA) 2021 to 2023 (OBIA)	Create long-term kelp time series
Eight *Nereocystis* sites	2016 to 2023	Planetscope (3.00 m)	OBIA	Create a short-term kelp time series
Macrocystis site	Aug 1, 2017	Worldview (1.84 m)	Not classified, a 30 m grid was overlaid and all grids with >50% kelp were visually identified as kelp	Validation of long-term kelp time series
Six *Nereocystis* sites	Aug 4, 2023, Aug 6, 2023	Worldview, GeoEye (0.460 m)	Not classified, a 10 m grid was overlaid and all grids with >50% kelp were visually identified as kelp	Validation of short-term kelp time series

3.3.3 Data analysis

Identifying environmental trends at different spatial scales and climate periods

The Mann-Kendall test (Mann, 1945, R package: Kendall; McLeod, 2005), a non-parametric test for monotonic trends, was used to investigate significant temporal trends of local summer SST climatologies, regional spring and summer SST climatologies, and MHWs. Here, a significant and positive Mann Kendall's τ would indicate an increasing trend, a significant and negative τ would indicate a decreasing trend, and a non-significant Mann Kendall's test result would indicate no significant temporal trends. We did not test for trends in PDO and ONI as these climatic oscillations are inherently cyclical (Norel et al., 2021).

The time series of environmental variables were statistically organized into climate periods to define kelp area changes between these periods. This is because kelp can generally show lagged fluctuations for one to two years in response to environmental conditions due to the potential multi-year impacts of environmental changes (Pfister et al., 2018; Mora-Soto et al., 2024a; Gendall et al., submitted). The climate periods were identified by defining changepoints, i.e., points in the time series where abrupt changes in temporal trends occur (Zhao et al., 2019), in the regional spring and summer SST. These climatologies were selected to define the transitions between climate periods because of the in-situ nature and the continuity of the time series *(Table 3)*; the local satellite-derived SST data was not fit for this analysis due to its temporally discontinuous nature (see section 3.3.2). The changepoint analysis was conducted using the Bayesian Estimator of Abrupt change, Seasonal change, and Trend (BEAST) algorithm, an ensemble algorithm that leverages time series decomposition models using Bayesian model averaging (Zhao et al., 2019, R package: rBeast). We further conducted Kruskal-Wallis tests to define significant differences in each environmental variable *(Table 3)* between climate periods, and Dunn's tests with the Benjamani-Hochberg adjustment for multiple testing were used for post hoc comparisons (Kruskal & Wallis, 1952; Dunn, 1964; Benjamini & Hochberg, 1997).

Long-term (1984 to 2023) and short-term (2016 to 2023) kelp response to environmental changes

The Mann-Kendall test (Mann, 1945) was used to define both long-term (1984 to 2023) and short-term (2016 to 2023) temporal trends in kelp area at each site. Here, a significant and positive Mann Kendall's τ would indicate increasing kelp area, a significant and negative τ would indicate

decreasing kelp area, and a non-significant Mann Kendall's test result would indicate no significant temporal trends. An increase or no significant change in kelp area would indicate temporal persistence.

In addition, for the long-term *Macrocystis* time series, the Kruskal-Wallis test (Kruskal & Wallis, 1952) was conducted to identify potential differences in kelp area between the climate periods. Dunn's test was used for post hoc comparisons, with the Benjamini-Hochberg correction for multiple testing (Dunn, 1964; Benjamini & Hochberg, 1997). Furthermore, a linear model with regional and global environmental predictors was tested to define the most significant environmental variables affecting changes in the kelp area. The Landsat-derived local SST climatologies were not used as predictors in this linear model due to the lack of data for several years of the time series. To construct this linear model, first, all the predictor variables were tested for collinearity with Kendall's correlation test and visual data exploration (Kendall, 1948), with the significant and highly correlated variables ($R > 0.5$) excluded from the analysis. The selected (non-highly correlated) variables for the linear model included mean regional summer SST, summer MHW, pre-summer MHW, ONI, and PDO. Second, the Akaike Information Criteria (AIC) (Akaike, 1974) was used to determine the most suitable combination of predictors for the linear model from the non-correlated variables, and the model with the lowest AIC was selected to be the final model. Finally, the assumptions of the final model were visually evaluated with histograms of the model residuals, residuals' quantile-quantile plots, plots of the fitted values vs residuals, and statistically evaluated for the normality assumption using Shapiro-Wilk tests (Shapiro & Wilk, 1965). A plot of the residuals vs the observed site numbers was used to identify patterns in the order of the data, which tests for the assumption of the independence of observations, whereas a plot of the models' fitted vs residuals values was used to test for the linearity and constant variance assumptions. All visualizations were consistent with the assumptions required by the model, and the result of the Shapiro-Wilk tests confirmed that the model residuals were normal.

A similar comparison of kelp area change across climate periods and linear model analysis of the effect of environmental conditions were not conducted for the *Nereocystis* sites due to the reduced time series. However, a descriptive characterization of the observed kelp percent area changes and the

local environmental conditions during and after the end of the Blob (2016 to 2023) was conducted. These included noting down the means and standard deviations of summer SST at each site, identifying the hottest and coolest sites, as well as years of kelp loss.

Spatial patterns of kelp persistence

Persistent kelp areas within the maximum kelp area were defined as areas (m2) where kelp was present for more than 50% of the time-series length (>19 years of presence for the long-term *Macrocystis* time series; >4 years for the short-term *Nereocystis* time series). Our definition of a persistent area was adapted from the "refugia" definition of Cavanaugh et al. (2023), who identified as refugia areas of kelp that occurred in 50% of the years in a Planetscope-derived time series (2016 to 2021 in their case). We simply defined these as "persistent" areas rather than "refugia", as the study area did not experience environmental conditions detrimental to kelps as the term "refugia" would imply (see results). We identified the spatial distribution of kelp persistence at each site using the 'Count overlapping features' tool in ArcGIS Pro 3.0 (ESRI, Redlands, United States), which indicated where and how many times the yearly kelp areas overlap, using the 'Count overlapping features' tool in ArcGIS Pro 3.0 (ESRI, Redlands, United States). Finally, the percent of the persistent kelp area ($\frac{persistent\ kelp\ area}{maximum\ kelp\ area}$) was calculated for each site.

3.4 Results

3.4.1 Environmental conditions

At the regional level, the mean spring SST ranged from 8.40°C to 11.1°C, and mean summer SST ranged from 9.61°C to 12.6°C *(Fig. 10, SST anomalies in Fig. B1)*, with no temporal trends in either regional spring or summer SST (Mann-Kendall's test: spring: $\tau = 0.187$, p=0.0911; summer: $\tau = 0.195$, p=0.0785; *Table 5*). Based on the mean summer and spring regional SST, the changepoints analysis *(Table B2)* indicated three climate periods: Period 1 represents generally warmer ocean temperatures from 1984 to 1998, Period 2 represents cooler temperatures from 1999 to 2013, and Period 3 represents the highest temperatures of the time series from 2014 to 2023 *(Fig. 10)*.

Accordingly, mean spring and summer regional SST were different across all periods *(Fig. 10, Table 3)*. For both spring and summer, Period 1 (spring SST: 9.82±0.413°C, spring SST anomaly: 0.129±0.413°C, summer SST: 10.7 ±0.311°C, summer SST anomaly: 0.0343±0.311°C) had significantly warmer SST than Period 2 (spring SST: 9.24±0.473°C, spring SST anomaly: -0.448±0.473°C, summer SST: 10.1 ±0.411°C, summer SST anomaly: -0.545±0.411°C, *Fig 10, Table 5*). Furthermore, Period 3 (spring SST: 10.5±0.375°C, spring SST anomaly: 0.804±0.374°C, summer SST: 11.6 ±0.531°C, summer SST anomaly: 0.946±0.531°C) had significantly warmer SST than both Periods 1 and 2 *(Fig. 10, Fig B1, Table 5)*.

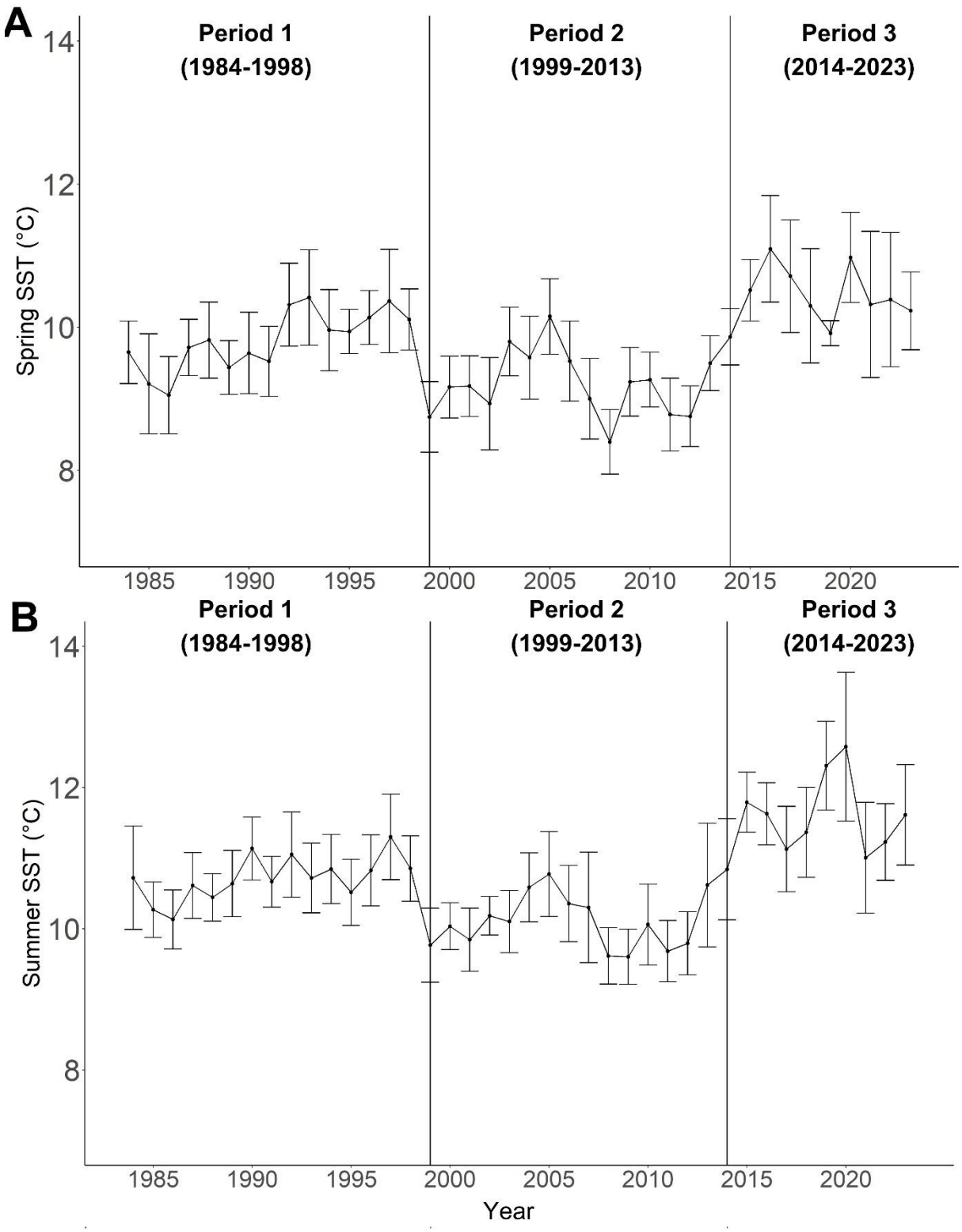

Fig. 10: A) Mean regional spring SST, and B) mean regional summer SST from 1984 to 2023. All data was derived from the Pine Island Lighthouse daily SST climatology (1984 to 2023), with error bars representing the standard deviations. The vertical black lines depict the transitions between the climate periods.

At the local scale, the Landsat-derived SST showed some variability, with the *Macrocystis* site presenting warmer SST (11.5±0.963°C) (climatological summer mean ± standard deviation) than the *Nereocystis* sites (10.1±1.05°C). On average, the hottest *Nereocystis* sites were ABL, ABE, and SLI (~10.3°C), and the coolest *Nereocystis* site was BH (9.41±0.716°C) *(Fig. 11A, Table B3)*. Across the three identified climate periods, the mean local SST significantly increased for the *Macrocystis* site and five *Nereocystis* sites (ABL, ABE, MIE, BH, WI) *(Fig. 11A, Table 5A)*, with ~1.40°C higher SST in Period 3 (*Macrocystis* site: 12.5±0.416°C, *Nereocystis* sites: 10.6±0.714°C) than in Period 1 (*Macrocystis* site: 10.3±0.198°C, *Nereocystis* sites: 9.17±0.542°C). However, neither Periods 1 nor 3 had significant differences with Period 2 regarding the mean local SST *(Fig. 11B, Table 5A).* For the other three *Nereocystis* sites (NR, PI, SLI), local SST measurements were not significantly different among the periods *(Fig. 11B, Table 5A)*, although local SST peaked in 2004 in sites NR and SLI, reaching mean summer temperatures of 14.2±1.50°C and 12.0±0.309°C, respectively.

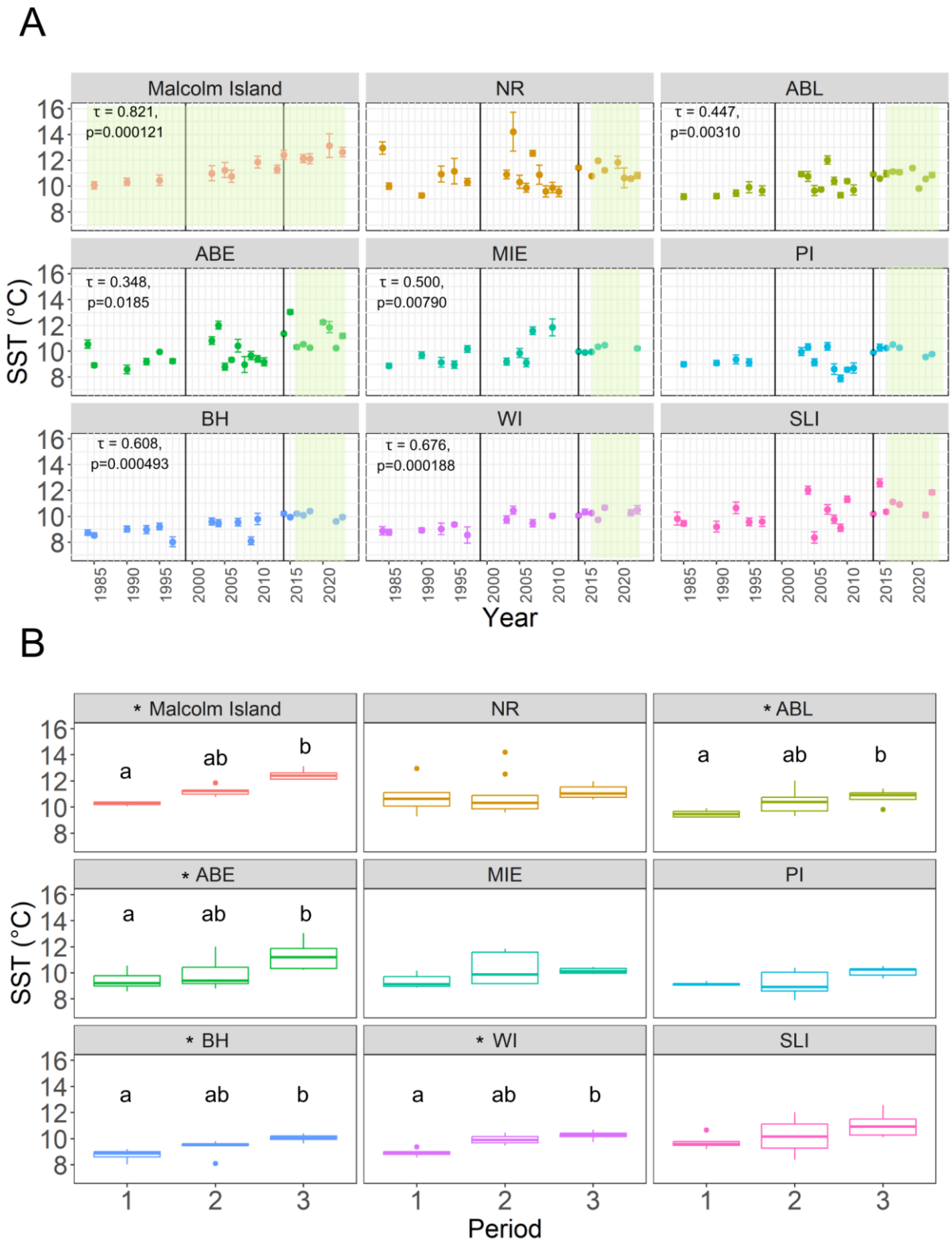

Fig. 11: A) Scatterplot showing the mean local summer SST for the Macrocystis site ("Malcolm Island") and each Nereocystis *site (as denoted by the abbreviated site names) from 1984 to 2023, with the error bars around each point representing the standard deviation for each year. The vertical black lines in 1999 and 2014 represent the boundaries between climate periods. The Mann-Kendall's τ and p-value are reported in the top left corner for sites with significant monotonic trends. The green*

shaded areas of each site's panel represent the length of the kelp time series analyzed for each site. B) The differences in mean local summer SST between each period. Sites with an asterisk (*) are sites with significant differences in local SST across periods. Different letters above each boxplot denote significant pairwise differences.

On the regional scale, 57 MHWs were identified between January 1983 and August 2023. Among these, 27 were in Category I, 23 in Category II, 6 in Category III, and 1 in Category IV *(Fig. 12A).* The most intense (Category IV) MHW occurred on 30 July 2020, lasting six days and reaching a maximum temperature intensity of 15.4°C (a +4.65°C anomaly), with a total cumulative intensity (calculated as the mean temperature anomaly of the MHW multiplied by the number of heatwave days) of 18.2°C days. The most cumulatively intense MHW occurred at the beginning of 2016, starting on 20 January and lasting 98 days, resulting in a cumulative total of 146 °C days, and reaching a maximum intensity (temperature) of 10.8°C (a +2.17°C anomaly). The pre-summer MHW time series did not display any temporal trends, but the summer MHW time series exhibited a statistically significant increase *(Table 5B).* Pre-summer MHW cumulative intensity was not significantly different across periods. However, summer MHW cumulative intensity was different across Periods 1 and 3, and 2 and 3, with Period 3 representing the highest MHW intensity (Period 1: 1.19 ±54.3°C days, Period 2: 1.67 ±6.21°C days, Period 3: 26.4 ±109°C days) *(Fig. B2, Table 5B).*

On the global scale, Period 1 (1984 to 1998) generally showed positive PDO (mean Z-score ± SD: 0.617± 0.855) and ONI (0.203 ± 1.13) values, reaching the highest PDO (2.09) and the second highest ONI (2.20) of the time series in 1997 *(Fig. 12B)*. Interestingly, the lowest ONI (-1.84) in the time series was also documented within Period 1 in 1988. Period 2 (1999 to 2023) displayed mostly negative PDO (-0.425±0.817) and ONI (-0.292±1.13), although a positive PDO and ONI were documented from 2002 to 2007. When comparing differences in oscillations between Periods 1 and 2, PDO was significantly more negative in Period 2 than in Period 1, whereas there were no significant differences in ONI *(Fig. 12B, Table 5C).* Period 3 (2014 to 2023) started with positive ONI (0.180±1.12) and PDO (-0.273±1.09), with the highest ONI of the time series (2.21) documented in 2015. However, from 2020 onwards, both ONI and PDO shifted negative, with PDO reaching its

lowest value of the time series (-1.91) in 2023, although ONI became positive again in 2023 (1.47). Ultimately, there were no significant differences in both ONI and PDO between Periods 1 and 3, and between Periods 2 and 3 *(Table 5C)*.

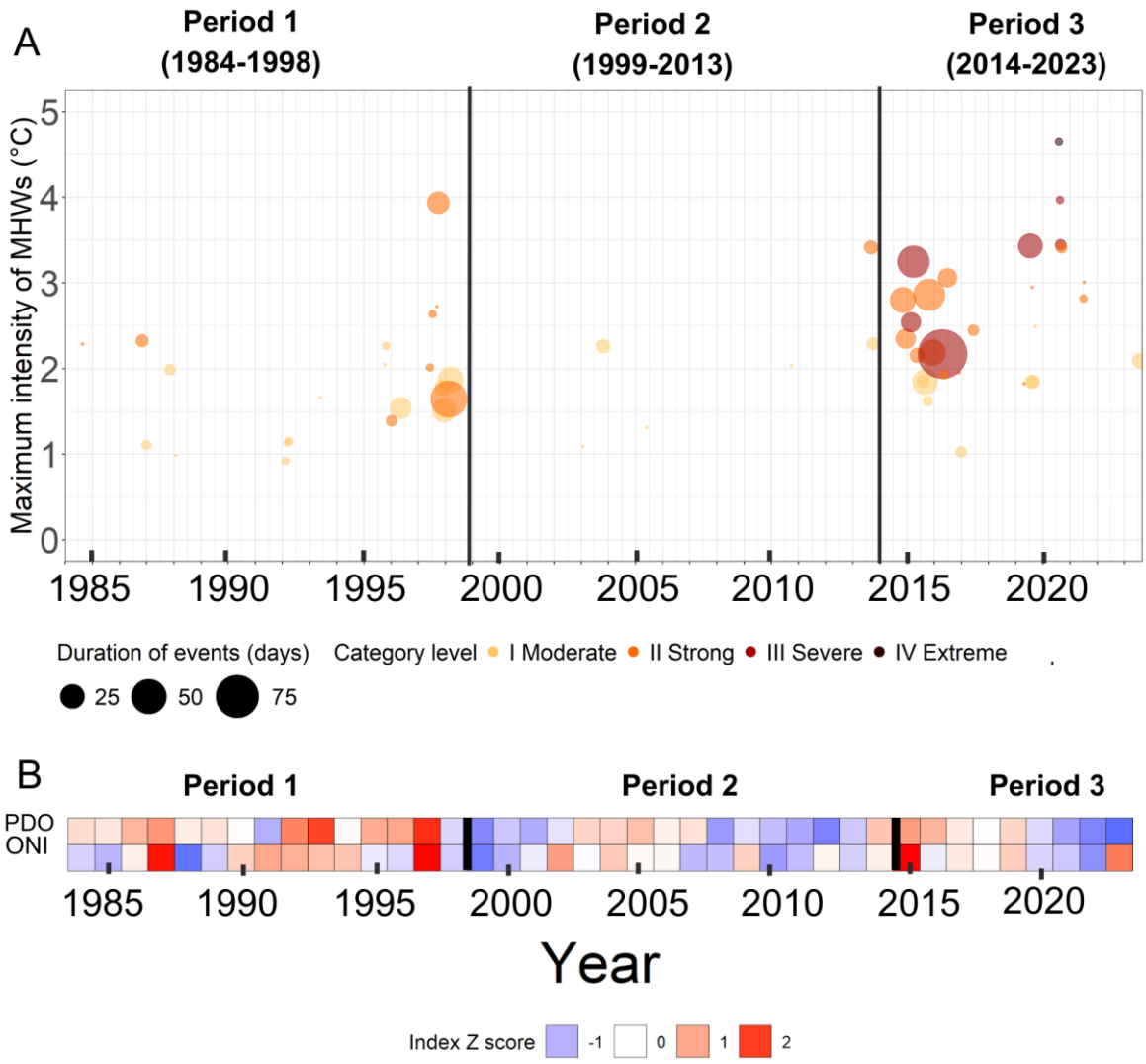

Fig. 12: Regional and global conditions across the three climatic periods identified (Period 1, Period 2, and Period 3). For both panels, the black lines represent the transitions between climate periods. A) MHWs and their associated duration and category level. The x-axis shows the date of each MHW's maximum intensity peak, and the y-axis shows the maximum intensity of each MHW. B) Pacific Decadal Oscillation (PDO) and Oceanic Niño Index (ONI) from 1984 to 2023.

Table 5: Mann-Kendall's test results testing for significant increases, decreases, or lack thereof in environmental variables from 1984 to 2023, with cells colored in grey, and Kruskal-Wallis and Dunn's test results representing environmental differences between climate periods with cells colored in white (P1 = Period 1, P2 = Period 2, P3 = Period 3) at A) local, B) regional, and C) global scales. Bolded values represent statistical significance.

	Testing for significant monotonic trends in each variable		Testing for significant differences between climate periods for each environmental variable				
Variable	Mann-Kendall's τ (if p-value is significant, + = increasing trend, - = decreasing trend)	Mann-Kendall's p-value	Kruskal-Wallis $\chi 2$	Kruskal-Wallis p-value	Dunn's test		
					Pair	*Z* statistic	Adjusted p-value (Benjamini-Hochberg method)
A: Local SST							
Malcolm Island (*Macrocystis* area)	**0.821**	**0.000121**	**9.18**	**0.0102**	P1-P2	1.76	0.0974
					P1-P3	**3.02**	**0.00744**
					P2-P3	1.66	0.0974
NR	0.0119	0.958	0.875	0.646	N/A	N/A	N/A
ABL	**0.447**	**0.00310**	**9.88**	**0.00716**	P1-P2	1.97	0.0988
					P1-P3	**3.14**	**0.00503**
					P2-P3	1.51	0.132
ABE	**0.348**	**0.0185**	**7.70**	**0.0213**	P1-P2	1.04	0.298
					P1-P3	**2.68**	**0.022**
					P2-P3	1.92	0.109
MIE	**0.500**	**0.00790**	4.81	0.0902	NA	NA	NA
PI	0.240	0.162	5.13	0.0770	NA	NA	NA
BH	**0.608**	**0.000493**	**11.2**	**0.00362**	P1-P2	1.68	0.0937
					P1-P3	**3.35**	**0.00240**

					P2-P3	1.68	0.0937
WI	**0.676**	**0.000178**	**12.2**	**0.00228**	P1-P2	2.19	0.0569
					P1-P3	**3.43**	**0.00181**
					P2-P3	1.08	0.280
SLI	0.333	0.0501	**5.68**	**0.0584**	P1-P2	0.16	0.349
					P1-P3	2.26	0.0549
					P2-P3	2.18	0.260
B: Regional							
Regional spring SST	0.187	0.0911	**22.4**	**1.39×10^{-5}**	**P1-P2**	**-2.58**	**1.51×10^{-2}**
					P1-P3	**2.43**	**1.51×10^{-2}**
					P2-P3	**4.68**	**8.59×10^{-6}**
Regional summer SST	0.195	0.0785	**26.4**	**1.88×10^{-6}**	**P1-P2**	**-2.77**	**7.71×10^{-3}**
					P1-P3	**2.66**	**7.71×10^{-3}**
					P2-P3	**5.08**	**1.10×10^{-6}**
Cumulative pre-summer MHW	0.0688	0.573	4.59	0.101	NA	NA	NA
Cumulative summer MHW	**0.399**	**0.00173**	15.90	0.000354	P1-P2	0.039	0.969
					P1-P3	**3.60**	**0.000931**
					P2-P3	**3.60**	**0.000931**
C: Global							
ONI	N/A	N/A	2.03	0.363	N/A	N/A	N/A
PDO	N/A	N/A	**8.03**	**0.0181**	**P1-P2**	**-2.57**	**0.0202**
					P1-P3	-1.93	0.106

					P2-P3	0.38	0.703

3.4.2 Long-term (1984 to 2023) and short-term (2016 to 2023) kelp response to environmental changes

The maximum kelp area at the *Macrocystis* site (1984 to 2023) covered 4.84 million m^2. Percent kelp area ranged from 24.0% (absolute area: 1.15 million m^2) to 71.0% (3.44 million m^2), with a mean of 50.0% (2.46 million m^2) of the maximum kelp area. Further, we found a statistically significant increase in kelp area (Mann Kendall's τ=0.247, p=0.0300, *Fig. 13A*) across all three climate periods. Among the climate periods, we observed statistically significant differences in kelp area between Periods 1 and 2 and between Periods 1 and 3, but not between Periods 2 and 3 *(Fig. 13A)*. Specifically, there was a slight increase in kelp area from 43.9±9.34% in Period 1 to 53.8±11.5% in Period 2, which remained high at 55.4±10.4% in Period 3 (*Fig. 13B*; Kruskal-Wallis $\chi2$ = 7.56, p=0.0228; Dunn's test: Period 1 vs Period 2: $\chi2$ = 2.35, p=0.0380; Period 1 vs Period 3, $\chi2$ = 2.35, p=0.0380, Period 2 vs period 3, $\chi2$ = 0.348, p=0.727).

Considering the kelp time series in its entirety, without division between climate periods, the final model with the lowest AIC included mean regional summer SST, cumulative summer MHW intensity, and ONI as predictors *(Table B4)*. However, regardless of the combination of predictor variables tested during the AIC-based selection process, the results of the linear model showed no effects of any of the predictors on kelp area *(Table B4)*.

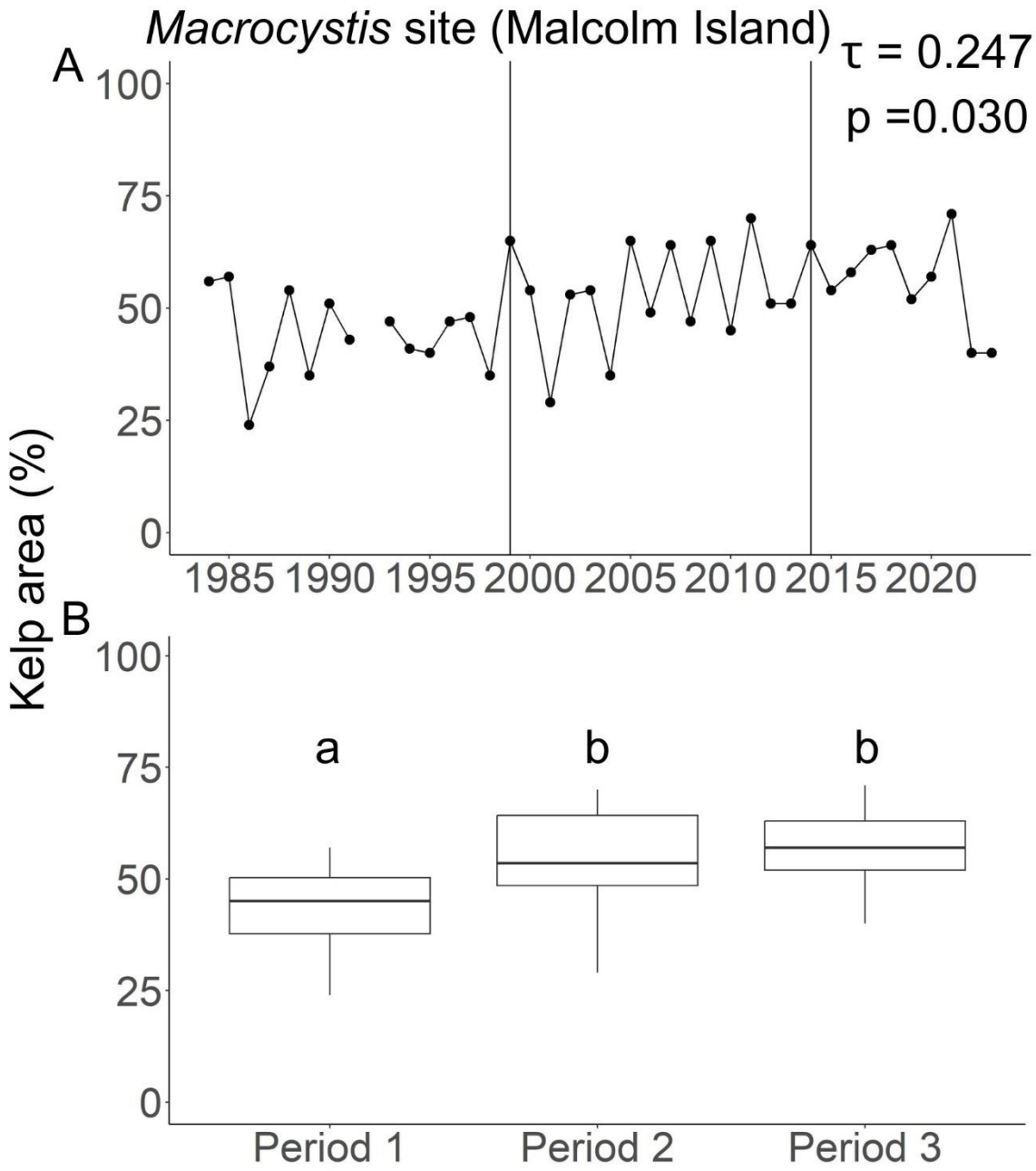

Fig. 13: Kelp area changes in the Macrocystis site (Malcolm Island). A) The temporal changes in the yearly kelp area from 1984 to 2023. Vertical lines in A) indicate the boundaries between periods. The τ is the Kendall rank correlation coefficient, representing the direction of monotonic change as determined by the Mann-Kendall's test, ranging from -1 (representing negative change) to +1 (positive change). The p represents the p-value. There is no data available for 1992. B) Boxplots showing the differences in the median kelp area and their associated interquartile ranges among climate periods. Identical letters above the boxes represent no significant differences in median kelp area between the pair of periods as determined by the Kruskal-Wallis test, whereas different letters above the boxes represent significant differences in median kelp area between the respective periods.

For the short-term time series, the maximum kelp areas across all *Nereocystis* sites ranged from 11,800 m^2 (BH) to 214,000 m^2 (MIE) *(Fig. 14)*. On a site level, mean percent kelp areas across all surveyed years ranged from 19.0±30.2% (4,010±6,360 m^2) at ABL to 58.5±13.3% at PI (111,000±25,100 m^2), with a total mean percent kelp area across all sites of 43.1 ± 19.3% *(Fig. 14)* Most sites' mean kelp areas exhibited parametric behavior, except ABL, which has a left-skewed pattern caused by kelp loss in the years 2018, 2019, 2022, and 2023 *(Fig. 14)*. The eight *Nereocystis* sites also displayed variable temporal trends in kelp areas from 2016 to 2023. Seven *Nereocystis* sites displayed no temporal trends (NR, ABL, MIE, PI, BH, WI, SLI), and one displayed a significantly increasing trend (ABE, Mann Kendall's $\tau = 0.857$, $p=0.00443$, *Fig. 14*).

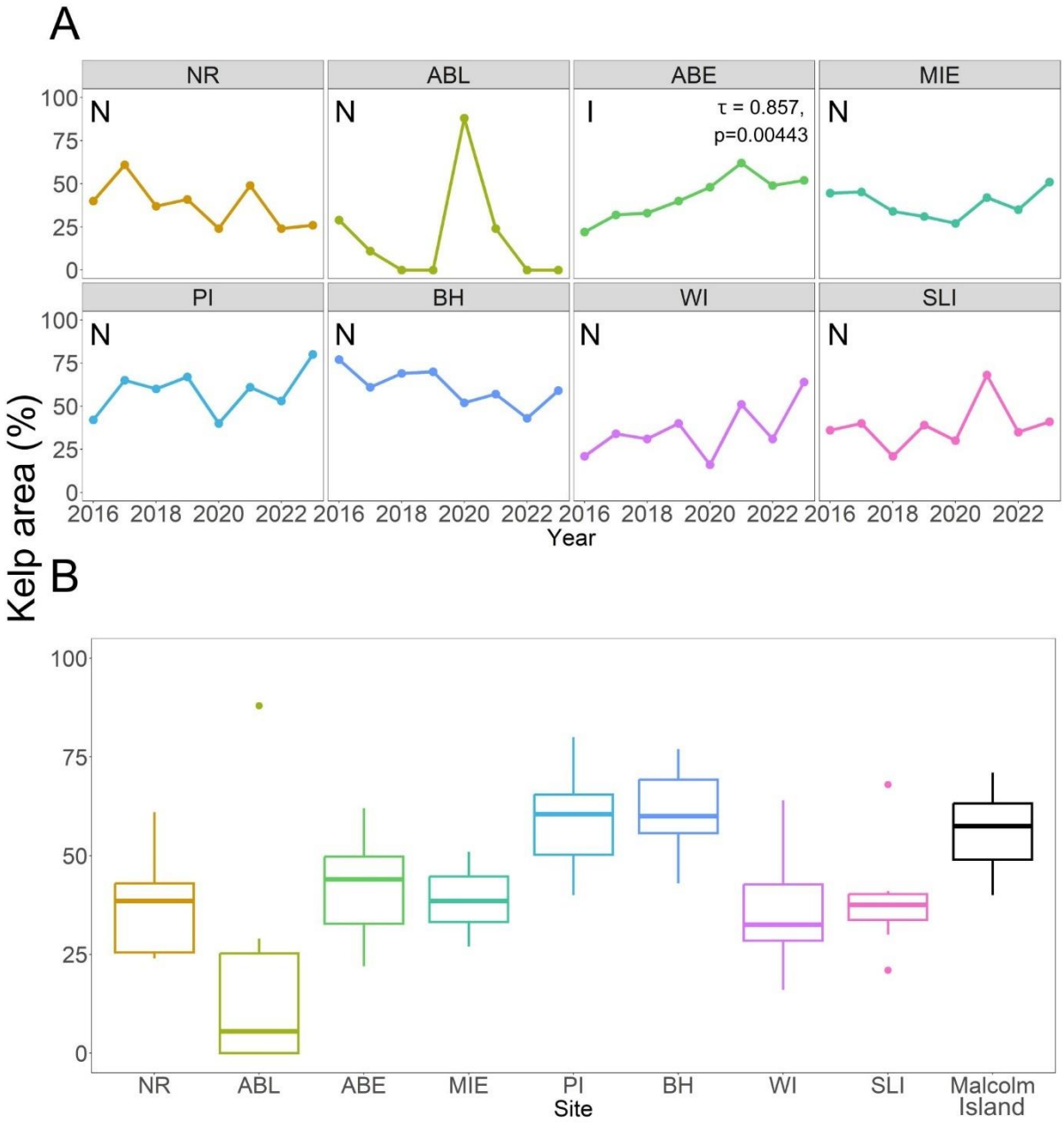

Fig. 14: ***A)*** *Changes in percent kelp area in the 8* Nereocystis *sites from 2016 to 2023. Sites with "N" under the site name are sites with no significant temporal trends, and the site with "I" had a significantly increasing trend, as per the Mann-Kendall test results. The significant Mann-Kendall test result is shown for the associated site.* ***B)*** *Boxplot showing median kelp area and their associated interquartile ranges from 2016 to 2023 at each site. The mean percent kelp area for the* Macrocystis *site ("Malcolm Island") from 2016 to 2023 is also included for reference, although it is not part of the short-term time series.*

3.4.3 Spatial patterns of kelp persistence

The spatial analysis indicated that the *Macrocystis* site had 77.0% persistence, i.e., 77.0% of the maximum kelp area was present for more than 19 years out of the 38-year time series *(Fig. 15)*.

The *Macrocystis* beds at the eastern part of the *Macrocystis* site were less spatially persistent than the western part *(Fig. 15)*. Five *Nereocystis* sites (NR, ABE, MIE, WI, SLI) had 20.6-33.8% persistence, i.e., area that was present for more than 4 years out of the 8-year time series *(Fig. 16)*. Sites PI and BH had larger proportions (53.1% and 53.6% respectively) of persistent kelp area, and ABL had no persistent kelp area (0.00% area). For both *Macrocystis* and *Nereocystis* sites, the persistent areas were mainly distributed in the center and inshore areas of each kelp bed *(Figs. 15-16)*.

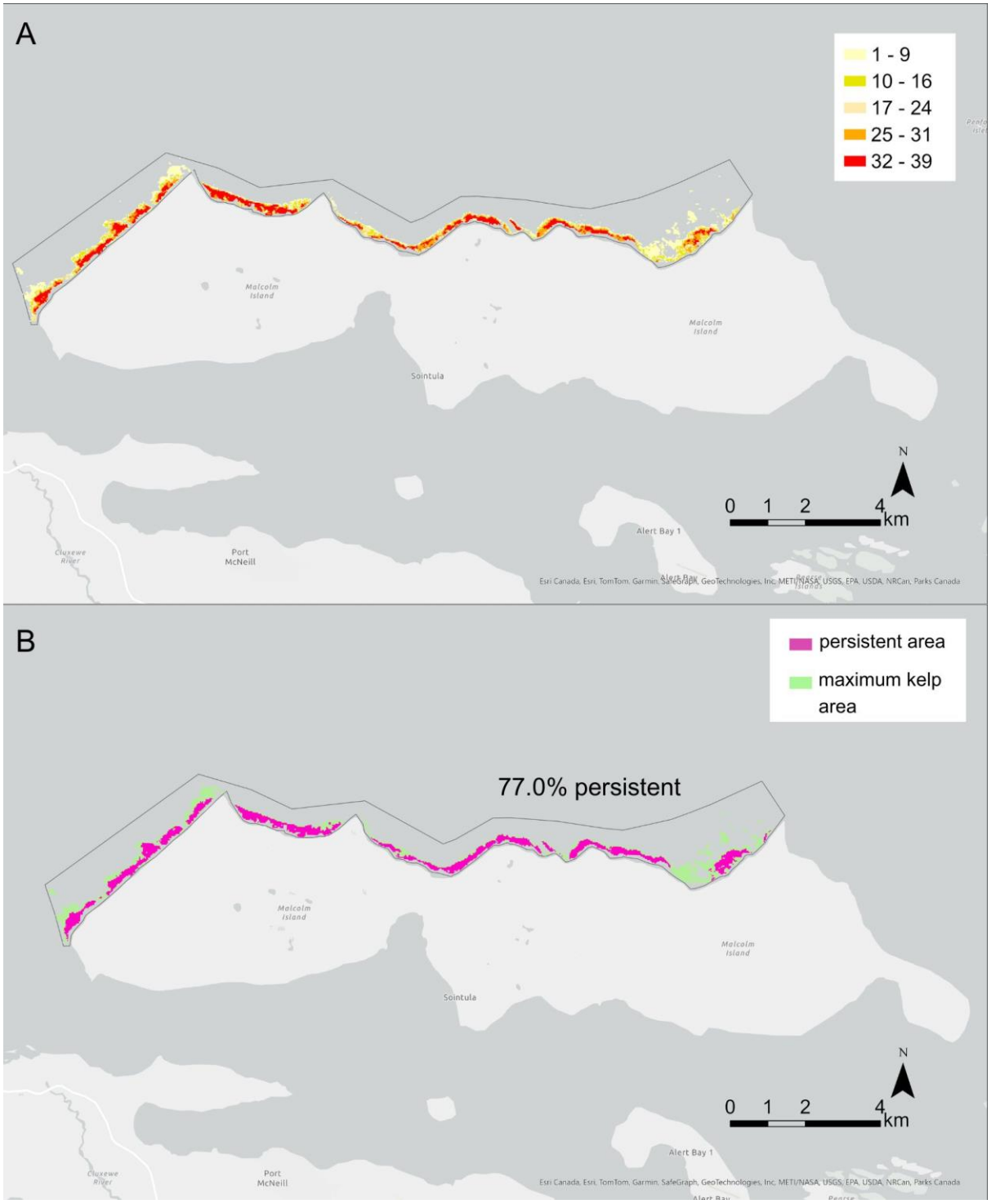

Fig. 15: Maps showing the spatial patterns of kelp persistence at the Macrocystis site: the north shore of Malcolm Island. A) shows the number of years of kelp presence, which was used to determine the areas of kelp persistence. The yellow-red scale indicates the number of years of kelp presence. B) shows the persistent area in pink and the maximum kelp area in green. The total percentage area of the maximum kelp area that is persistent is indicated in B. For both panels, the frame around the kelp beds shows the area considered for the analysis. Refer to Fig. 8 for the location of the Macrocystis site.

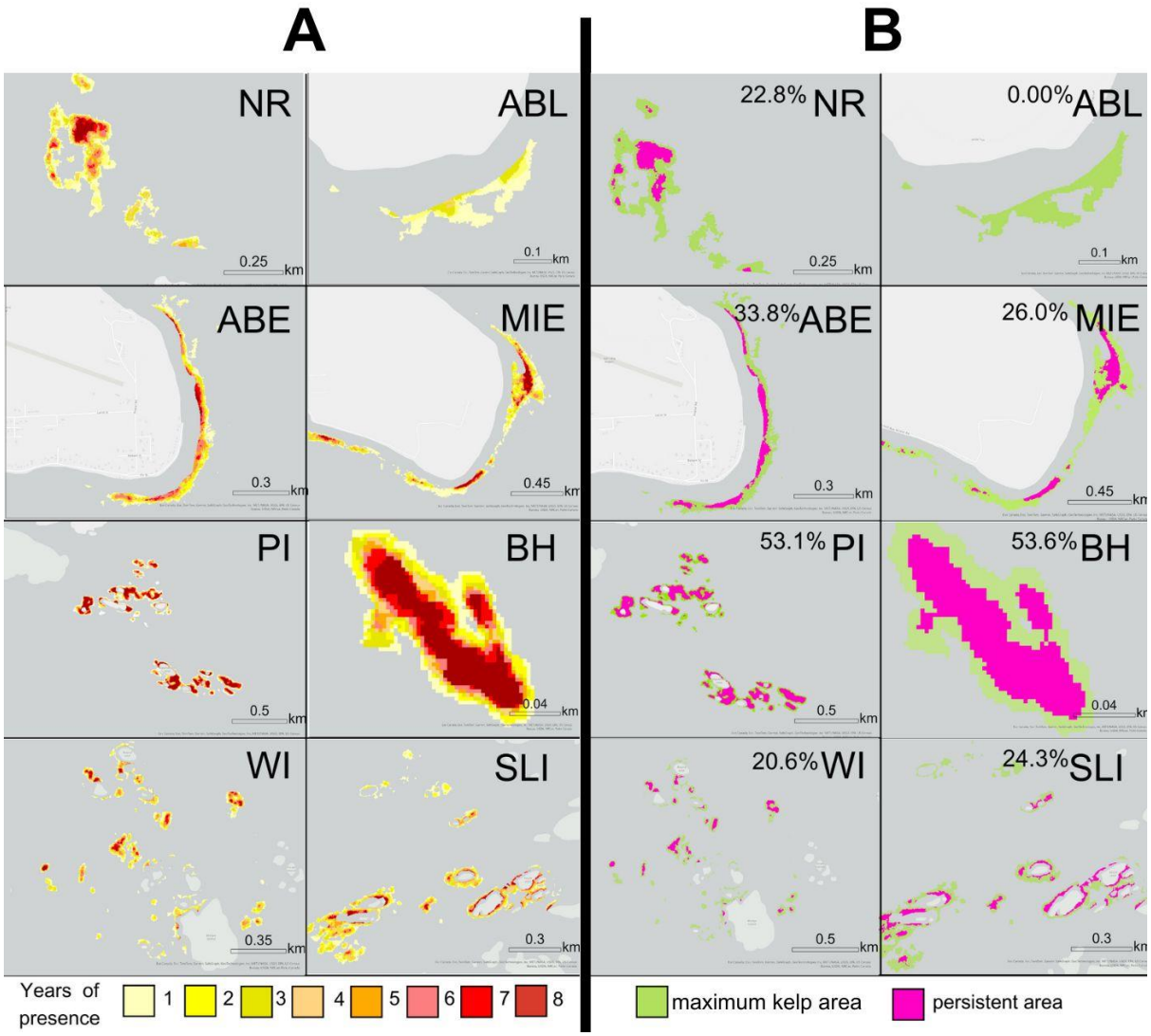

Fig. 16: Maps showing the spatial patterns of kelp persistence at each Nereocystis *site. A) shows the number of years of kelp presence, which was used to determine the areas of kelp persistence. The yellow-red scale indicates the number of years of kelp presence. B) shows the persistent area in pink and the maximum kelp area in green. The total percentage area of the maximum kelp area that is persistent is indicated in B. Refer to Fig. 8 for the location of each* Nereocystis *site.*

3.5 Discussion

We found that kelp was both spatially and temporally persistent in the dynamic subregion of the Broughton Archipelago, with increases in the area occupied by *Macrocystis*. Specifically, we identified temporal trends in kelp area and associated them with the changing environmental conditions using a long-term kelp change time series from 1984 to 2023 of the *Macrocystis* site and a short-term kelp change time series from 2016 to 2023 of the *Nereocystis* sites. We also identified spatial patterns of persistence by spatially combined kelp areas for each site.

3.5.1 Long-term (1984 to 2023) and short-term (2016 to 2023) kelp response to environmental changes

Overall, kelp area in the Broughton Archipelago was mostly temporally persistent. Kelp percent area increased monotonically in the *Macrocystis* site from 1984 to 2023, specifically increasing by 9.90% in Period 2 and staying high throughout Period 3. The increase in kelp area at the *Macrocystis* site on the north shore of Malcolm Island corroborates reports from community members (SCFS, unpublished, 2023). This temporal increase indicated persistence in *Macrocystis* area from 1984 to 2023, which may be explained by the increase in local SST from ~10.0 to 13.0 °C. This potentially represents a move towards more ideal environmental conditions for *Macrocystis*, which has an optimal thermal range from 12.0 to 17.0°C (Lüning & Neushul, 1978), although this range could vary among populations and life stages (e.g. spores, gametophytes, or sporophytes) (Muth et al., 2019; Hollarsmith et al., 2020; Le et al., 2022). For example, an increase from 9.50 to 12.9°C was experimentally associated with a ~5.00 μm increase in *Macrocystis* gametophyte germ-tube length (Le et al., 2022), and a 10.0 to 14.0°C increase to be associated with a ~2% increase in the relative growth rate of *Macrocystis* blades (Fernández et al., 2020). The local SST increases in the study area always remained below the upper thermal limits for *Macrocystis*, which lie around 18.0-25.0°C (Hay, 1990; Le et al., 2022; Ladah & Zertuche-Gonzalez, 2007)

On the contrary, regional and global environmental conditions were not linked to significant changes in kelp area (based on the linear model results, *Table B4*). This is likely as regional and

global conditions occasionally diverged from the conditions kelps were facing locally in the nearshore environment (Brewer-Dalton et al., 2014; Lin & Bianucci, 2023). For example, the colder SST in Period 2 was only observed in the regional SST and inferred from the negative PDO, but not the local SST time series, which increased continuously throughout all three climate periods. Furthermore, occasional intense MHWs and higher local SST were observed during and after 2020, despite a shift to more negative ONI and PDO during the same time. A similar disparity was found between local SST and global climatic oscillations in other parts of BC. For instance, local SST continuously increased after 2020 in the Salish Sea, despite climatic oscillations transitioning to negative phases (e.g. Amos et al., 2015; Mora-Soto et al., 2024a), suggesting that the local SST increase in the Broughton Archipelago may be linked to local oceanographic conditions and variation in coastal geomorphology (Brewer-Dalton et al., 2014; Lin & Bianucci, 2023). Despite mismatches in environmental conditions of different scales during certain years of the time series, generally speaking, Period 3 had higher local and regional SST, a higher frequency and magnitude of MHWs, and more positive PDO and ONI. Similar conditions observed in the Strait of Georgia and Barkley Sound resulted in a subsequent decrease in kelp area (Mora-Soto et al., 2024a; Starko et al, 2022). However, in the dynamic subregion of the Broughton Archipelago, both local and regional measurements of SST remained within *Macrocystis'* optimal thermal range during Period 3, and consequently, we did not observe decreases in kelp area. This reinforces the observation that local temperature gradients can greatly influence kelp responses in the face of regional events such as MHWs (Starko et al., 2024b). It is unknown whether the climatic oscillations affected other environmental conditions not investigated in this study (e.g. nutrient availability) (Whitney, 2015; Bond et al., 2015), which may have impacted kelp physiology (Hollarsmith et al., 2022). Regardless, climatic oscillations did not directly relate to significant changes in kelp area at the *Macrocystis* site.

Aside from environmental changes, there may be other conditions at play, such as a low abundance of sea urchins (Eisaguirre et al., 2020). In Chapter 2, we found no sea urchins during a one-time sampling effort during the summer of 2023 at the *Macrocystis* site, suggesting that the absence or low abundance of sea urchins may have been conducive to kelp persistence at the

Macrocystis site. Continuous time-series data about other environmental and biotic conditions could elucidate what specifically drove the increase in *Macrocystis* area in the study area.

Our observations of *Macrocystis* persistence cooler waters corroborate patterns observed in cooler areas throughout the Northeast Pacific coast. For instance, centennial increases in the *Macrocystis* area were also observed in Southeast Alaska by Hollarsmith et al. (2024), which the authors attributed to various factors including temperature increases and the reintroduction of the sea otter, a keystone predator. Persistence in *Macrocystis* area was also observed in Cumshewa Inlet and Ella Beach, BC, and the outer coast of Washington, where local summer SST increases (~10.0 to 14.0°C) over the past few decades were similar to those observed in the Broughton Archipelago and did not reach the upper thermal limits of *Macrocystis* (Gendall et al., submitted; Mora-Soto et al., 2024a; Pfister et al., 2018). Similarly, these cooler, northern regions (BC and Washington) displayed *Macrocystis* persistence in response to the Blob of 2016. Conversely, the warmer southern regions (Central to Southern California, and Baja California Norte and Sur), which reached summer temperatures of ~17.0-24.0°C, experienced areal decreases to ~2-57% of their pre-Blob baseline (Mora-Soto et al., 2024b; Pfister et al., 2018; Cavanaugh et al., 2019; Bell et al., 2023).

Kelp persisted in most of the *Nereocystis* sites from 2016 to 2023, although some sites showed different trends in kelp area. Specifically, ABL did not display a significant temporal trend, but exhibited kelp losses in four of the eight studied years, corroborating community anecdotes of kelp decrease in the area (SCFS, unpublished, 2023). Similarly, the observed increase in kelp area at ABE reinforces local reports of a recent increase in kelp area after past decreases (SCFS, unpublished, 2023). Some of our results, however, contrasted with some other community reports of kelp trends: e.g., a kelp decrease was reported near NR (SCFS, unpublished, 2023), and a kelp increase at MIE after urchin harvesting began in that area, although the start date of urchin harvesting was not reported (Mountain, pers comm, 2023). Such discrepancies between the local community members' observations and our results may be linked to different study periods or time scales since they did not report the years where the changes in the kelp area were observed (SCFS, unpublished, 2023;

Mountain, pers comm, 2023). Thus, it is possible that the changes identified by the local community were observed outside of the timeframe covered in this study between 2016 to 2023. Furthermore, short-term studies (<20 years) are less likely than long-term studies (>20 years) to capture patterns of kelp decrease due to kelp's high interannual variability and environmental conditions' multi-year or decadal dynamics (Wernberg et al., 2019). Therefore, it is also possible that our short-term time series was simply not long enough to detect the changes reported by local communities, or that *Nereocystis'* high interannual variability in canopy-forming area may have skewed community observations based on when the observations were made.

The observed overall kelp persistence in the *Nereocystis* sites may also be explained by the local SST (~9.00-12.0°C), similar to the patterns observed in the *Macrocystis* site, Local SST increased at some of the *Nereocystis* sites but mostly remained below the upper thermal limits of *Nereocystis* (around 12-16.0°C for sporophytes, and 16.0-18.0°C for gametophytes, depending on the population) (Pontier et al., 2024; Korabik et al., 2023; Weigel et al., 2023). However, the variability in kelp responses between *Nereocystis* sites cannot be explained solely by environmental conditions, as the ABE site with increased kelp area and the ABL site with occasional kelp loss did not have any significantly different environmental conditions than the other six sites, which displayed no significant temporal change. Thus, the different temporal kelp trends in ABE and ABL may potentially be attributed to other environmental and/or biotic factors not researched in this study. Similar to the *Macrocystis* site, regional and global environmental conditions did not appear to affect the overall kelp persistence in the *Nereocystis* sites, likely because these conditions differed from local SST conditions.

Kelp area in the *Nereocystis* sites remained mostly persistent during and after the Blob *(Fig. 14)*. It is important to note that the time series for the *Nereocystis* sites started at the end of the Blob (2016), lacking a pre-Blob baseline for the *Nereocystis* sites. Therefore, our results could mean that *Nereocystis* was either not affected by the Blob or was affected by the Blob and did not recover to possible higher pre-Blob abundances. This echoes findings of *Nereocystis* persistence after the Blob in Oregon (Hamilton et al., 2020) and in the southern Salish Sea (Mora-Soto et al., 2024a, 2024b), where SST remained cooler (~12.0-15.0°C). On the other hand, this contrasts with findings of

Nereocystis trends in Northern California (McPherson et al., 2021; Cavanaugh et al., 2023; Bell et al., 2023), Southern Puget Sound (Berry et al., 2021), and the northern and central Salish Sea (Mora-Soto et al., 2024b; Starko et al., 2024a), where *Nereocystis* area declined after the Blob and showed limited recovery. However, the reasons for these kelp declines vary from higher SST (summer temperatures: ~13.0 to 20.0°C) to an increase in sea urchins after the loss of a keystone predator (sunflower sea stars) after the Blob (Hamilton et al., 2021), neither of which have been documented in the Broughton Archipelago.

Overall, we identified primarily persistent kelp forests, including *Macrocystis* and *Nereocystis* kelp areas, in the dynamic subregion of the Broughton Archipelago. As the documented SST trends remained within the favorable range for kelps throughout both time series, we cannot conclude if the kelps would be resilient to further SST increases (up to 20.0°C) in the study area, such as those observed SST increases in the northern Salish Sea, Southern Puget Sound, the sheltered parts of Barkley Sound, and in California. Regardless, the kelp forests have likely persisted for a long time in the study area, as all but two sites (BH and WI) were historically documented to have kelp present in the 1850s to 1950s based on records in the British Admiralty nautical charts (*Fig 17,* Costa et al., 2020). Note that this historical information only serves as a record of kelp presence, not kelp absence (Costa et al., 2020), thus, the lack of historical kelp documentation at BH does not necessarily mean that kelp was absent from the 1850s to the 1950s. The likely centennial persistence of kelp suggests that the dynamic subregion of the Broughton Archipelago represents a climate refuge for kelp. It is important to consider that this observation of persistence in the dynamic subregion may not apply to other parts of the Broughton Archipelago, such as the fjord subregion, which have smaller, fringing kelp beds that are subject to significantly different environmental conditions (Ch. 2). Indeed, local community members have anecdotally noted decreases in kelp distribution and area in the fjord subregion, including near now-decommissioned open-net salmon farms (Mountain, pers comm, 2023). Future research can investigate kelp area changes in the fjord subregion using very-high-resolution satellite imagery (e.g. Worldview-2 at 0.460 m spatial resolution), which may be capable of

accurately detecting the smaller, fringing kelp beds.

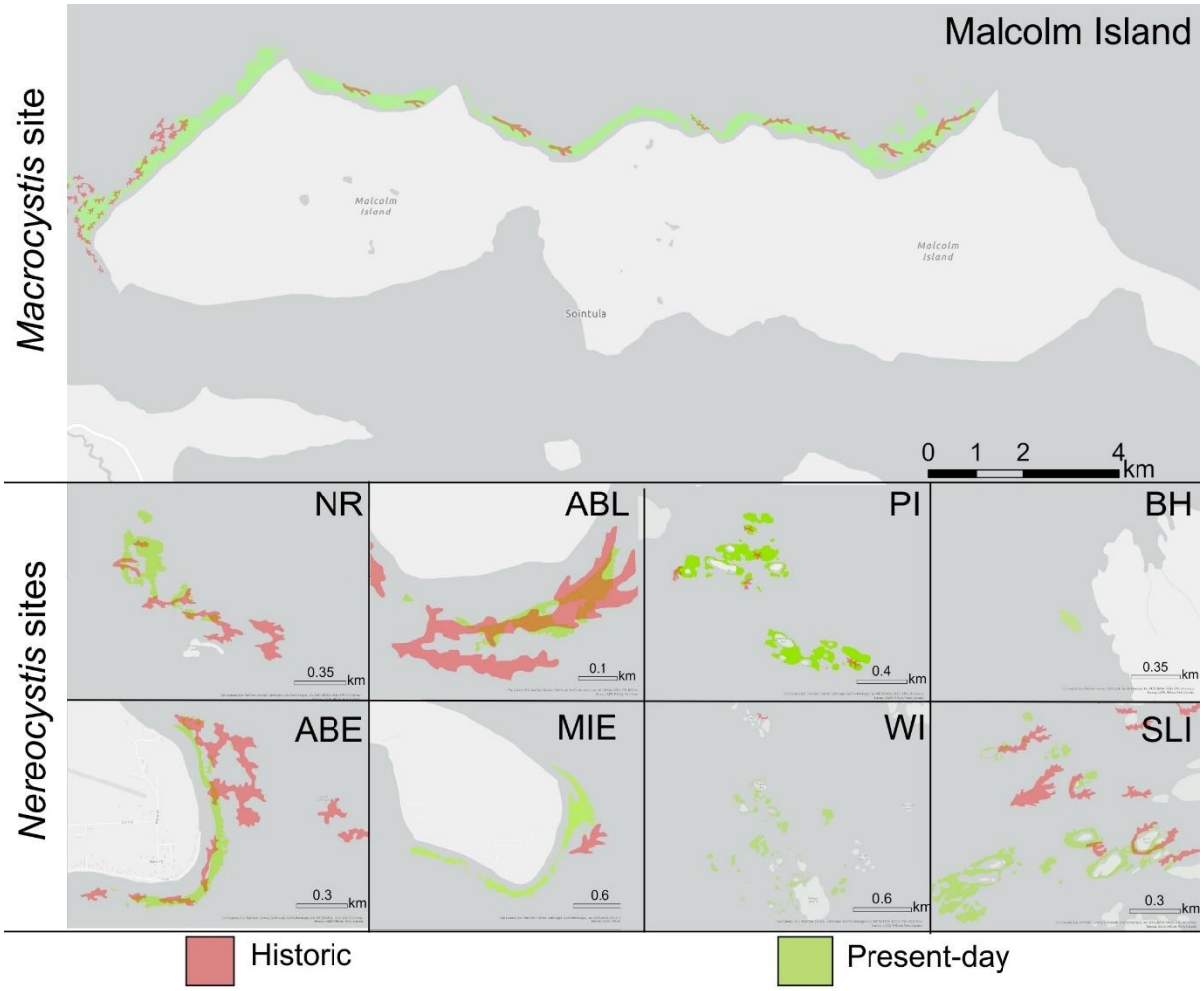

*Fig. 17: Map showing the location of historic kelp forests (1850s to 1950s) as documented in the British Admiralty nautical charts (red) and the maximum kelp area as derived from 'present-day' (*Macrocystis *site: aggregate from 1984 to 2023, 8 Nereocystis sites: aggregate from 2016 to 2023) satellite imagery (green). Note that the historic kelp polygons are only evidence of kelp presence, not kelp absence, and their shapes and sizes may not be related to the size of the actual kelp beds present during that time (Costa et al., 2020). Refer to Fig 8 for the location of each* Macrocystis *and Nereocystis site.*

.

3.5.2 Spatial patterns of kelp persistence

Kelp beds of both species had similar spatial patterns of persistence, with the center and inshore areas of kelp beds being more persistent than the edges. This reinforces spatial patterns found in *Macrocystis* forests in Southern California (Young et al., 2016), and *Nereocystis* forests in Northern California (Arafeh-Dalmau et al., 2023), Oregon (Hamilton et al., 2020; Arafeh-Dalmau et al., 2023),

and the outer coast of Washington (Arafeh-Dalmau et al., 2023). The spatial pattern of persistence may be associated with local variations in environmental and biotic factors, including current conditions, kelp dispersal, and sea urchin abundance (Jackson & Winant, 1983; Graham, 2003; Reeves et al., 2022). For instance, water current velocities are higher at the edges of the kelp bed than on the inside due to kelp plants' ability to buffer water currents (Jackson & Winant, 1983). Therefore, physical disturbances to kelps are more prone to happen at the kelp bed edges (Bekkby et al., 2019), potentially affecting its spatial persistence (e.g. Young et al., 2016). Currents may also play a role in kelp spore dispersal, with currents typically traveling further away at the kelp bed edge than in the interior, carrying zoospores away from the bed (Graham, 2003). In contrast, in the kelp forest interior, the drag from the high density of kelp sporophytes modifies current flow to primarily oscillate within the kelp bed, maintaining high levels of spore supply (Graham, 2003), and potentially contributing to the higher spatial persistence in the kelp bed interior. Biotic factors, such as increased urchin grazing at the edges of a kelp bed compared to the inside, may also cause lower kelp persistence at the edges (Reeves et al., 2022). However, it is unlikely that this is the situation at most of our study sites, as only some were documented to have abundant urchins (Ch. 2).

Beyond the potential influence of environmental and biotic drivers on the spatial patterns of persistence, the variable environmental conditions during the satellite imagery acquisition could have also affected the observed kelp area. Potential environmental conditions affecting the observed kelp area in the satellite images include the tidal height, which can submerge the edges of the kelp bed (short-term dataset tidal height: 0.716-2.50 m), and the currents that move kelps in different directions (Timmer et al., 2024). Timmer et al. (2024) found that kelp bed area can decrease by an average of 22.5% around the edges of the kelp bed per meter of tidal increase during low current speeds (<0.100 m/s) and 35.5% at high current speeds (>10.0 m/s). However, that study was conducted using drone imagery, thus the specific impacts of a tidal height increase on kelp bed edge submersion as detected from satellite imagery may slightly differ due to the difference in spatial resolution. We have reduced the influence of tidal height on detected kelp area by 1) aggregating images acquired under the different tidal heights for the long-term dataset and 2) testing and confirming with a linear mixed model the lack of a significant effect of tidal height on kelp area for the short-term dataset. No

information on current speeds during the time of satellite imagery acquisition was available, however, according to the regional model by Foreman et al. (2009), tidal current speeds are generally high (~0.390 m/s) at the *Nereocystis* sites, thus it is possible that some kelp was submerged by the tidal currents. Nonetheless, the non-persistent areas in the short-term time series were all larger than 35.5% of the maximum kelp areas, thus it is unlikely that the spatial pattern of persistence can be entirely attributed to tidal height and tidal current speeds.

The proportion of persistent kelp area varied within the *Macrocystis* site. A visual assessment of the *Macrocystis* site showed that the western parts have more persistent kelp areas, whereas the eastern part had a smaller percentage of persistent kelp areas. Fieldwork conducted for Ch. 2 and historical data from the BC Shorezone Mapping System[1] revealed submerged eelgrass beds interspersed between the *Macrocystis* at the eastern end of the north shore and homogenous *Macrocystis* patches at the western end. Thus, interspecific competition between *Macrocystis* and eelgrass may lead to smaller areas of persistence, a phenomenon that has been documented between other seaweed and seagrass species (Alexandre et al., 2017).

The kelp beds in the *Nereocystis* sites generally had lower proportions of spatially persistent area than in the *Macrocystis* site. ABL, the only *Nereocystis* site with years of kelp loss, was not spatially persistent, even in the center of its maximum kelp area. The sites that displayed no significant temporal changes, i.e., temporal persistence, had 20.6-53.6% spatially persistent areas; and the site where kelp was increasing (ABE) had a 33.8% spatially persistent area. It is important to note that for the *Nereocystis* sites, the threshold for kelp persistence was only 4 years out of the 8-year time series, much lower than that of the longer time series (19 out of 38 years), which may have led to the different percentages of persistent area between the long-term and short-term datasets. However, the lower persistence levels in the *Nereocystis* sites, as compared to the *Macrocystis* sites, may also be partially explained by *Nereocystis'* ruderal quality and annual life history, which leads to higher interannual variability than other perennial kelp species, such as *Macrocystis* (Dayton, 1984; Springer et al., 2010). The phenomenon of *Nereocystis* having higher spatial variability than *Macrocystis* was

[1] https://bcmca.ca/datafiles/individualfiles/bcmca_eco_vascplants_eelgrass_bioband_atlas.pdf

also observed on the Washington coast (Pfister et al., 2018), which the study authors also attributed to *Nereocystis'* ruderal nature.

3.6 Conclusion

This study examined kelp forest responses to environmental changes in the dynamic subregion of the Broughton Archipelago across different spatial and temporal scales. Temporally, we documented overall kelp persistence in the dynamic subregion of the Broughton Archipelago, including areal increases from 1984 to 2023 in the *Macrocystis* site and primarily no significant change in kelp area at *Nereocystis* sites from 2016 to 2023. Increased local SST into the thermal optimum of *Macrocystis* was associated with increases in *Macrocystis* area, whereas regional SST, MHWs, and climatic oscillations did not affect it. *Nereocystis* area did not appear to be affected by environmental conditions at local, regional, and global scales, likely as temperatures remained within its thermal optimum. Spatially, we found that most sites had spatially persistent kelp, and areas in the center of a kelp bed were more likely to be persistent than the edges. The *Macrocystis* site had more spatially persistent areas than the *Nereocystis* sites.

In a broader context, our findings add to the understanding of kelp forest trends and patterns of persistence in the face of environmental changes in BC, the Northeast Pacific Ocean, and other temperate regions globally. The patterns observed in the dynamic subregion of the Broughton Archipelago reinforce findings that regional events such as MHWs may not negatively impact kelp populations if local conditions are favorable. Ultimately, by filling in the geographic gaps of kelp change, this study can inform marine spatial planning efforts such as the creation of protected areas, kelp harvest regulations, and restoration decisions.

4.0 Summary and Conclusion

4.1 Thesis overview

This thesis aimed to define the spatiotemporal distribution, abundance, and persistence of kelp forests in the Broughton Archipelago, which was accomplished with the following objectives.

The first objective: 1) Identify environmental and biotic variables that drive spatial differences in kelp forest distribution and abundance, was addressed in Chapter 2. We achieved this by mapping floating kelp abundance at 31 focal sites across the environmental gradient using UAV and very-high-resolution satellite imagery, compiling environmental data from in-situ sources and environmental models, and characterizing grazer (*Strongylocentrus* spp. and *Mesocentrotus franciscanus*, "sea urchins") and predator (sunflower sea stars, *Pycnopodia helianthoides*) abundances using ROV footage. From the environmental variables, we identified two environmentally distinct subregions in the Broughton Archipelago: a cooler, more dynamic archipelago subregion to the west, and a warmer, more sheltered fjord subregion to the east and north. Next, we found that lower SST, flatter bottom slopes, and higher tidal current speeds, typical of the archipelago subregion, were positively associated with kelp abundance, whereas the higher SST, steeper bottom slopes, and lower tidal current speeds of the fjord subregion were negatively associated with kelp abundance. Conversely, sea urchin and *Pycnopodia* abundances did not significantly relate to kelp abundance; nevertheless, they formed spatial patterns where sea urchin abundances were the highest within the archipelago subregion, and *Pycnopodia* abundances were the highest within the fjord subregion. These results reinforce other literature on the interactions between the environment and kelps and provide additional insight into how environmental gradients may potentially interact with kelp-urchin-*Pycnopodia* relationships. Furthermore, these findings informed our site selection for Objective 2--to understand the temporal kelp change of the more abundant kelp forests in the region.

The second objective: 2) Investigate spatiotemporal persistence and resilience of kelp forests in the face of environmental change, was addressed in Chapter 3. This was achieved for one large *Macrocystis* site and eight *Nereocystis* sites in the archipelago subregion by using satellite imagery

and environmental data to (1) identify long-term (1984 to 2023) and short-term (2016 to 2023) kelp responses to environmental changes, and spatially combining kelp areas to (2) identify spatial patterns of kelp persistence. Kelp areas remained mostly persistent across both timescales despite showing interannual variability. For the *Macrocystis* site (1984 to 2023), kelp areas showed an increasing monotonic trend across the entire time series, with significant increases occurring after 1999. For the eight *Nereocystis* sites (2016 to 2023), kelp was persistent in seven sites, with six sites not significantly changing in area and one site significantly increasing in area. Only one site displayed non-persistence, with some years of kelp loss. *Macrocystis* beds had a higher percent persistent area than *Nereocystis* beds, suggesting life history and/or other factors may be at play. This suggests that the dynamic archipelago subregion region may be a climate refuge for kelps, likely due to its cool water temperatures that remain within kelps' optimal thermal ranges. Importantly, we did not conduct a time series analysis for the fjord subregion, which was established as a subregion with more suboptimal conditions for kelp than the archipelago subregion, thus we cannot extrapolate the findings of kelp persistence to this the fjord subregion. Overall, this chapter demonstrated the persistence of kelp systems in the dynamic archipelago subregion of the Broughton Archipelago.

Ultimately, this research addresses a gap in geographic coverage of kelp forest research, synthesizing our knowledge on kelp forest distribution, abundance, and factors driving changes at different spatial and temporal scales. Notably, it enhances our understanding of the environmental and biological factors influencing kelp distribution and abundance in BC, a region with a complex coastline that presents diverse, often undocumented conditions at the local level. This work also contributes to a broader understanding of kelp dynamics in BC, which currently lacks extensive, long-term data on kelp forest changes. Furthermore, it enriches the literature on the remote sensing of kelp forests, focusing on BC, where satellite remote sensing is challenging due to the area's intricate topography and relatively smaller kelp forests. Ultimately, the spatial patterns observed in kelp distribution, abundance, and persistence, along with related environmental and biotic factors, underscore the need to monitor kelp forests across environmental gradients. This work laid a strong foundation for future efforts in monitoring, managing, and protecting these ecosystems, informing

marine spatial planning efforts such as the creation of protected areas, kelp harvest regulations, and restoration decisions.

4.2 Limitations and Future Research

This research's primary limitation lies in the spatial and temporal availability of high-quality kelp imagery and associated environmental and biotic driver data. Chapter 2 utilized UAV and satellite imagery with high spatial resolution (2.30-46.0 cm), ROV surveys, and CTD deployments to investigate the drivers of the kelp forest distribution and abundance at 31 sites across the environmentally and biotically distinct archipelago and fjord subregions**.** However, this study had low temporal resolution (summer of 2023), thus, our characterization of kelp distribution and abundance may have been affected by environmental and biotic conditions unique to that year. Conversely, Chapter 3 utilized datasets of higher temporal resolution (long-term: 1984 to 2023, short-term: *Nereocystis* datasets), resulting in a more in-depth understanding of kelp change over time. However, spatially, it only covered eight focal sites in the archipelago subregion and did not include the fjord subregion at all, thus our conclusion of kelp forest persistence may not apply to those in the fjord subregion due to its more suboptimal environmental conditions for kelp. Moreover, despite the inclusion of continuous regional and global-scale environmental data, our characterization of the local drivers of change was limited. Local SST data was discontinuous due to high cloud cover limiting satellite imagery availability, and we lacked biotic driver data due to the lack of consistent subtidal biomonitoring efforts in the region. Ultimately, the two chapters, with their respective emphasis on the spatial and temporal dimensions, somewhat compensate for their limitations on spatial and temporal availability, resulting in a comprehensive understanding of the kelp dynamics in the Broughton Archipelago.

Future work can expand on this research in regional and global scales. To improve our understanding of kelp persistence and resilience in the Broughton Archipelago, researchers can use very-high-resolution Worldview satellite imagery (0.46-1.84 m) to investigate temporal kelp change

in the fjord subregion as well as coastlines not covered by the sites in both chapters. Higher spatial resolution results in less pixel mixing between land, kelp, and water, offering higher accuracy in detecting smaller kelp beds in the fjord subregion. Furthermore, drone flights, ROV surveys, and CTD deployments can be repeated in some of the focal sites in future summers to investigate potential temporal changes in the environmental and biotic drivers. Finally, to gain temporally continuous satellite-derived SST data, it is worth exploring other satellite platforms with higher revisit frequency than Landsat (e.g. MODIS and Sentinel-3), with the trade-offs of lower spatial resolutions (MODIS: 1 km, Sentinel-3: 300 m, Landsat: 30 m) and temporal availability (MODIS: 2002-present, Sentinel-3: 2016-present, Landsat: 1984 to 2023). This would allow the more frequent characterization of local SST temporal change without having to conduct field measurements repeatedly. Regionally, future work can continue to fill in the geographic gaps across the coast of BC to better understand kelp persistence and resilience across this diverse coastline.

5.0 References

Abdi, H., & Williams L.J. (2010). Principal component analysis. *Wiley interdisciplinary reviews*: computational statistics, *2*(4), 433-459. https://doi.org/10.1002/wics.101

Akaike H (1974). A new look at the statistical model identification. *IEEE transactions on automatic control*, *19*(6), 716-723.

Alexandre, A., Baeta, A., Engelen, A. H., & Santos, R. (2017). Interactions between seagrasses and seaweeds during surge nitrogen acquisition determine interspecific competition. *Scientific Reports*, *7*(1), 13651. https://doi.org/10.1038/s41598-017-13962-4

Amos, C. L., Martino, S., Sutherland, T. F., & Al Rashidi, T. (2015). Sea surface temperature trends in the coastal zone of British Columbia, Canada. *Journal of Coastal Research*, *31*(2), 434-446. https://doi.org/10.2112/jcoastres-d-14-00114.1

Arafeh-Dalmau, N., Montaño-Moctezuma, G., Martinez, J.A., Beas-Luna, R., Schoeman, D.S., Torres-Moye, G. (2019). Extreme Marine Heatwaves Alter Kelp Forest Community Near Its Equatorward Distribution Limit. *Frontiers in Marine Science. 6*, 499 https://doi.org/10.3389/fmars.2019.00499

Arafeh-Dalmau N, Olguín-Jacobson C., Bell TW, Micheli F, & Cavanaugh KC (2023). Shortfalls in the protection of persistent bull kelp forests in the USA. *Biological Conservation, 283*, 110133. https://doi.org/10.1016/j.biocon.2023.110133

Bates, D., Maechler, M., Bolker, B., Walker, S., Christensen, R. H. B., Singmann, H., ... & Bolker, M. B. (2015). Package 'lme4'. *convergence*, *12*(1), 2.

Bayley D, Brickle P, Brewin P, Golding N. and Pelembe, T. (2021). Valuation of kelp forest ecosystem services in the Falkland Islands: A case study integrating blue carbon sequestration potential. *One Ecosystem*, *6*, 62811. https://doi.org/10.3897/oneeco.6.e62811

BC Parks (2003) Broughton Archipelago Park. https://bcparks.ca/broughton-archipelago-park/ [Accessed 5 August 2024].

Beas-Luna, R., Micheli, F., Woodson, C. B., Carr, M., Malone, D., Torre, J., ... & Torres-Moye, G. (2020). Geographic variation in responses of kelp forest communities of the California Current to recent climatic changes. *Global Change Biology*, *26*(11), 6457-6473. https://doi.org/10.1111/gcb.15273

Bekkby, T., Smit, C., Gundersen, H., Rinde, E., Steen, H., Tveiten, L., Gitmark, J.K., Fredriksen, S., Albretsen, J. and Christie, H. (2019). The abundance of kelp is modified by the combined impact of depth, waves and currents. *Frontiers in Marine Science*, *6*,.475. https://doi.org/10.3389/fmars.2019.00475

Bell, T.W., Allen, J.G., Cavanaugh, K.C. and Siegel, D.A. (2020). Three decades of variability in California's giant kelp forests from the Landsat satellites. *Remote Sensing of Environment*, *238*, 110811. https://doi.org/10.1016/j.rse.2018.06.039

Bell, T. W., Cavanaugh, K. C., Reed, D. C., & Siegel, D. A. (2015). Geographical variability in the controls of giant kelp biomass dynamics. *Journal of Biogeography*, *42*(10), 2010-2021.https://doi.org/10.1111/jbi.12550

Bell, T. W., Cavanaugh, K. C., Saccomanno, V. R., Cavanaugh, K. C., Houskeeper, H. F., Eddy, N., ... & Gleason, M. (2023). Kelpwatch: A new visualization and analysis tool to explore kelp canopy dynamics reveals variable response to and recovery from marine heatwaves. *Plos one*, *18*(3), e0271477. https://doi.org/10.1371/journal.pone.0271477

Benjamini, Y., & Hochberg, Y. (1995). Controlling the false discovery rate: a practical and powerful approach to multiple testing. *Journal of the Royal statistical society: series B (Methodological)*, *57*(1), 289-300.https://doi.org/10.1111/j.2517-6161.1995.tb02031.x

Berry, H. D., Mumford, T. F., Christiaen, B., Dowty, P., Calloway, M., Ferrier, L., ... & VanArendonk, N. R. (2021). Long-term changes in kelp forests in an inner basin of the Salish Sea. *PloS one*, *16*(2), e0229703. https://doi.org/10.1371/journal.pone.0229703

Blaschke, T. (2010). Object based image analysis for remote sensing. *ISPRS journal of photogrammetry and remote sensing*, *65*(1), 2-16. https://doi.org/10.1016/j.isprsjprs.2009.06.004

Bonaviri, C., Graham, M., Gianguzza, P. and Shears, N.T. (2017). Warmer temperatures reduce the influence of an important keystone predator. *Journal of Animal Ecology*, *86*(3), 490-500. https://doi.org/10.1111/1365-2656.12634

Bond, N. A., Cronin, M. F., Freeland, H., & Mantua, N. (2015). Causes and impacts of the 2014 warm anomaly in the NE Pacific. *Geophysical Research Letters*, *42*(9), 3414-3420. https://doi.org/10.1002/2015gl063306

Burt, J.M., Tinker, M.T., Okamoto, D.K., Demes, K.W., Holmes, K. and Salomon, A.K. (2018). Sudden collapse of a mesopredator reveals its complementary role in mediating rocky reef regime shifts. *Proceedings of the Royal Society B: Biological Sciences*, 285(1883), 20180553. https://doi.org/10.6084/m9.figshare.c.4161416.v2

Brewer-Dalton, K., Page, F. H., Chandler, P., & Ratsimandresey, A. (2014). *Oceanographic conditions of salmon farming areas with attention to those factors that may influence the biology and ecology of sea lice, Lepeophtherius salmonis and Caligus spp., and their control.* DFO Can. Sci. Advis. Sec. Res. Doc, 48.

Broughton Aquaculture Transition Initiative. (2020). Winter 2020 Update.

Broughton Aquaculture Transition Initiative. (2021). Declining Kelp Forests in the Broughton Area. Spring 2021 Update.

Buscher, E., Mathews, D. L., Bryce, C., Bryce, K., Joseph, D., & Ban, N. C. (2020). Applying a low cost, mini remotely operated vehicle (ROV) to assess an ecological baseline of an indigenous seascape in Canada. *Frontiers in Marine Science*, *7*, 669. doi.org/10.3389/fmars.2020.00669

Cabaitan, P., Licuanan, W., & Gomez, E. (2007). Comparison Between Videographic and Photographic Methods in Assessing Coral Reef Bethnic Communities. *Science Diliman*, *19*(1).

Campbell, A. and Harbo, R.M. (2020). The sea urchin fisheries in British Columbia, Canada. In *Biology of Echinodermata.* 191-199. CRC Press.

Cavanaugh, K.C., Bell, T., Costa, M., Eddy, N.E., Gendall, L., Gleason, M.G., Hessing-Lewis, M., Martone, R., McPherson, M., Pontier, O. and Reshitnyk, L. (2021). A review of the opportunities and challenges for using remote sensing for management of surface-canopy forming kelps. *Frontiers in Marine Science*, *8*, 753531. https://doi.org/10.3389/fmars.2021.753531

Cavanaugh, K. C., Cavanaugh, K. C., Pawlak, C. C., Bell, T. W., & Saccomanno, V. R. (2023). CubeSats show persistence of bull kelp refugia amidst a regional collapse in California. *Remote Sensing of Environment*, *290*, 113521. https://doi.org/10.1016/j.rse.2023.113521

Cavanaugh, K. C., Kendall, B. E., Siegel, D. A., Reed, D. C., Alberto, F., & Assis, J. (2013). Synchrony in dynamics of giant kelp forests is driven by both local recruitment and regional environmental controls. *Ecology*, *94*(2), 499-509. https://doi.org/10.1890/12-0268.1

Cavanaugh, K.C., Siegel, D.A., Reed, D.C. and Dennison, P.E. (2011). Environmental controls of giant-kelp biomass in the Santa Barbara Channel, California. *Marine Ecology Progress Series, 429*, pp.1-17.. https://doi.org/10.3354/meps09141

Charrad, M., Ghazzali, N., Boiteau, V. and Niknafs, A. (2014). NbClust: an R package for determining the relevant number of clusters in a data set. *Journal of statistical software*, *61*, 1-36. https://doi.org/10.18637/jss.v061.i06

Cheng, L., von Schuckmann, K., Abraham, J. P., Trenberth, K. E., Mann, M. E., Zanna, L., ... & Lin, X. (2022). Past and future ocean warming. *Nature Reviews Earth & Environment*, *3*(11), 776-794.https://doi.org/10.1038/s43017-022-00345-1

Connell, J. H., & Sousa, W. P. (1983). On the evidence needed to judge ecological stability or persistence. *The American Naturalist*, *121*(6), 789-824. https://doi.org/10.1086/284105

Costa, M., Le Baron, N., Tenhunen, K., Nephin, J., Willis, P., Mortimor, J.P., Dudas, S. and Rubidge, E. (2020). Historical distribution of kelp forests on the coast of British Columbia: 1858–1956. *Applied geography*, *120*, 102230. https://doi.org/10.1016/j.apgeog.2020.102230

Cowdrey T. (2021). *Mapping Bull Kelp (Nereocystis luetkeana) forests in Puget Sound with a consumer-level unmanned aerial vehicle.* [master's thesis]. [Olympia (WA)]: Evergreen State College.

Cowdrey, T. & Claar, D. (2024). *Monitoring Puget Sound Bull Kelp Forests with Multispectral UAS: An Index-Based Approach.* Washington State Dept of Natural Resources. https://www.dnr.wa.gov/publications/aqr_nrsh_monitoring_bull_kelp_multispectral_uas.pdf. [Accessed August 5 2024]

Cowen, R. K., Agegian, C. R., & Foster, M. S. (1982). The maintenance of community structure in a central California giant kelp forest. *Journal of experimental marine biology and ecology*, *64*(2), 189-201.

Davies, S.C., Gregr, E. J., Lessard, J., Bartier, P., Wills, P. (2018). *Coastal digital elevation models integrating ocean bathymetry and land topography for marine ecological analyses in Pacific Canadian waters*.Can. Tech. Rep. Fish. Aquat. Sci. 3321: vi + 38 p

Dayton, P. K. (1985). The structure and regulation of some South American kelp communities. *Ecological monographs*, *55*(4), 447-468.

Dayton, P. K., Currie, V., Gerrodette, T., Keller, B. D., Rosenthal, R., & Tresca, D. V. (1984). Patch dynamics and stability of some California kelp communities. *Ecological monographs*, *54*(3), 253-289. https://doi.org/10.2307/1942498

Dayton, P. K., Tegner, M. J., Edwards, P. B., & Riser, K. L. (1999). Temporal and spatial scales of kelp demography: the role of oceanographic climate. *Ecological Monographs*, *69*(2), 219-250.. *Ecological Monographs*. https://doi.org/10.1890/0012-9615(1999)069[0219:tassok]2.0.co;2

Dean, T. A., & Jacobsen, F. R. (1984). Growth of juvenile Macrocystis pyrifera (Laminariales) in relation to environmental factors. *Marine Biology*, *83*, 301-311.

Department of Fisheries & Oceans (2015) *Report on the Progress of Recovery Strategy Implementation for Northern Abalone (Haliotis kamtschatkana) in Pacific Canadian Waters for the Period 2007-2012*. Fisheries and Oceans Canada. https://wildlife-species.canada.ca/species-risk-registry/virtual_sara/files/Pr-NorthernAbalone-v01-2015Jul13-Eng.pdf [Accessed August 5, 2024]

Deysher, L., Dean, T.A. (1986). In situ recruitment of sporophytes of the giant kelp, Macrocystis pyrifera (L.) C.A. Agardh: *Effects of physical factors. Journal of Experimental Marine Biology and Ecology*. https://doi.org/10.1016/0022-0981(86)90131-0

Di Lorenzo, E., & Mantua, N. (2016). Multi-year persistence of the 2014/15 North Pacific marine heatwave. *Nature Climate Change*, *6*(11), 1042-1047. https://doi.org/10.1038/nclimate3082

Di Lorenzo, E., Schneider, N., Cobb, K. M., Franks, P. J. S., Chhak, K., Miller, A. J., ... & Rivière, P. (2008). North Pacific Gyre Oscillation links ocean climate and ecosystem change. Geophysical research letters, 35(8).https://doi.org/10.1029/2007gl032838

Drinkwater, K. F., & Jones, E. P. (1987). Density stratification, nutrient and chlorophyll distributions in the Hudson Strait region during summer and their relation to tidal mixing. *Continental Shelf Research*, *7*(6), 599-607.

Druehl, L. D. (1977). The distribution of Macrocystis integrifolia in British Columbia as related to environmental parameters. *Canadian Journal of Botany*, *56*(1), 69–79.

Druehl, L., & Clarkston, B. (2016). *Pacific seaweeds: Updated and expanded edition*. Harbour publishing.

Duggins, D. O. (1983). Starfish predation and the creation of mosaic patterns in a kelp-dominated community. *Ecology*, *64*(6), 1610-1619.

Dunn, O. J. (1964). Multiple comparisons using rank sums. *Technometrics*, *6*(3), 241-252.

Dunn P. K. (2022). Tweedie: Evaluation of Tweedie Exponential Family Models. R package version 2.3.5. https://cran.r-project.org/web/packages/tweedie/index.html. [Accessed August 5, 2024]

Eger, A.M., Marzinelli, E.M., Beas-Luna, R., Blain, C.O., Blamey, L.K., Byrnes, J.E., Carnell, P.E., Choi, C.G., Hessing-Lewis, M., Kim, K.Y. and Kumagai, N.H., 2023. The value of ecosystem services in global marine kelp forests. *Nature communications*, *14*(1), p.1894. https://doi.org/10.1038/s41467-023-37385-0

Eisaguirre, J. H., Eisaguirre, J. M., Davis, K., Carlson, P. M., Gaines, S. D., & Caselle, J. E. (2020). Trophic redundancy and predator size class structure drive differences in kelp forest ecosystem dynamics. *Ecology, 101*(5), e02993.https://doi.org/10.1002/ecy.2993

European Space Agency. (n.d.). About WorldView Series. Retrieved from: https://earth.esa.int/eogateway/missions/worldview [Accessed September 25, 2024]

European Space Agency. (n.d.). Planetscope Overview. Retrieved from: https://earth.esa.int/eogateway/missions/planetscope/description [Accessed September 25, 2024]

Fernández, P. A., Gaitán-Espitia, J. D., Leal, P. P., Schmid, M., Revill, A. T., & Hurd, C. L. (2020). Nitrogen sufficiency enhances thermal tolerance in habitat-forming kelp: implications for acclimation under thermal stress. *Scientific Reports*, *10*(1), 3186. https://doi.org/10.1038/s41598-020-60104-4

Filbee-Dexter, K., & Scheibling, R. E. (2014). Detrital kelp subsidy supports high reproductive condition of deep-living sea urchins in a sedimentary basin. *Aquatic Biology*, *23*(1), 71-86. https://doi.org/10.3354/meps10573

Filbee-Dexter, K., Starko, S., Pessarrodona, A., Wood, G., Norderhaug, K. M., Piñeiro-Corbeira, C., & Wernberg, T. (2024). Marine protected areas can be useful but are not a silver bullet for kelp conservation. *Journal of Phycology*, *60*(2), 203-213. https://doi.org/10.1111/jpy.13446

Filbee-Dexter, K., & Wernberg, T. (2018). Rise of turfs: a new battlefront for globally declining kelp forests. *Bioscience*, *68*(2), 64-76. https://doi.org/10.1093/biosci/bix147

Fisheries & Oceans Canada. *British Columbia Lightstation Sea-Surface Temperature and Salinity Data (Pacific), 1914-present.* Retrieved from: https://open.canada.ca/data/en/dataset/719955f2-bf8e-44f7-bc26-6bd623e82884 [Accessed August 5, 2024]

Foreman, M. G. G., Stucchi, D. J., Zhang, Y., & Baptiste, A. M. (2006). Estuarine and tidal currents in the Broughton Archipelago. *Atmosphere-Ocean*, *44*(1), 47-63. https://doi.org/10.3137/ao.440104

Foreman, M. G. G., Czajko, P., Stucchi, D. J., & Guo, M. (2009). A finite volume model simulation for the Broughton Archipelago, Canada. *Ocean Modelling*, *30*(1), 29-47. https://doi.org/10.1016/j.ocemod.2009.05.009

Fox, J., & Weisberg, S. (2018). An R companion to applied regression. Sage publications.

Frölicher, T.L., Fischer, E.M., Gruber, N. (2018). Marine heatwaves under global warming. *Nature*. https://doi.org/10.1038/s41586-018-0383-9

Galloway, A. W. E., Gravem, S. A., Kobelt, J. N., Heady, W. N., Okamoto, D. K., Sivitilli, D. M., ... & Whippo, R. (2023). Sunflower sea star predation on urchins can facilitate kelp forest

recovery. *Proceedings of the Royal Society B*, *290*(1993), 20221897. https://doi.org/10.1098/rspb.2022.1897

Gendall, L., Schroeder, S. B., Wills, P., Hessing-Lewis, M., & Costa, M. (2023). A multi-satellite mapping framework for floating kelp forests. *Remote Sensing*, *15*(5), 1276. https://doi.org/10.3390/rs15051276

Gendall, L.; Hessing-Lewis, M;; Wachmann, A; Schroeder S., Reshitnyk, L., Crawford S., Lee L., Guujaaw N., Costa, M., submitted. Drivers of Change in Haida Gwaii Kelp Forests: Combining Satellite Imagery with Historical Data to Understand Spatial and Temporal Variability.

Getis, A., & Ord, J. K. (1992). The analysis of spatial association by use of distance statistics. *Geographical analysis*, *24*(3), 189-206. https://doi.org/10.1111/j.1538-4632.1992.tb00261.x

Giesbrecht, I. J., Tank, S. E., Frazer, G. W., Hood, E., Gonzalez Arriola, S. G., Butman, D. E., ... & Lertzman, K. P. (2022). Watershed classification predicts streamflow regime and organic carbon dynamics in the Northeast Pacific coastal temperate rainforest. *Global Biogeochemical Cycles*, *36*(2), e2021GB007047. https://doi.org/10.1029/2021GB007047

Graham, M.H., 2003. Coupling propagule output to supply at the edge and interior of a giant kelp forest. *Ecology*. https://doi.org/10.1890/0012-9658(2003)084[1250:cpotsa]2.0.co;2

Gregr, E.J., Christensen, V., Nichol, L., Martone, R.G., Markel, R.W., Watson, J.C., Harley, C.D., Pakhomov, E.A., Shurin, J.B. and Chan, K.M., 2020. Cascading social-ecological costs and benefits triggered by a recovering keystone predator. *Science*, *368*(6496), pp.1243-1247. https://doi.org/10.1126/science.aay5342

Gregr, E., Peterman, M., & Lessard, J. (2018). *Coastline Fetch estimates for Pacific Canada.* Marine Spatial Ecology Section, Fisheries and Oceans Canada. Retrieved from: https://open.canada.ca/data/en/dataset/412431c4-7363-410e-86a4-76feb9a6dcde [Accessed on September 25, 2024]

Gregr, E. J., Palacios, D. M., Thompson, A., & Chan, K. M. (2019). Why less complexity produces better forecasts: an independent data evaluation of kelp habitat models. *Ecography*, *42*(3), 428-443. https://nsojournals.onlinelibrary.wiley.com/doi/10.1111/ecog.03470

Greene, H. G., Yoklavich, M. M., Starr, R. M., O'Connell, V. M., Wakefield, W. W., Sullivan, D. E., ... & Cailliet, G. M. (1999). A classification scheme for deep seafloor habitats. *Oceanologica acta*, *22*(6), 663-678.

Gonzalez-Aragon, D., Rivadeneira, M. M., Lara, C., Torres, F. I., Vásquez, J. A., & Broitman, B. R. (2024). A species distribution model of the giant kelp Macrocystis pyrifera: worldwide changes and a focus on the Southeast Pacific. *Ecology and Evolution*, *14*(3), e10901. https://doi.org/10.1002/ece3.10901

Gupta, N., & Bhadauria, H. S. (2014, September). Object-oriented approach of information extraction from panchromatic satellite images based on fuzzy logic. In *2014 5th International Conference-Confluence The Next Generation Information Technology Summit (Confluence)* (pp. 651-656). IEEE. https://doi.org/10.1109/CONFLUENCE.2014.6949274

Hadjimitsis, D.G., Clayton, C.R.I., Retalis, A. (2004). On the darkest pixel atmospheric correction algorithm: a revised procedure applied over satellite remotely sensed images intended for environmental applications. *Remote Sensing*. https://doi.org/10.1117/12.511520

Haggarty, D., Gregr, E., Lessard, J., Fields, C., Davies, S. (2020). *Shallow substrate model (20m) of the Pacific Canadian coast.* Department of Fisheries and Oceans. https://osdp-psdo.canada.ca/dp/en/search/metadata/NRCAN-FGP-1-b100cf6c-7818-4748-9960-9eab2aa6a7a0. [Accessed on August 5, 2024].

Hamilton, S.L., Bell, T.W., Watson, J.R., Grorud-Colvert, K., Menge, B.A. (2020). Remote sensing: generation of long-term kelp bed data sets for evaluation of impacts of climatic variation. *Ecology*. https://doi.org/10.1002/ecy.3031

Hamilton, S. L., Saccomanno, V. R., Heady, W. N., Gehman, A. L., Lonhart, S. I., Beas-Luna, R., ... & Gravem, S. A. (2021). Disease-driven mass mortality event leads to widespread extirpation and variable recovery potential of a marine predator across the eastern Pacific. *Proceedings of the Royal Society B*, *288*(1957), 20211195. https://doi.org/10.1098/rspb.2021.1195

Hartigan, J. A., & Wong, M. A. (1979). Algorithm AS 136: A k-means clustering algorithm. *Journal of the royal statistical society. series c (applied statistics)*, *28*(1), 100-108.

Harvell, C. D., Montecino-Latorre, D., Caldwell, J. M., Burt, J. M., Bosley, K., Keller, A., ... & Gaydos, J. K. (2019). Disease epidemic and a marine heat wave are associated with the continental-scale collapse of a pivotal predator (Pycnopodia helianthoides). *Science advances*, *5*(1), eaau7042. https://doi.org/10.1126/sciadv.aau7042

Hawkins, D. M. (2004). The problem of overfitting. *Journal of chemical information and computer sciences*, *44*(1), 1-12. https://doi.org/10.1021/ci0342472

Hay, C. H. (1990). The distribution of Macrocystis (Phaeophyta: Laminariales) as a biological indicator of cool sea surface temperature, with special reference to New Zealand waters. *Journal of the Royal Society of New Zealand*, *20*(4), 313-336.

Held, M. B., & Harley, C. D. (2009). Responses to low salinity by the sea star Pisaster ochraceus from high-and low-salinity populations. *Invertebrate Biology*, *128*(4), 381-390. https://doi.org/10.1111/j.1744-7410.2009.00175.x

Hemery, L. G., Marion, S. R., Romsos, C. G., Kurapov, A. L., & Henkel, S. K. (2016). Ecological niche and species distribution modelling of sea stars along the Pacific Northwest continental shelf. *Diversity and Distributions*, *22*(12), 1314-1327. https://doi.org/10.1111/ddi.12490

Hobday, A.J., Alexander, L.V., Perkins, S.E., Smale, D.A., Straub, S.C., Oliver, E.C.J., Benthuysen, J.A., Burrows, M.T., Donat, M.G., Feng, M., Holbrook, N.J., Moore, P.J., Scannell, H.A., Gupta, A.S., Gupta, A.S., Wernberg, T. (2016). A hierarchical approach to defining marine heatwaves. *Progress in Oceanography*. https://doi.org/10.1016/j.pocean.2015.12.014

Hodson, A., Mumford, P., & Lister, D. (2004). Suspended sediment and phosphorus in proglacial rivers: bioavailability and potential impacts upon the P status of ice-marginal receiving waters. *Hydrological processes*, *18*(13), 2409-2422. https://doi.org/10.1002/hyp.1471

Hollarsmith, J. A., Andrews, K., Naar, N., Starko, S., Calloway, M., Obaza, A., ... & Therriault, T. W. (2022). Toward a conceptual framework for managing and conserving marine habitats: A case study of kelp forests in the Salish Sea. *Ecology and Evolution*, *12*(1), e8510. https://doi.org/10.1002/ece3.8510

Hollarsmith, J. A., Buschmann, A. H., Camus, C., & Grosholz, E. D. (2020). Varying reproductive success under ocean warming and acidification across giant kelp (Macrocystis pyrifera) populations. *Journal of Experimental Marine Biology and Ecology*, *522*, 151247. https://doi.org/10.1016/j.jembe.2019.151247

Hollarsmith, J. A., Cornett, J. C., Evenson, E., & Tugaw, A. (2024). A century of canopy kelp persistence and recovery in the Gulf of Alaska. *Annals of Botany*, *133*(1), 105-116. https://doi.org/10.1093/aob/mcad149

Holling, C.S. (1973). Resilience and Stability of Ecological Systems. *Annual Review of Ecology*, Evolution, and Systematics. https://doi.org/10.1146/annurev.es.04.110173.000245

Houskeeper, H. F., Rosenthal, I. S., Cavanaugh, K. C., Pawlak, C., Trouille, L., Byrnes, J. E., ... & Cavanaugh, K. C. (2022). Automated satellite remote sensing of giant kelp at the Falkland Islands (Islas Malvinas). *PLoS One*, *17*(1), e0257933. https://doi.org//10.1371/journal.pone.0257933

Huovinen, P., Ramírez, J., Palacios, M., & Gómez, I. (2020). Satellite-derived mapping of kelp distribution and water optics in the glacier impacted Yendegaia Fjord (Beagle Channel, Southern Chilean Patagonia). *Science of the Total Environment*, *703*, 135531.https://doi.org/10.1016/j.scitotenv.2019.135531

Jackson, G. A., & Winant, C. D. (1983). Effect of a kelp forest on coastal currents. *Continental Shelf Research*, *2*(1), 75-80. https://doi.org/10.1016/0278-4343(83)90023-7

Jayathilake, D. R., & Costello, M. J. (2021). Version 2 of the world map of laminarian kelp benefits from more Arctic data and makes it the largest marine biome. *Biological Conservation*, *257*, 109099. https://doi.org/10.1016/j.biocon.2021.109099

Karez, R., Engelbert, S., Kraufvelin, P., Pedersen, M. F., & Sommer, U. (2004). Biomass response and changes in composition of ephemeral macroalgal assemblages along an experimental gradient of nutrient enrichment. *Aquatic botany*, *78*(2), 103-117. https://doi.org/10.1016/j.aquabot.2003.09.008

Kendall, M. G. (1948). Rank correlation methods. Griffin.

Knudby, A. (2021). Remote sensing.

Korabik, A. R., Winquist, T., Grosholz, E. D., & Hollarsmith, J. A. (2023). Examining the reproductive success of bull kelp (Nereocystis luetkeana, Phaeophyceae, Laminariales) in climate change conditions. *Journal of Phycology*, *59*(5), 989-1004. https://doi.org/10.1111/jpy.13368

Krause-Jensen, D., & Duarte, C. M. (2016). Substantial role of macroalgae in marine carbon sequestration. *Nature Geoscience*, *9*(10), 737-742. https://doi.org/10.1038/ngeo2790

Kriegisch, N., Reeves, S. E., Flukes, E. B., Johnson, C. R., & Ling, S. D. (2019). Drift-kelp suppresses foraging movement of overgrazing sea urchins. *Oecologia*, *190*, 665-677. https://doi.org/10.1007/s00442-019-04445-6

Krumhansl, K. A., Okamoto, D. K., Rassweiler, A., Novak, M., Bolton, J. J., Cavanaugh, K. C., ... & Byrnes, J. E. (2016). Global patterns of kelp forest change over the past half-century. *Proceedings of the National Academy of Sciences*, *113*(48), 13785-13790. https://doi.org/10.1073/pnas.1606102113

Kruskal, W. H., & Wallis, W. A. (1952). Use of ranks in one-criterion variance analysis. *Journal of the American statistical Association*, *47*(260), 583-621.

Konar, B. and Estes, J.A., 2003. The stability of boundary regions between kelp beds and deforested areas. *Ecology*, *84*(1), pp.174-185. https://doi.org/10.1890/0012-9658(2003)084[0174:TSOBRB]2.0.CO;2

Kvile, K. Ø., Andersen, G. S., Baden, S. P., Bekkby, T., Bruhn, A., Geertz-Hansen, O., ... & Gundersen, H. (2022). Kelp forest distribution in the Nordic region. *Frontiers in Marine Science*, 9, 850359. https://doi.org/10.3389/fmars.2022.850359

Laben, C. A., & Brower, B. V. (2000). U.S. Patent No. 6,011,875. Washington, DC: U.S. Patent and Trademark Office.

Ladah, L. B., & Zertuche-González, J. A. (2007). Survival of microscopic stages of a perennial kelp (Macrocystis pyrifera) from the center and the southern extreme of its range in the Northern Hemisphere after exposure to simulated El Niño stress. *Marine Biology*, *152*, 677-686. https://doi.org/10.1007/s00227-007-0723-z

Lamy, T., Koenigs, C., Holbrook, S. J., Miller, R. J., Stier, A. C., & Reed, D. C. (2020). Foundation species promote community stability by increasing diversity in a giant kelp forest. *Ecology*, *101*(5), e02987. https://doi.org/10.1002/ecy.2987

Le, D. M., Desmond, M. J., Buschmann, A. H., Pritchard, D. W., Camus, C., Hurd, C. L., & Hepburn, C. D. (2022). Reproduction, hatchery and culture applications for the giant kelp (Macrocystis pyrifera): a methodological appraisal. *Applied Phycology*, *3*(1), 368-382. https://doi.org/10.1371/journal.pone.0278268

Levitus, S., Antonov, J. I., Boyer, T. P., & Stephens, C. (2000). Warming of the world ocean. *Science*, *287*(5461), 2225-2229. https://doi.org/10.1126/science.287.5461.2225

Li, H., Monteiro, C., Heinrich, S., Bartsch, I., Valentin, K., Harms, L., ... & Bischof, K. (2020). Responses of the kelp Saccharina latissima (Phaeophyceae) to the warming Arctic: from physiology to transcriptomics. *Physiologia plantarum*, *168*(1), 5-26. https://doi.org/10.1111/ppl.13009

Lin, Y., & Bianucci, L. (2023). Seasonal Variability of the Ocean Circulation in Queen Charlotte Strait, British Columbia. *Atmosphere-Ocean*, 1-23. https://doi.org/10.1080/07055900.2023.2184321

Lind, A. C., Konar, B. (2017). Effects of abiotic stressors on kelp early life-history stages. *Algae*, *32*(3), 223-233. https://doi.org/10.4490/algae.2017.32.8.7

Ling, S. D., Scheibling, R. E., Rassweiler, A., Johnson, C. R., Shears, N., Connell, S. D., ... & Johnson, L. E. (2015). Global regime shift dynamics of catastrophic sea urchin overgrazing. *Philosophical Transactions of the Royal Society B: Biological Sciences*, *370*(1659), 20130269. http://dx.doi.org/10.1098/rstb.2013.0269

Loos, E., Costa, M., & Johannessen, S. (2017). Underwater optical environment in the coastal waters of British Columbia, Canada. *Facets*, *2*(2), 872-891. https://doi.org/10.1139/facets-2017-0074

Lowman, H. E., Emery, K. A., Dugan, J. E., & Miller, R. J. (2022). Nutritional quality of giant kelp declines due to warming ocean temperatures. *Oikos*, *2022*(7). https://doi.org/10.1111/oik.08619

Lüning, K., & Neushul, M. (1978). Light and temperature demands for growth and reproduction of laminarian gametophytes in southern and central California. *Marine Biology*, *45*, 297-309. https://doi.org/10.1007/BF00391816

MacNeill, M. R. (1974). The mid-depth temperature minimum in B. C. inlets. [master's thesis]. [Vancouver (BC)]: University of British Columbia.

Mann, H.B. (1945). NONPARAMETRIC TESTS AGAINST TREND. *Econometrica*. https://doi.org/10.2307/1907187

McPherson, M. L., Finger, D. J., Houskeeper, H. F., Bell, T. W., Carr, M. H., Rogers-Bennett, L., & Kudela, R. M. (2021). Large-scale shift in the structure of a kelp forest ecosystem co-occurs with an epizootic and marine heatwave. *Communications biology*, *4*(1), 298. https://doi.org/10.1038/s42003-021-01827-6

Miller, R. J., Lafferty, K. D., Lamy, T., Kui, L., Rassweiler, A., & Reed, D. C. (2018). Giant kelp, Macrocystis pyrifera, increases faunal diversity through physical engineering. P*roceedings of the Royal Society B: Biological Sciences*, *285*(1874), 20172571. https://doi.org/10.1098/rspb.2017.2571

Mohamad, I. B., & Usman, D. (2013). Standardization and its effects on k-means clustering algorithm. *Res J Appl Sci Eng Technol*, *6*(17), 3299-3303. https://.doi.org/10.19026/rjaset.6.3638

Mora-Soto, A., Capsey, A., Friedlander, A. M., Palacios, M., Brewin, P. E., Golding, N., ... & Macias-Fauria, M. (2021). One of the least disturbed marine coastal ecosystems on Earth: Spatial and temporal persistence of Darwin's sub-Antarctic giant kelp forests. *Journal of Biogeography*, *48*(10), 2562-2577. https://doi.org/10.1111/jbi.14221

Mora-Soto, A., Schroeder, S., Gendall, L., Wachmann, A., Narayan, G. R., Read, S., ... & Costa, M. (2024). Kelp dynamics and environmental drivers in the southern Salish Sea, British Columbia, Canada. *Frontiers in Marine Science*, *11*, 1323448. https://doi.org/10.3389/fmars.2024.1323448

Mora-Soto, A., Schroeder, S., Gendall, L., Wachmann, A., Narayan, G., Read, S., ... & Costa, M. (2024). Back to the past: Long-term persistence of bull kelp forests in the Strait of Georgia, Salish Sea, Canada. *Frontiers in Marine Science*, *11*, 1446380. https://doi.org/10.3389/fmars.2024.1446380

Muth, A. F., Graham, M. H., Lane, C. E., & Harley, C. D. (2019). Recruitment tolerance to increased temperature present across multiple kelp clades. https://doi.org/10.1002/ecy.2594

NASA. (n.d.) Timeline | Landsat Science. Retrieved from: https://landsat.gsfc.nasa.gov/satellites/timeline/ [Acccessed September 25, 2024]

Nijland, W., Reshitnyk, L., & Rubidge, E. (2019). Satellite remote sensing of canopy-forming kelp on a complex coastline: a novel procedure using the Landsat image archive. *Remote Sensing of Environment, 220*, 41-50. https://doi.org/10.1016/j.rse.2018.10.032

NOAA (2024a). *Cold and warm episodes by season.* Retrieved from: https://origin.cpc.ncep.noaa.gov/products/analysis_monitoring/ensostuff/ONI_v5.php [Accessed September 25, 2024)

NOAA (2024b). *Pacific Decadal Oscillation.* Retrieved from: https://www.ncei.noaa.gov/access/monitoring/pdo/ [Accessed September 25, 2024]

Norel, M., Kałczyński, M., Pińskwar, I., Krawiec, K., & Kundzewicz, Z. W. (2021). Climate variability indices—a guided tour. *Geosciences, 11*(3), 128. https://doi.org/10.3390/geosciences11030128

Pessarrodona, A., Assis, J., Filbee-Dexter, K., Burrows, M. T., Gattuso, J. P., Duarte, C. M., ... & Wernberg, T. (2022). Global seaweed productivity. *Science Advances, 8*(37), eabn2465. https://doi.org/10.1126/sciadv.abn2465

Pfister, C. A., Berry, H. D., & Mumford, T. (2018). The dynamics of Kelp Forests in the Northeast Pacific Ocean and the relationship with environmental drivers. *Journal of Ecology, 106*(4), 1520-1533. https://doi.org/10.1111/1365-2745.12908

Planet Developers (2024). RapidEye Overview. Retrieved from: https://developers.planet.com/docs/data/rapideye/ [Accessed September 25, 2024]

Pontier, O., Rhoades, O., Twist, B., Okamoto, D. and Hessing-Lewis, M., 2024. Bull kelp (Nereocystis luetkeana) growth rates as climate stress indicators for Canada's Pacific coast. *FACETS, 9*(1), pp.1-19. https://doi.org/10.1139/facets-2023-0237

R Core Team (2022). R: A language and environment for statistical computing. R Foundation for Statistical Computing, Vienna, Austria. https://www.R-project.org/. [Accessed August 5, 2024]

Raffaelli, D., Hawkins, S. (1999). Community dynamics. *Intertidal Ecology*, 98-146. https://doi.org/10.1007/978-94-009-1489-6_4

Randell, Z., Wiliams, M., Bogdanova E., McQueen C., Larson S., Meyer E. *Urban Kelp Research Project 2023 year-end report to the Port of Seattle.* Seattle Aquarium. https://www.dropbox.com/scl/fi/r9h8rwams3n2h39q5hpib/2023_YearEnd_Report_Urban-Kelp-Research-Project.pdf?rlkey=35ua56ufnezqcyuomed3wgnep&e=2&dl=0 [Accessed August 5, 2024]

Reed, D. C., Rassweiler, A. R., Miller, R. J., Page, H. M., & Holbrook, S. J. (2015). The value of a broad temporal and spatial perspective in understanding dynamics of kelp forest ecosystems. *Marine and Freshwater Research, 67*(1), 14-24. http://dx.doi.org/10.1071/MF14158

Reed, D., Washburn, L., Rassweiler, A., Miller, R., Bell, T., & Harrer, S. (2016). Extreme warming challenges sentinel status of kelp forests as indicators of climate change. *Nature Communications*, *7*(1), 13757. https://doi.org/10.1038/ncomms13757

Reeves, S. E., Kriegisch, N., Johnson, C. R., & Ling, S. D. (2022). Kelp habitat fragmentation reduces resistance to overgrazing, invasion and collapse to turf dominance. *Journal of Applied Ecology*, *59*(6), 1619-1631.https://doi.org/10.1111/1365-2664.14171

Reid, M., Collins, M.L., Hall, S.R.J., Mason, E., McGee, G. and Frid, A. (2022). Protecting our coast for everyone's future: Indigenous and scientific knowledge support marine spatial protections proposed by Central Coast First Nations in Pacific Canada. *People and Nature*, *4*(5), pp.1052-1070. https://doi.org/10.1002/pan3.10380

Reshitnyk, L., Aguilar, A., Bell, Tom W., Hessing-Lewis, M., Houskeeper, H., Man, L., Pontier, O. (2024). Multi-scale mapping of charismatic megaflora: leveraging long-term site and regional level spatial data to inform satellite-based remote sensing of kelp forests in British Columbia, Canada (unpublished)

Roberts, D. A., Gardner, M., Church, R., Ustin, S., Scheer, G., & Green, R. O. (1998). Mapping chaparral in the Santa Monica Mountains using multiple endmember spectral mixture models. *Remote sensing of environment*, *65*(3), 267-279. https://doi.org/10.1016/S0034-4257(98)00037-6

Rogers-Bennett, L., & Catton, C. A. (2019). Marine heat wave and multiple stressors tip bull kelp forest to sea urchin barrens. *Scientific reports*, *9*(1), 15050. https://doi.org/10.1038/s41598-019-51114-y

Rogers-Bennett, L., & Okamoto, D. (2020). Mesocentrotus franciscanus and Strongylocentrotus purpuratus. In *Developments in Aquaculture and Fisheries Science* (Vol. 43, pp. 593-608). Elsevier. https://doi.org/10.1016/B978-0-12-819570-3.00032-9

Saccomanno, V. R., Bell, T., Pawlak, C., Stanley, C. K., Cavanaugh, K. C., Hohman, R., ... & Gleason, M. (2023). Using unoccupied aerial vehicles to map and monitor changes in emergent kelp canopy after an ecological regime shift. *Remote Sensing in Ecology and Conservation*, *9*(1), 62-75. https://doi.org/10.1002/rse2.295

Salmon Coast Field Station (2023). Salmon Coast Field Station Participatory Mapping with Community Members in the Broughton Archipelago.

Salmon Coast Field Station., (2023). Sea lice on juvenile wild salmon in the Broughton Archipelago, British Columbia. 2023 report. Retrieved from: https://salmoncoast.org/wp-content/uploads/2023/12/Salmon-Coast-Sea-Lice-Report-2023.pdf

Schroeder, S. B., Boyer, L., Juanes, F., & Costa, M. (2020). Spatial and temporal persistence of nearshore kelp beds on the west coast of British Columbia, Canada using satellite remote sensing. *Remote Sensing in Ecology and Conservation*, *6*(3), 327-343. https://doi.org/10.1002/rse2.142

Schroeder, S. B., Dupont, C., Boyer, L., Juanes, F., & Costa, M. (2019). Passive remote sensing technology for mapping bull kelp (Nereocystis luetkeana): A review of techniques and regional

case study. *Global Ecology and Conservation*, *19*, e00683. https://doi.org/10.1016/j.gecco.2019.e00683

Selgrath, J. C., Carlton, J. T., Pearse, J., Thomas, T., & Micheli, F. (2024). Setting deeper baselines: kelp forest dynamics in California over multiple centuries. *Regional Environmental Change*, *24*(3), 1-15. https://doi.org/10.1007/s10113-024-02260-1

Shaffer, A., Gross, J., Black, M., Kalagher, A., & Juanes, F. (2023). Dynamics of juvenile salmon and forage fishes in nearshore kelp forests. *Aquatic Conservation: Marine and Freshwater Ecosystems*, *33*(8), 822-832. https://doi.org/10.1002/aqc.3957

Shapiro, S. S., & Wilk, M. B. (1965). An analysis of variance test for normality (complete samples). *Biometrika*, *52*(3-4), 591-611.

Shugar, D. H., Walker, I. J., Lian, O. B., Eamer, J. B., Neudorf, C., McLaren, D., & Fedje, D. (2014). Post-glacial sea-level change along the Pacific coast of North America. *Quaternary Science Reviews*, *97*, 170-192. https://doi.org/10.1016/j.quascirev.2014.05.022

Shorezone (n.d.). *BC Shorezone*. https://www.shorezone.org/interactive-shorezone-maps/#BC_Map [Accessed August 5, 2024]

Simonson, E. J., Scheibling, R. E., & Metaxas, A. (2015). Kelp in hot water: I. Warming seawater temperature induces weakening and loss of kelp tissue. *Marine Ecology Progress Series*, *537*, 89-104. https://doi.org/10.3354/meps11438

Smale, D. A. (2020). Impacts of ocean warming on kelp forest ecosystems. *New Phytologist*, *225*(4), 1447-1454. https://doi.org/10.1111/nph.16107

Smith, K. E., Aubin, M., Burrows, M. T., Filbee-Dexter, K., Hobday, A. J., Holbrook, N. J., ... & Smale, D. A. (2024). Global impacts of marine heatwaves on coastal foundation species. *Nature Communications*, *15*(1), 5052. https://doi.org/10.1038/s41467-024-49307-9

Springer, Y. P., Hays, C. G., Carr, M. H., & Mackey, M. R. (2010). Toward ecosystem-based management of marine macroalgae—The bull kelp, Nereocystis luetkeana. *Oceanography and marine biology*, *48*, 1.

Starko, S., Neufeld, C. J., Gendall, L., Timmer, B., Campbell, L., Yakimishyn, J., ... & Baum, J. K. (2022). Microclimate predicts kelp forest extinction in the face of direct and indirect marine heatwave effects. *Ecological Applications*, *32*(7), e2673. https://doi.org/10.1002/eap.2673

Starko, S., Timmer, B., Reshitnyk, L., Csordas, M., McHenry, J., Schroeder, S., ... & Neufeld, C. J. (2024). Local and regional variation in kelp loss and stability across coastal British Columbia. *Marine Ecology Progress Series*, *733*, 1-26. https://doi.org/10.3354/meps14548

Starko, S., van der Mheen, M., Pessarrodona, A., Wood, G. V., Filbee-Dexter, K., Neufeld, C. J., ... & Wernberg, T. (2024). Impacts of marine heatwaves in coastal ecosystems depend on local environmental conditions. *Global change biology*, *30*(8), e17469. https://doi.org/10.1111/gcb.17469

Stehman, S.V., Czaplewski, R.L. (1998). Design and Analysis for Thematic Map Accuracy Assessment: Fundamental Principles. *Remote Sensing of Environment*. https://doi.org/10.1016/s0034-4257(98)00010-8

Stekoll, M. S., Deysher, L., & Hess, M. (2006). A remote sensing approach to estimating harvestable kelp biomass. *Journal of Applied Phycology*. *1*, 97-108. https://doi.org/10.1007/s10811-006-9029-7

Steneck, R. S., Graham, M. H., Bourque, B. J., Corbett, D., Erlandson, J. M., Estes, J. A., & Tegner, M. J. (2002). Kelp forest ecosystems: biodiversity, stability, resilience and future. *Environmental conservation*, 29(4), 436-459. https://doi.org/10.1017/s0376892902000322

Steneck, R. S., Johnson, C. R. (2013). Dynamic patterns, processes and feedbacks. *Marine community ecology*, 315-336.

Suchy, K. D., Dower, J. F., Varela, D. E., & Lagunas, M. G. (2016). Interannual variability in the relationship between in situ primary productivity and somatic crustacean productivity in a temperate fjord. *Marine Ecology Progress Series, 545*, 91-108. https://doi.org/10.3354/meps11608

Suchy, K. D., Le Baron, N., Hilborn, A., Perry, R. I., & Costa, M. (2019). Influence of environmental drivers on spatio-temporal dynamics of satellite-derived chlorophyll a in the Strait of Georgia. *Progress in oceanography*, *176*, 102134. https://doi.org/10.1016/j.pocean.2019.102134

Supratya, V. P., Coleman, L. J., & Martone, P. T. (2020). Elevated temperature affects phenotypic plasticity in the bull kelp (Nereocystis luetkeana, Phaeophyceae). *Journal of phycology*, *56*(6), 1534-1541. https://doi.org/10.1111/jpy.13

Sutherland, I.R., (1990). Kelp Inventory, 1989 The Vancouver Island and Malcolm Island shores of Queen Charlotte Strait, including a summary of historical inventory information for the area. British Columbia Aquaculture and Commercial Fisheries Branch, Fish. Development Rep. No. 36. 41 pp. plus 3 charts.

Tait, L. W. (2019). Giant kelp forests at critical light thresholds show compromised ecological resilience to environmental and biological drivers. *Estuarine, Coastal and Shelf Science*, *219*, 231-241. https://doi.org/10.1016/j.ecss.2019.02.026

Thompson, Markus (2021) MaPP Kelp Monitoring Protocol. Marine Plan Partnership. https://mappocean.org/wp-content/uploads/2021/07/MaPP_Kelp_Monitoring_Methods_2021.pdf [Acessed August 5, 2024]

Timmer, B., Reshitnyk, L. Y., Hessing-Lewis, M., Juanes, F., & Costa, M. (2022). Comparing the use of red-edge and near-infrared wavelength ranges for detecting submerged kelp canopy. *Remote Sensing*, *14*(9), 2241. https://doi.org/10.3390/rs14092241

Timmer, B., Reshitnyk, L. Y., Hessing-Lewis, M., Juanes, F., Gendall, L., & Costa, M. (2024). Capturing accurate kelp canopy extent: integrating tides, currents, and species-level morphology in kelp remote sensing. *Frontiers in Environmental Science*, *12*, 1338483. https://doi.org/10.3389/fenvs.2024.1338483

Traiger, S. B., & Konar, B. (2018). Mature and developing kelp bed community composition in a glacial estuary. *Journal of Experimental Marine Biology and Ecology*, *501*, 26-35. https://doi.org/10.1016/j.jembe.2017.12.016

Turner, N. J. (2001). Coastal peoples and marine plants on the Northwest Coast. *Proceedings of the International Association of Aquatic and Marine Science Libraries and Information Centers.* Victoria, British Columbia.

Tweedie, M. C. K. (1984). An index which distinguishes between some important exponential families. In Statistics: Applications and New Directions. Proceedings of the Indian Statistical Institute Golden Jubilee International Conference. (Eds. J. K. Ghosh and J. Roy), pp. 579-604. Calcutta: Indian Statistical Institute

Umista Cultural Society. (n.d.) *Our Land.* https://umistapotlatch.ca/notre_terre-our_land-eng.php

Vadas, R. L. (1972). Ecological implications of culture studies on Nereocystis Luetkeana 1. *Journal of Phycology*, *8*(2), 196-203. https://doi.org/10.1111/j.1529-8817.1972.tb04025.x

Vettori, D., Nikora, V., & Biggs, H. (2020). Implications of hyposaline stress for seaweed morphology and biomechanics. *Aquatic Botany*, *162*, 103188. https://doi.org/10.1016/j.aquabot.2019.103188

Wachmann, A., Starko, S., Neufeld, C.J. and Costa, M. (2024). Validating Landsat Analysis Ready Data for Nearshore Sea Surface Temperature Monitoring in the Northeast Pacific. *Remote Sensing*, *16*(5), p.920. https://doi.org/10.3390/rs16050920

Watson, J., & Estes, J. A. (2011). Stability, resilience, and phase shifts in rocky subtidal communities along the west coast of Vancouver Island, Canada. *Ecological Monographs*, *81*(2), 215-239. https://doi.org/10.1890/10-0262.1

Weigel, B.L., Small, S.L., Berry, H., Dethier, M.N. (2023). Effects of temperature and nutrients on microscopic stages of the bull kelp (Nereocystis luetkeana, Phaeophyceae). *Journal of Phycology*. https://doi.org/10.1111/jpy.13366

Wernberg, T., Bennett, S., Babcock, R. C., De Bettignies, T., Cure, K., Depczynski, M., ... & Wilson, S. (2016). Climate-driven regime shift of a temperate marine ecosystem. *Science*, *353*(6295), 169-172. https://doi.org/10.1126/science.aad8745

Wernberg, T., Krumhansl, K., Filbee-Dexter, K., & Pedersen, M.F. (2019) Status and trends for the world's kelp forests. In *World seas: An environmental evaluation* (pp. 57-78). Academic Press. https://doi.org/10.1016/b978-0-12-805052-1.00003-6

Wernberg, T., Smale, D. A., Tuya, F., Thomsen, M. S., Langlois, T. J., De Bettignies, T., ... & Rousseaux, C. S. (2013). An extreme climatic event alters marine ecosystem structure in a global biodiversity hotspot. *Nature Climate Change*, *3*(1), 78-82. https://doi.org/10.1038/nclimate1627

Wernberg, T., Thomsen, M. S., Baum, J. K., Bishop, M. J., Bruno, J. F., Coleman, M. A., ... & Vanderklift, M. A. (2024). Impacts of climate change on marine foundation species. *Annual review of marine science*, *16*(1), 247-282. https://doi.org/10.1146/annurev-marine-042023-093037

Whitney, F.A. (2015). Anomalous winter winds decrease 2014 transition zone productivity in the NE Pacific. *Geophysical Research Letters*, *42*(2), pp.428-431. http://dx.doi.org/10.1002/2014GL062634

Young, M., Cavanaugh, K., Bell, T., Raimondi, P., Edwards, C.A., Drake, P.T., Erikson, L. and Storlazzi, C. (2016). Environmental controls on spatial patterns in the long-term persistence of giant kelp in central California. *Ecological Monographs, 86*(1), pp.45-60. https://esajournals.onlinelibrary.wiley.com/doi/10.1890/15-0267

Zhao, K., Wulder, M.A., Hu, T., Bright, R., Wu, Q., Qin, H., Li, Y., Toman, E., Mallick, B., Zhang, X. and Brown, M. (2019). Detecting change-point, trend, and seasonality in satellite time series data to track abrupt changes and nonlinear dynamics: A Bayesian ensemble algorithm. *Remote sensing of Environment, 232*, p.111181. https://doi.org/10.1016/j.rse.2019.04.034

Appendix A - Supplementary material of Chapter 2

A1 UAV flight plan specifications

Two different types of UAV surveys were conducted. (1) When kelp beds were absent, manual flights were conducted to take oblique aerial photos for a qualitative overview of the site if weather conditions allowed (not directly used for analysis). (2) When at least one kelp bed was present (kelp bed defined as a cluster of floating *Nereocystis* or *Macrocystis* spanning ~3 meters or more in any direction, with <10m between each plant (Thompson 2021)), a flight plan (survey grids of parallel lines) was conducted at 70.0-120 m above sea level (ASL) covering the entire kelp bed or chain of kelp beds present at the site. The flight altitude was selected per site based on the size and density of the kelp bed to enhance the survey efficiency and the ease of ortho-mosaicking the images during the processing process. The flight lines were oriented to be 45 degrees away from the solar azimuth to minimize glint on the water surface, with a minimum of 70% side and frontal overlap in image coverage (Cowdrey, 2021). As both field campaigns were conducted on boats, often with no safe way to embark on land, no ground control points were used for the surveys.

A2 Orthomosaicking methods of UAV imagery

Multispectral UAV images were imported into Agisoft Metashape (Agisoft, St. Petersburg, Russia) under a multi-camera system. Images were initially aligned using the “medium” quality and the resulting point cloud was visually evaluated and manually edited for realignment following

methods detailed in Cowdrey (2021). If the point cloud was not of satisfactory quality, realignment was conducted using the "high" quality. The refined point cloud was subsequently used to generate a digital elevation model (DEM) and an orthomosaic TIFF file, and the orthomosaics were exported in the EPSG:32609 (WGS 84 / UTM zone 9N) coordinate reference system.

A3 Imagery processing and classification methods

Image classification

An eCognition (Trimble Geospatial Imaging, Munich, Germany) supervised classification, object-based image analysis (OBIA) method (Blaschke, 2010) for multispectral imagery was used to classify multispectral orthomosaics and high-resolution satellite imagery, adapting methods used in Schroeder et al., 2019b; Gendall et al., 2023; Mora-Soto et al. 2024a. The green, red, red-edge (RE), and NIR bands were used as inputs for multiresolution segmentation with 0, 1, 1, and 2 as the respective weights for each band. A segmentation scale of 100 to 200, shape value of 0.1, and compactness value of 0.5 were used, and all segmentation products were manually checked to ensure that each segment didn't have a mix of water and kelp to facilitate the training process (Gendall et al., 2023). Training classes "water", "kelp", and "mask" were selected using expert knowledge, and the feature space optimization tool was used to select the best combination of spatial, spectral, and contextual information used for the classification. All outputs were manually edited for quality in eCognition and ArcGIS using a knowledge-based approach, producing a measure of kelp area for each site in the end.

A4 Photosynthetically available radiation measurements

The profiler data was processed using ProSoft (v7.4, Satlantic, Halifax, NS, Canada). Photosynthetically available radiation (PAR) (quanta cm^{-2} s^{-1}) at each meter depth was automatically derived from downwelling irradiance measurement using the equation $\int_{400nm}^{700nm} \frac{\lambda}{hc} E_d(\lambda) d\lambda$ (where λ = wavelength (nm), h = Planck's constant $6.63x10^{-34}$ Js, c = speed of light 3.00x10.8 m/s) within

ProSoft. Absolute PAR at each meter depth was then converted to mol photons m^{-2} day^{-1}. The mean percentage PAR (PAR available at depth *n* divided by PAR at the surface) for depths 1 to 5 was also automatically derived within ProSoft. As the downwelling irradiance sensor's measurements were affected by the tilt of the profiler instrument during the survey, the tilt values along both the X and Y axes were visually assessed for each profiler drop, and profile drops with a significant amount of tilt values higher than 20 degrees were removed from subsequent PAR metric calculations. The mean PAR (converted to mol photons m^{-2} day^{-1}) and percent PAR of 1 m, 2 m, 3 m, 4 m, and 5 m depths for each site were recorded. Only percent PAR means were used in the subsequent statistical analysis.

A5 Supplementary tables

Table A. 1: Table showing each study site's environmental attributes

Site	Lat	Lon	Sub-region	Surface tempera-ture (°C)	Midwater tempera-ture (°C)	Bottom tempera-ture (°C)	Surface salinity (PSU)	Midwater salinity (PSU)	Bottom salinity (PSU)	Stratification index (kg m^{-3})	PAR at 1 m (%)	PAR at 2 m (%)	Par at 3 m (%)	PAR at 4 m (%)	PAR at 5 m (%)	PAR at 1 m (mol photons m^{-2} day^{-1})	PAR at 2 m (mol photons m^{-2} day^{-1})	Par at 3 m (mol photons m^{-2} day^{-1})	PAR at 4 m (mol photons m^{-2} day^{-1})	PAR at 5 m (mol photons m^{-2} day^{-1})	Tidal current (m/s)	Slope (°)	Fetch (km)
1	50.58103	-126.829	A	9.56	9.41	9.39	34.3	34.3	34.3	0.175	73.3	54.3	42.3	34.1	28.2	22.4	16.44	12.8	10.3	8.53	0.590	5.73	244
2	50.6654	-126.965	A	9.98	9.94	10.3	34.4	34.2	34.1	0.411	49.8	23.6	12.7	8.6	5.75	14.7	6.97	3.79	2.55	1.70	0.100	2.17	911
3	50.66445	-126.916	A	9.47	9.39	9.94	34.9	34.9	34.9	0.0362	68.9	48.5	35.3	27.3	21.6	19.3	13.63	9.89	7.66	6.05	0.120	0.810	1,060
4	50.61558	-126.831	A	11.3	10.6	9.33	34.4	34.4	34.4	0.0997	75.2	55.8	45.0	38.7	33.8	3.50	2.60	2.09	1.80	1.57	0.520	3.22	283
5	50.61911	-126.623	A	10.1	9.81	9.65	33.1	33.2	33.3	0.292	65.5	43.6	30.2	21.9	16.2	4.77	3.17	2.19	1.59	1.18	0.200	4.10	35.0
6	50.62561	-126.503	F	14.3	12.9	10.1	22.3	25.9	31.6	3.23	53.3	29.8	16.5	9.5	5.58	12.6	7.05	3.90	2.24	1.32	0.0900	12.6	77.0
7	50.64031	-126.438	F	11.4	10.3	9.48	29.5	30.4	31.5	1.49	59.8	35.7	22.8	15.9	11.2	9.94	5.94	3.79	2.65	1.86	0.140	16.2	94.0
8	50.6935	-126.687	A	9.80	9.45	9.30	34.0	34.0	34.1	0.313	62.7	39.4	26.3	19.8	15.4	6.59	4.15	2.76	2.06	1.61	0.180	7.46	51.0
9	50.74256	-126.719	A	9.95	9.87	9.54	33.3	33.4	33.5	0.0828	66.0	44.1	30.9	22.4	17.4	2.72	1.81	1.27	0.910	0.710	0.0800	10.7	545
10	50.65104	-126.264	F	12.8	12.2	11.9	23.1	24.4	25.1	1.25	62.2	38.5	25.6	16.2	11.2	13.0	8.05	5.35	3.37	2.32	0.0800	16.2	63.0
11	50.67859	-126.253	F	14.0	11.7	11.1	19.9	25.6	27.0	5.12	60.1	39.2	24.1	14.8	9.59	42.1	27.43	16.8	10.4	6.72	0.120	19.3	103
12	50.79088	-126.484	F	13.3	11.5	11.3	31.6	31.5	31.7	1.22	55.8	31.6	18.7	11.2	7.27	26.7	15.07	8.93	5.35	3.47	0.0900	12.0	59.0

13	50.82344	-126.555	F	13.5	10.9	10.5	29.2	31.9	32.2	3.80	52.3	27.6	15.3	8.8	5.31	7.31	3.86	2.14	1.22	0.740	0.0800	21.6	125
14	50.62218	-126.743	A	9.55	9.46	9.45	34.1	34.2	34.2	0.162	72.8	54.1	41.5	33.0	27.5	12.8	9.50	7.30	5.81	4.83	0.350	9.09	1,910
15	50.58745	-126.946	A	9.65	9.64	9.59	34.6	34.5	34.6	0.0126	83.2	67.0	60.4	49.5	41.3	16.1	13.0	11.7	9.65	7.99	0.200	2.61	98.0
16	50.62158	-126.701	A	11.1	9.93	9.34	29.5	32.5	33.6	3.19	61.8	38.8	25.3	17.8	13.0	3.78	2.37	1.55	1.09	0.79	0.160	8.62	112
17	50.75882	-126.714	F	11.7	11.2	N/A	31.1	31.6	N/A	0.715	58.7	34.6	21.7	15.0	12.5	6.21	3.66	2.28	1.56	1.16	0.130	28.1	183
18	50.80696	-126.425	F	12.5	11.6	10.2	29.9	30.8	32.0	1.35	62.2	36.7	25.0	17.2	12.8	1.81	1.06	0.72	0.500	0.370	0.130	12.3	108
19	50.84872	-126.323	F	13.1	11.0	9.25	28.1	30.7	32.5	3.42	59.7	35.9	22.8	14.4	9.99	7.50	4.52	2.87	1.81	1.26	0.130	35.3	774
20	50.79376	-126.473	F	14.1	11.2	10.0	28.6	30.9	32.0	3.56	74.9	46.9	42.4	26.7	15.1	20.5	12.74	10.9	6.88	3.77	0.110	7.89	56.0
21	50.8243	-126.568	F	14.7	10.7	10.5	30.8	32.4	32.5	4.07	55.6	33.5	19.1	10.2	4.85	38.9	23.30	13.3	7.06	3.29	0.0300	5.98	10.0
22	50.83788	-126.572	F	16.8	12.3	N/A	22.9	32.4	N/A	9.09	54.4	31.6	17.9	10.4	N/A	4.93	2.83	1.57	0.900	N/A	0.0800	14.29	217
23	50.87377	-126.593	F	18.7	13.1	10.8	21.0	33.2	33.1	11.2	64.1	44.3	29.1	19.2	12.5	17.2	11.90	7.80	4.93	2.83	0.0200	12.0	64.0
24	50.92485	-126.48	F	20.1	12.8	11.1	14.5	34.5	33.6	16.5	76.2	59.0	47.8	33.5	23.7	28.4	21.74	17.6	13.8	9.72	0.0600	30.7	145
25	50.58029	-126.962	A	9.92	9.71	9.67	34.1	34.5	34.5	0.468	56.7	40.0	24.7	22.7	28.3	5.00	3.50	1.94	1.87	1.89	0.240	2.46	193
26	50.5899	-126.758	A	9.72	9.47	9.40	34.8	34.6	34.5	0.0917	77.7	61.7	51.2	41.3	35.1	35.5	28.06	22.2	17.6	14.9	0.0500	7.87	224
27	50.58971	-126.762	A	9.39	9.28	9.27	34.5	34.5	34.4	0.0470	70.1	58.6	41.8	32.3	26.9	39.7	32.18	22.0	16.6	14.3	0.0500	10.9	342
28	50.6907	-126.262	F	13.2	11.3	10.8	21.9	26.1	27.5	4.00	58.5	35.8	21.8	14.1	9.13	38.7	23.69	14.4	9.34	6.05	0.0900	24.6	109
29	50.69272	-126.199	F	13.9	11.3	10.4	18.2	24.6	27.0	5.71	60.2	38.0	24.0	16.9	10.1	22.3	13.61	8.26	5.43	5.58	0.150	2.71	21.0
30	50.67402	-126.097	F	12.5	10.8	9.01	21.1	25.3	29.2	3.93	56.8	33.6	20.0	13.2	8.91	7.42	4.40	2.61	1.72	1.16	0.100	33.6	207

31	50.8402	-126.663	F	18.4	11.2	10.3	21.0	32.9	32.9	12.1	64.3	45.7	30.1	19.1	12.3	42.1	29.02	19.1	12.1	7.80	0.020	10.0	97.0

Table A. 2: Table showing differences in each environmental variable between subregions. Bolded variables are the variables selected for the cluster analysis

	Archipelago subregion mean and SD	Fjord subregion mean and SD	Kruskal-Wallis $\chi 2$	P-value
Surface temperature	**9.95±0.583°C**	**14.3±2.47°C**	**21.9**	**2.82×10^{-6}**
Midwater temperature	9.69±0.357°C	11.6±0.787°C	21.6	3.39×10^{-6}
Benthic temperature	9.55±0.301°C	10.4±0.762°C	8.89	0.0029
Surface salinity	30.8±1.71 PSU	19.6±5.12 PSU	21.2	4.15×10^{-6}
Midwater salinity	**31.2±0.818 PSU**	**25.5±3.18 PSU**	**21.9**	2.82×10^{-6}
Benthic salinity	34.2±0.517 PSU	27.2±2.78 PSU	20.8	5.10×10^{-6}
Stratification index	0.414±0.848 kg m^{-3}	5.10±4.37 kg m^{-3}	20.1	7.34×10^{-6}
Percent PAR at 1 m depth	**68.0±8.99%**	**60.5±6.47%**	**6.36**	**0.012**
Percent PAR at 2 m depth	48.4±11.7%	37.7±7.45%	8.54	0.0035
Percent PAR at 3 m depth	36.0±12.7%	24.7±8.45%	8.08	0.0045
Percent PAR at 4 m depth	28.4±11.1%	15.9±6.14%	11.3	0.00077
Percent PAR at 5 m depth	23.9±10.0%	10.7±4.41%	14.4	0.00015
Tidal current	**0.218±0.171 m/s**	**0.0917±0.0397 m/s**	**6.09**	**0.010**
Slope	**4.83±3.47°**	**17.5±9.57°**	**14.7**	**0.00012**
Fetch	**462±539 km**	**139±168 km**	**6.16**	**0.013**

Table A. 3: Table showing all study sites' coordinates, subregions, kelp species (if present), and all kelp metrics and biotic metrics

Site	Lat	Lon	Sub-region	Kelp Species	Classified kelp area (m^2)	Kelp bed area (m^2)	Kelp density (%)	Kelp abundance index	Urchin abundance (counts/ image)	*Pycnopodia* abundance (counts/ image)
1	50.58103	-126.829	A	*Nereocystis*	55,000	242,000	22.7	10.1	15.3	0.000
2	50.6654	-126.965	A	*Macrocystis*	16,700	29,800	56.1	8.70	0.000	0.000
3	50.66445	-126.916	A	*Macrocystis*	25,600	213,000	12.0	9.70	0.000	0.000
4	50.61558	-126.831	A	*Nereocystis*	136,000	484,000	28.1	10.80	3.71	0.000
5	50.61911	-126.623	A	*Nereocystis*	1,790	12,900	13.9	7.40	0.0440	0.00700
6	50.62561	-126.503	F	*Nereocystis*	9,370	158,000	4.10	9.20	0.000	0.000
7	50.64031	-126.438	F	*Nereocystis*	1,510	34,000	4.30	7.70	0.0700	0.115
8	50.6935	-126.687	A	*Nereocystis*	5,490	61,300	9.00	8.50	0.000	0.000
9	50.74256	-126.719	A	*Nereocystis*	2,600	50,300	5.20	8.10	3.01	0.000
10	50.65104	-126.264	F	*Nereocystis*	240	8,720	2.70	6.30	0.000	0.377
11	50.67859	-126.253	F	None	0.000	0.000	0.000	0.000	0.000	0.0520
12	50.79088	-126.484	F	*Nereocystis*	14.0	589	2.30	3.90	3.30	0.000
13	50.82344	-126.555	F	*Nereocystis*	26.0	2,500	1.00	4.80	0.000	0.000
14	50.62218	-126.743	A	*Nereocystis*	5,310	11,800	45.0	7.80	14.8	0.000
15	50.58745	-126.946	A	*Nereocystis*	1,760	15,800	11.1	7.40	0.000	0.000
16	50.62158	-126.701	A	*Nereocystis*	2,240	28,600	7.80	7.80	3.19	0.00500
17	50.75882	-126.714	F	None	0.000	0.000	0.000	0.000	11.0	0.000
18	50.80696	-126.425	F	*Nereocystis*	78.0	4,670	1.70	5.60	3.78	0.000
19	50.84872	-126.323	F	*Nereocystis*	40.0	5,020	7.90	5.30	0.00800	0.000
20	50.79376	-126.473	F	*Nereocystis*	125	6,880	1.80	5.90	0.000	0.000
21	50.8243	-126.568	F	None	0.000	0.000	0.000	0.000	0.000	0.000
22	50.83788	-126.572	F	None	0.000	0.000	0.000	0.000	0.0550	0.000
23	50.87377	-126.593	F	None	0.000	0.000	0.000	0.000	0.000	0.000
24	50.92485	-126.48	F	None	0.000	0.000	0.000	0.000	10.5	0.000
25	50.58029	-126.962	A	*Nereocystis*	25,800	83,200	31.1	9.30	0.000	0.000
26	50.5899	-126.758	A	Mixed	834	9,660	8.60	6.90	0.000	0.000
27	50.58971	-126.762	A	*Nereocystis*	36.0	1,960	2.00	4.80	0.266	0.000
28	50.6907	-126.262	F	None	0.000	0.000	0.000	0.000	0.000	0.000
29	50.69272	-126.199	F	*Nereocystis*	77.0	14,900	0.500	6.10	0.00400	0.0380
30	50.67402	-126.097	F	None	0.000	0.000	0.000	0.000	0.00	0.000
31	50.8402	-126.663	F	None	0.000	0.000	0.000	0.000	0.0100	0.000

Table A. 2: Table showing differences in environmental and biotic variables between the kelp and non-kelp sites in the fjord subregion.

Variable	Kelp sites in fjord subregion (n=9)	No kelp sites in fjord subregion (n=9)
Bottom substrate	Mixed (n=4), rocky (n=5)	Mixed (n=3), rocky (n=3), sandy (n=3)
Surface temperature	13.2±0.891°C	15.6±3.02°C
Midwater temperature	11.4±0.740°C	11.7±0.859°C
Benthic temperature	10.4±0.835°C	10.5±0.715°C
Surface salinity	26.7±4.46 PSU	22.7±5.25 PSU
Midwater salinity	*29.0±3.09PSU*	*30.5 ±3.70 PSU*
Benthic salinity	30.6±2.65 PSU	30.8±2.86 PSU
Stratification index	**2.11±1.56 kg m^{-3}**	**6.74±5.23kg m^{-3}**
Percent PAR at 1 m depth	60.0±6.67%	61.0±6.65%
Percent PAR at 2 m depth	35.7±5.66%	39.7±8.76%
Percent PAR at 3 m depth	23.7±7.95%	25.7±9.29%
Percent PAR at 4 m depth	15.2±5.37%	16.6±7.09%
Percent PAR at 5 m depth	9.83±3.25%	11.6±5.93%
Tidal current	*0.111±0.0271 m/s*	*0.0722±0.0421 m/s*
Slope	15.2±9.23°	19.8±9.87°
Fetch	153±235 km	126±685km
Urchin abundance	0.795±1.56 counts / image	2.49±4.73 counts / image
Pycnopodia abundance	0.0574±0.0125 counts / image	0.0589±0.0172 counts / image

Table A. 3: Results from linear models 1 and 2 showing significant (bold) environmental predictors that affected the kelp abundance index. Model 1 was significant ($p=8.17\times10^{-7}$) and explained 67.8% of the variation in the kelp abundance index, whereas model 2 was significant (p=0.002) and explained 58.0% of the variation. Bolded text indicates significant variables (p<0.05), italicized text indicates variables approaching significance (p<0.1), and normal text indicates variables that are not significant

Model 1: All sites (R2 = 0.67)

Variables	Coefficient estimate	Standardized coefficient	Coefficient standard error	T-value	P-value
Intercept	13.4	1.72×10^{-16}	2.28	5.85	8.17×10^{-7}
Tidal current	*7.20*	*0.248*	*3.60*	*2.00*	*0.0558*
Slope	**-0.133**	**-0.338**	**0.0475**	**-2.79**	**0.00949**
SST	**-0.598**	**-0.467**	**0.165**	**-3.63**	**0.00118**
Model 2: Only sites with kelp (R2=0.580)					
Variables	Coefficient estimate	Standardized coefficient	Coefficient standard error	T-value	P-value
Intercept	13.5	2.55×10^{-16}	3.80	3.54	0.00254
Tidal current	**6.86**	**0.517**	**2.32**	**2.60**	**0.00880**
SST	-0.285	-0.271	0.20	-1.42	0.175
Slope	*-0.0794*	*-0.332*	*0.04*	*-1.80*	*0.0891*

Table A. 4: Results of the hotspot analysis: GI statistic for urchin abundance.*

Urchin abundance hotspots					
Site	Urchin abundance (counts/image)	GI* statistic Z-score	Gi* statistic p-value	Hotspot	Confidence interval
1	15.2	1.79	0.0736	Yes	90%
2	0.00	-1.08	0.281	No	N/A
3	0.00	-0.63	0.530	No	N/A
4	3.71	1.80	0.0720	Yes	90%
5	0.0447	0.766	0.444	No	N/A
6	0.00	-0.902	0.367	No	N/A
7	0.0702	-0.723	0.469	No	N/A
8	0	1.92	0.0546	Yes	95%
9	3.01	1.00	0.316	No	N/A
10	0.00	-1.08	0.281	No	N/A
11	0.00	-1.08	0.281	No	N/A
12	3.30	-0.638	0.523	No	N/A
13	0.00	-1.00	0.323	No	N/A
14	14.8	1.80	0.0713	Yes	90%
15	0.00	0.570	0.569	No	N/A
16	3.19	0.629	0.529	No	N/A
17	11.0	1.00	0.316	No	N/A
18	3.78	-0.445	0.656	No	N/A
19	0.00877	-0.108	0.914	No	N/A
20	0.00	-0.638	0.523	No	N/A
21	0.00	-1.19	0.236	No	N/A
22	0.0556	-1.19	0.236	No	N/A
23	0.00	-0.283	0.777	No	N/A
24	10.5	1.01	0.314	No	N/A
25	0.00	0.761	0.447	No	N/A
26	0.00	2.45	0.0143	Yes	95%
27	0.266	2.45	0.0143	Yes	95%
28	0.00	-1.08	0.281	No	N/A
29	0.00362	-1.23	0.219	No	N/A
30	0.00	-0.735	0.462	No	N/A

31	0.0102	-1.22	0.222	No	N/A

Table A. 5: Results of the hotspot analysis: GI statistic for* Pycnopodia *abundance*

Site	*Pycnopodia* abundance (counts/image)	GI* statistic Z-score	GI* statistic p-value	Hotspot	Confidence interval
1	0.000	-0.819	0.413	No	N/A
2	0.000	-0.584	0.559	No	N/A
3	0.000	-0.584	0.559	No	N/A
4	0.000	-0.868	0.3985	No	N/A
5	0.007	-0.585	0.558	No	N/A
6	0.000	0.561	0.574	No	N/A
7	0.120	0.801	0.423	No	N/A
8	0.000	-0.668	0.504	No	N/A
9	0.000	-0.497	0.619	No	N/A
10	0.380	2.97	0.00294	Yes	99%
11	0.0517	2.97	0.00294	Yes	99%
12	0.000	-0.743	0.457	No	N/A
13	0.000	-0.895	0.371	No	N/A
14	0.000	-0.827	0.408	No	N/A
15	0.000	-0.743	0.457	No	N/A
16	0.00451	-0.748	0.454	No	N/A
17	0.000	-0.497	0.619	No	N/A
18	0.000	-0.665	0.506	No	N/A
19	0.000	-0.398	0.690	No	N/A
20	0.000	-0.743	0.457	No	N/A
21	0.000	-0.819	0.413	No	N/A
22	0.000	-0.819	0.413	No	N/A
23	0.000	-0.743	0.457	No	N/A
24	0.000	-0.398	0.690	No	N/A
25	0.000	-0.584	0.559	No	N/A
26	0.000	-0.714	0.475	No	N/A
27	0.000	-0.714	0.475	No	N/A
28	0.000	2.97	0.00294	Yes	99%
29	0.0381	2.58	0.00995	Yes	99%

30	0.000	-0.00211	0.998	No	N/A
31	0.000	-0.6765	0.506	No	N/A

Table A. 6: Results from generalized linear model 3 showing significant (bold) predictors that affected kelp density. This model explained 50.8% of the variation in kelp density

Model 3: Interactions between environmental and biotic drivers on kelp (R2 = 0.508)				
Variables	Coefficient estimate	Coefficient standard error	T-value	P-value
Intercept	**0.324**	**0.329**	**0.983**	**0.35**
Urchin abundance	-0.0679	0.118	-0.577	0.569
Pycnopodia abundance	27.9	69.9	0.398	0.693
Subregion	**1.09**	**0.308**	**3.54**	**0.00168**
Subregion * urchin abundance	0.0569	0.117	0.487	0.631
Subregion * *Pycnopodia* abundance	-14.7	35.0	-0.419	0.679
Urchin abundance * *Pycnopodia* abundance	10.9	22.0	0.496	0.624

Table A. 7: Table showing differences in all absolute PAR measurements between subregion.

	Archipelago subregion mean and SD	Fjord subregion mean and SD	Kruskal-Wallis $\chi 2$	P-value
Absolute PAR at 1 m depth (mol photons m^{-2} day^{-1})	14.4±12.2	19.3±13.8	1.44	0.230
Absolute PAR at 2 m depth (mol photons m^{-2} day^{-1})	10.6±9.96	12.2±9.17	0.578	0.447
Absolute PAR at 3 m depth (mol photons m^{-2} day^{-1})	7.80±7.50	7.90±6.09	0.292	0.603
Absolute PAR at 4 m depth (mol photons m^{-2} day^{-1})	6.11±5.85	5.07± 4.08	0.0785	0.779
Absolute PAR at 5 m depth (mol photons m^{-2} day^{-1})	5.08 ±5.01	3.50±2.75	0.296	0.572

A6 Supplementary figures

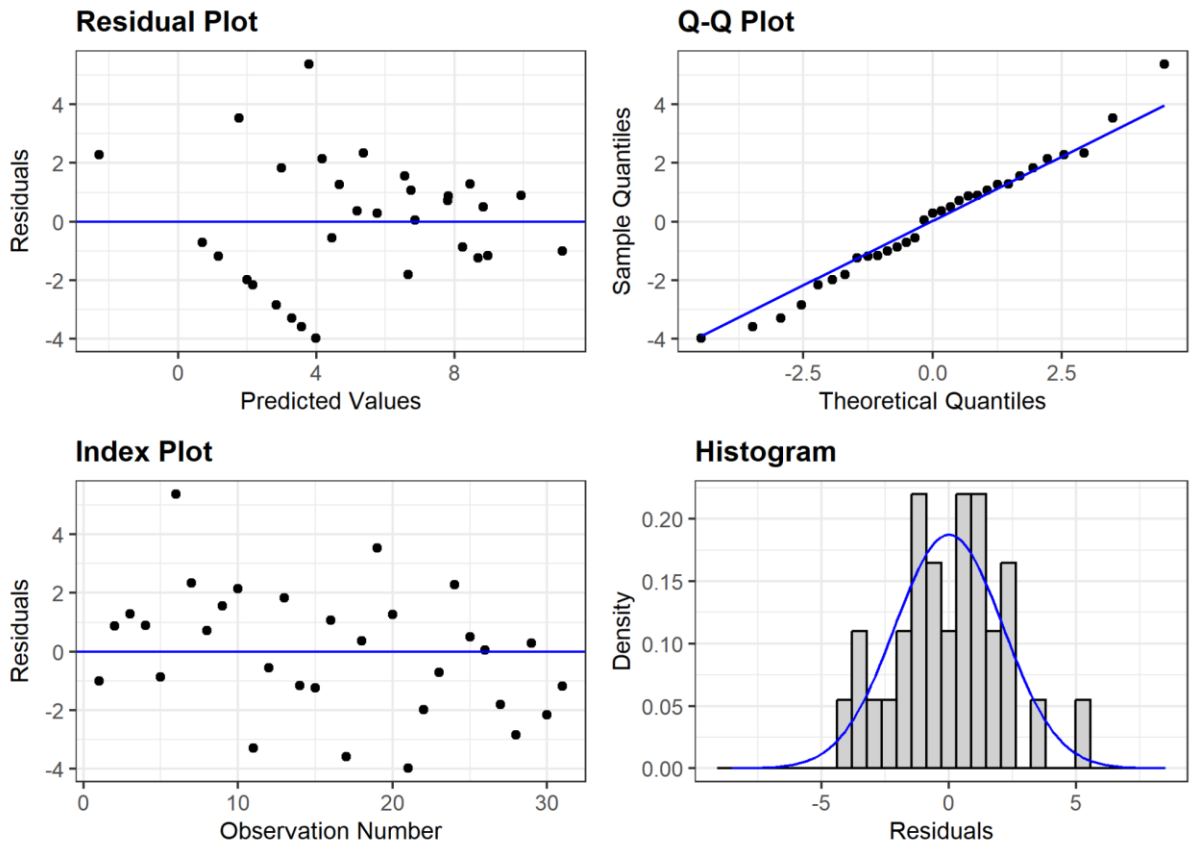

Fig. A 1: Assessing the fit of linear model 1 (for all 31 sites: kelp abundance index ~ SST + tidal current speeds + slope): Plots of the model's fitted values vs residuals, residuals' quantile-quantile plots, residuals with observation number, and a histogram of the models' residuals.

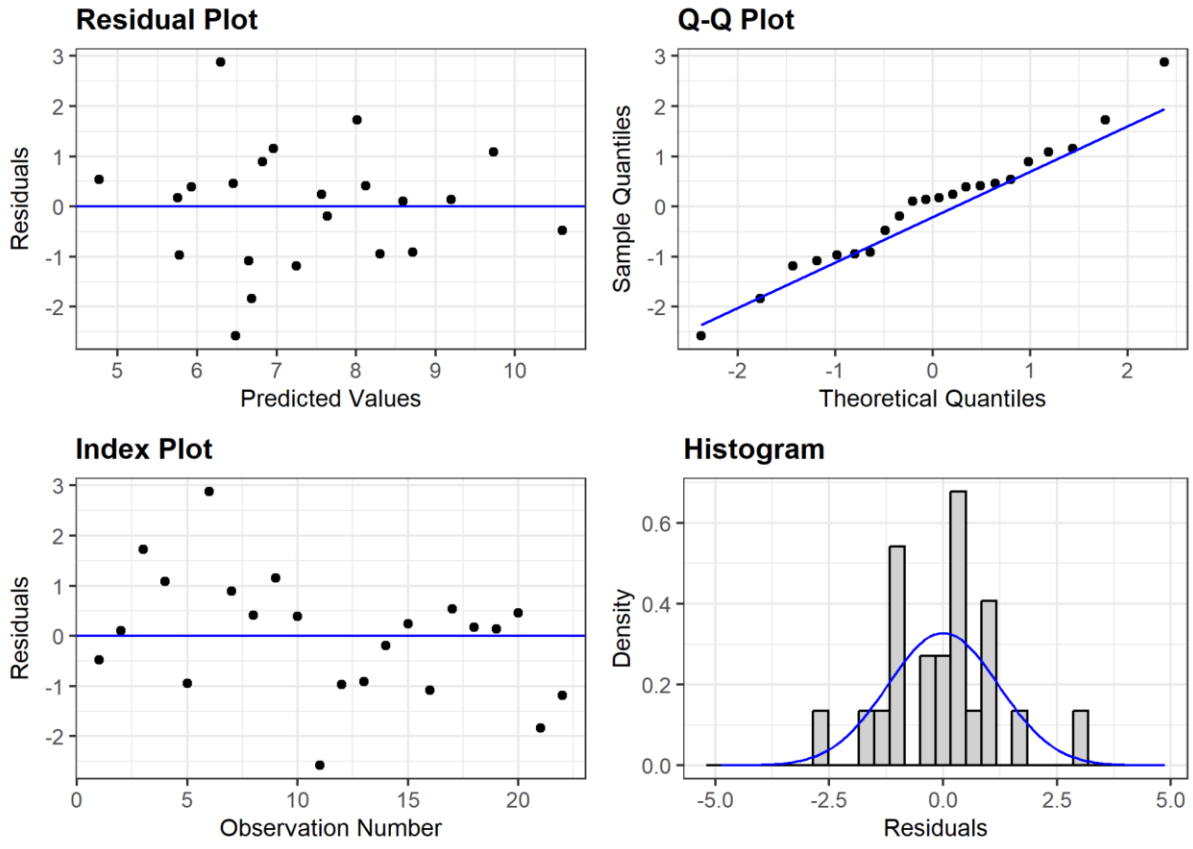

Fig. A 2: Assessing the fit of linear model 2 (for sites with kelp: kelp abundance index ~ SST + tidal current speeds + slope): Plots of the model's fitted values vs residuals, residuals' quantile-quantile plots, residuals with observation number, and a histogram of the models' residuals.

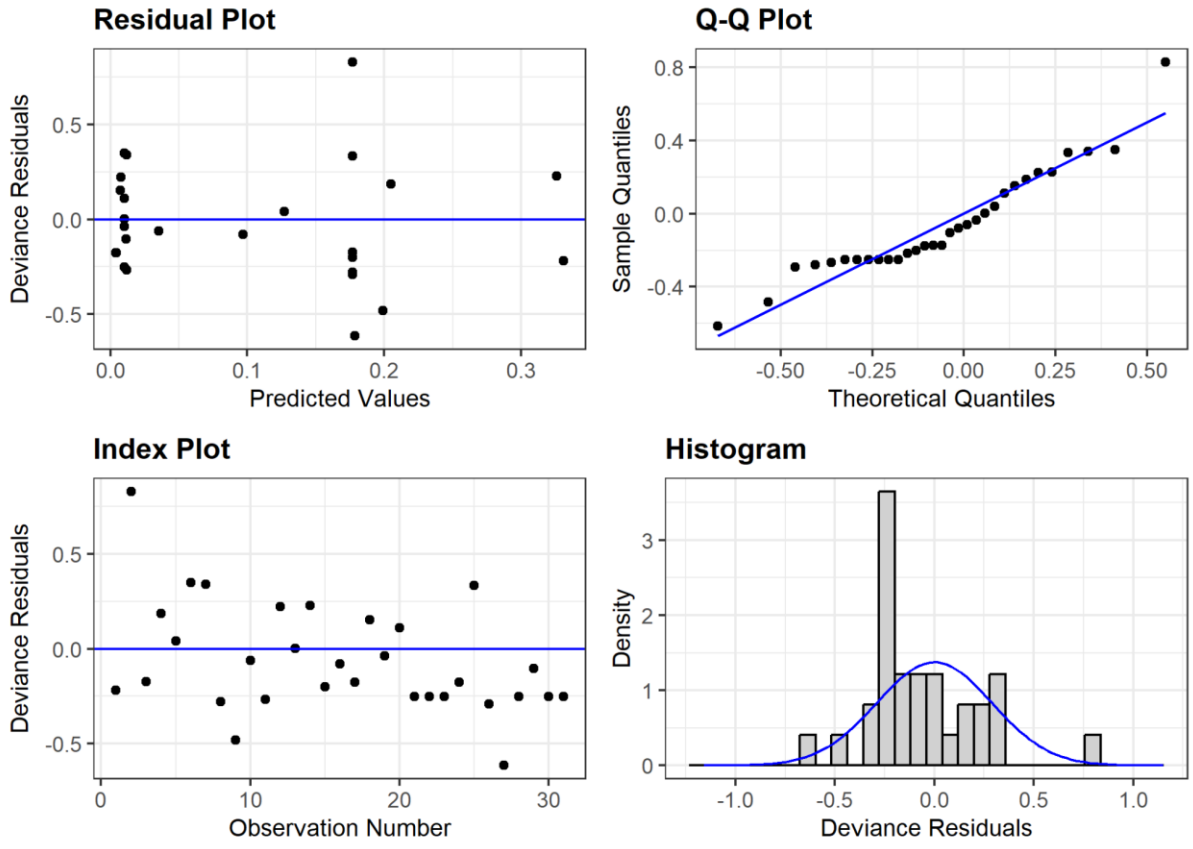

Fig. A 3: Assessing the fit of the Tweedie generalized linear model (kelp density ~ subregion + urchin abundance + Pycnopodia *abundance + subregion*urchin abundance + subregion**Pycnopodia *abundance + urchin abundance* * Pycnopodia *abundance): Plots of the model's fitted values vs residuals, residuals' quantile-quantile plots, residuals with observation number, and a histogram of the models' residuals.*

Appendix B - Supplementary material of Chapter 3

B1 *Macrocystis* site land mask creation

A land mask was created for the *Macrocystis* site based on a single, cloud-free, low-tide (0.2 m tidal height) Landsat 5 TM scene acquired on June 5, 1996. This scene represented the lowest tide and cloud-free image within the 1984 to 2023 time series. A Modified Normalized Difference Water Index (MNDWI) was applied to the image, and a threshold to differentiate land from water was manually identified. The Landsat scene was reclassified as either "land" or "water" and clipped to the study area.

B2 Object-based image analysis classification methods

An eCognition (Trimble Geospatial Imaging, Munich, Germany) supervised classification, object-based image analysis (OBIA) method was used to classify both the 2021 to 2023 images for the long-term time series and the years 2016 to 2023 for the short-term time series, adapting methods used in Schroeder et al. (2019); Gendall et al. (2023); Mora-Soto et al. (2024). For the long-term time series, the green (G), red (R), NDVI, and NIR bands were used as inputs for multiresolution segmentation, with 0, 1, 1, and 2 as the respective weights for each band. For the short-term time series, the NIR/G band ratio was used instead of the NDVI. A segmentation scale of 10 to 20, shape value of 0.1, and compactness value of 0.5 were used, and all segmentation products were manually checked to ensure no over or under-segmentation, and that each segment only contained either water or kelp. Training objects for three classes (water, kelp, and mask) were selected using expert knowledge of the image area. The feature space optimization tool was used to select the best combination of spatial, spectral, and contextual information used for the classification (Gupta & Bhadauria, 2010). All outputs were manually edited for quality in eCognition and ArcGIS, producing a measure of kelp area for each site in the end.

B3 Accuracy assessment methods

A stratified random sampling approach (Knudby, 2021) was used for the validation of kelp classifications, using an equal number of randomly generated points for ‘kelp’ and ‘non-kelp’ classes. For the long-term dataset, 200 validation points were generated for kelp and water classes respectively, resulting in a total of 400 validation points. A 30 x 30 m grid (corresponding to the pixel size of Landsat) was overlaid over the kelp classification and the validation image, and grids that overlapped with the randomly generated points were used for the accuracy assessment. For each site in the short-term dataset, 50-100 validation points for kelp and water classes were generated depending on the site area. A 10 x 10 m grid (corresponding to a common size found in OBIA

objects) was overlaid over the short-term dataset sites instead. For both long-term and short-term time series, if a grid had more than 1 validation point, the duplicate point would be removed.

For both long-term and short-term time series, each grid was assessed using both the satellite imagery classification and the validation imagery, such that if a grid was >50% kelp, that grid would be labeled a 'kelp' grid, and if it was <50% kelp, the grid would be labeled a 'water' grid. Each grid would have a validation label: 'true kelp' or 'true water', and a classification label: 'classified kelp' or 'classified water'. Using the validation label and classification labels, a confusion matrix was produced for the accuracy assessment (Stehman & Czaplewski, 1998).

B4 Supplementary tables

Table B. 1: Precision and recall of kelp classification of satellite imagery

Year	**Imagery source**	**Site**	**Precision**	**Recall**	**Total Accuracy**
2017	Landsat	Malcolm Island *(Macrocystis* site)	92.8%	89.1%	89.7%
2023	Planetscope	PI	79.2%	95.3%	87.8%
2023	Planetscope	MIE	91.6%	85.4%	88.7%
2023	Planetscope	BH	84.8%	87.5%	87.8%
2023	Planetscope	WI	74.6%	96.4%	86.2%
2023	Planetscope	ABE	84.1%	90.2%	88.3%
2023	Planetscope	NR	97.6%	93.0%	95.6%

Table B. 2: Table describing the results of the changepoint analysis.

Variable	Number of changepoints	Probability of having that number of changepoints	Changepoint year	Probability associated with that changepoint year

Regional				
In-situ spring SST	2	35.7%	2014, 1999	97.1%, 85.3%
In-situ summer SST	2	51.9%	2014, 1999	98.6%, 63.0%

Table B. 3: Table describing the climatological summer mean and standard deviation of local SST at each Nereocystis site.

Nereocystis site	Climatological summer local SST from 1984 to 2023 (mean ± standard deviation)
ABL	10.3±0.779°C
ABE	10.3±1.21°C
MIE	9.96±0.855°C
BH	9.41±0.716°C
WI	9.71±0.689°C
NR	10.9±1.17°C
PI	9.51±0.754°C
SLI	10.3±1.09°C

Table B. 4: Table describing the results of the linear model used to identify potential environmental drivers of percent kelp area change. The combination of predictors listed below was decided using the lowest AIC, however, note that no combinations of predictors resulted in any significant relationship between environmental conditions and the percent kelp area.

$R^2 = 0.0872$			
Predictors	*Estimates*	*Confidence Interval*	*p-value*
Intercept	0.572	-0.238-1.38	0.160
1-year summer SST mean	-0.00726	-0.0844-0.0699	0.849
Cumulative summer MHW	0.00153	-0.00146-0.00451	0.306
ONI	-0.0288	-0.0685-0.109	0.149

B5 Supplementary figures

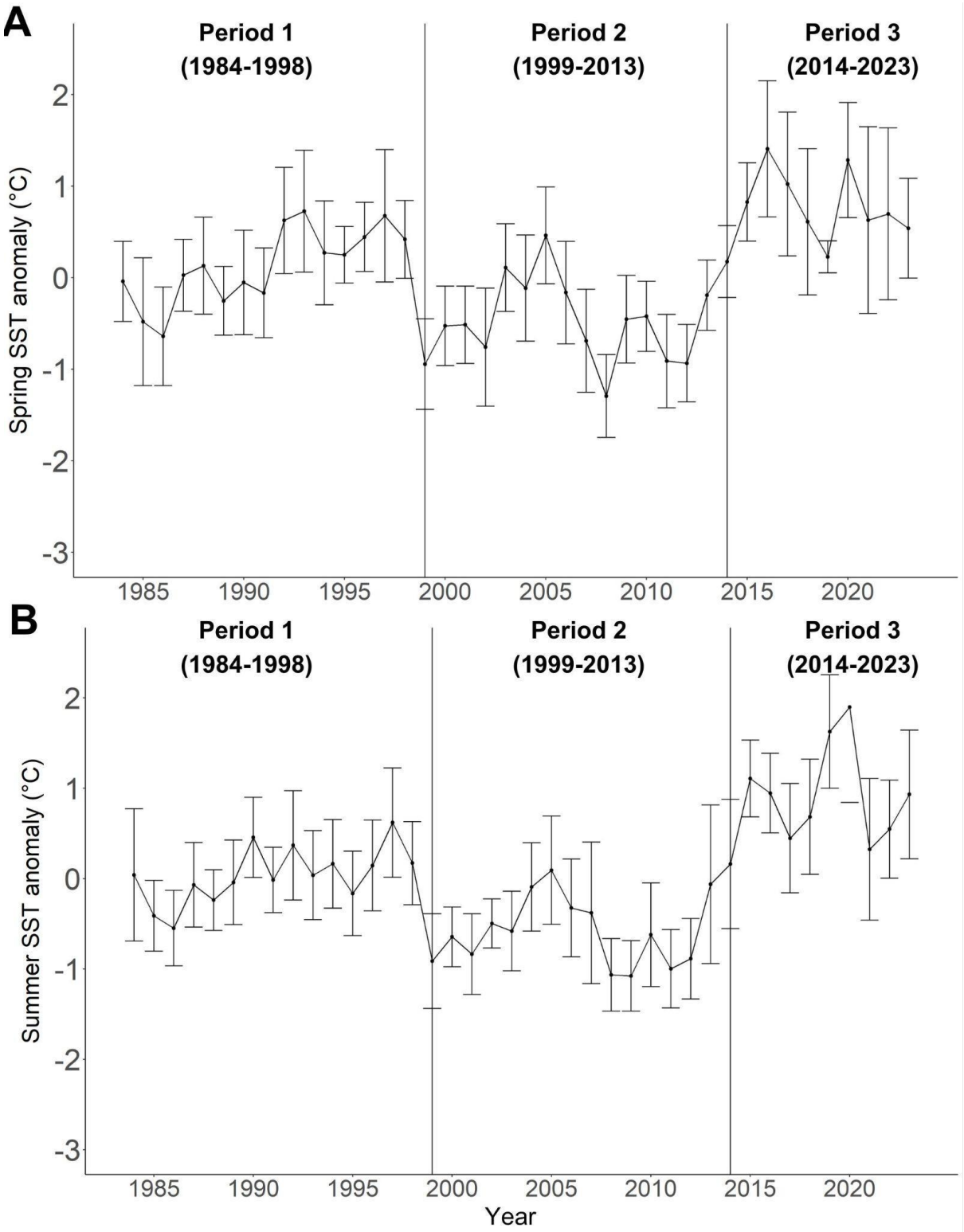

Fig. B 1: A) Mean regional spring SST anomaly, and B) mean regional summer SST anomaly, derived from the yearly seasonal mean subtracting the climatological mean calculated with daily values from 1984 to 2023. All data was derived from the Pine Island Lighthouse daily SST climatology (1984 to 2023), with error bars representing the standard deviations. The vertical black lines depict the transitions between the climate periods.

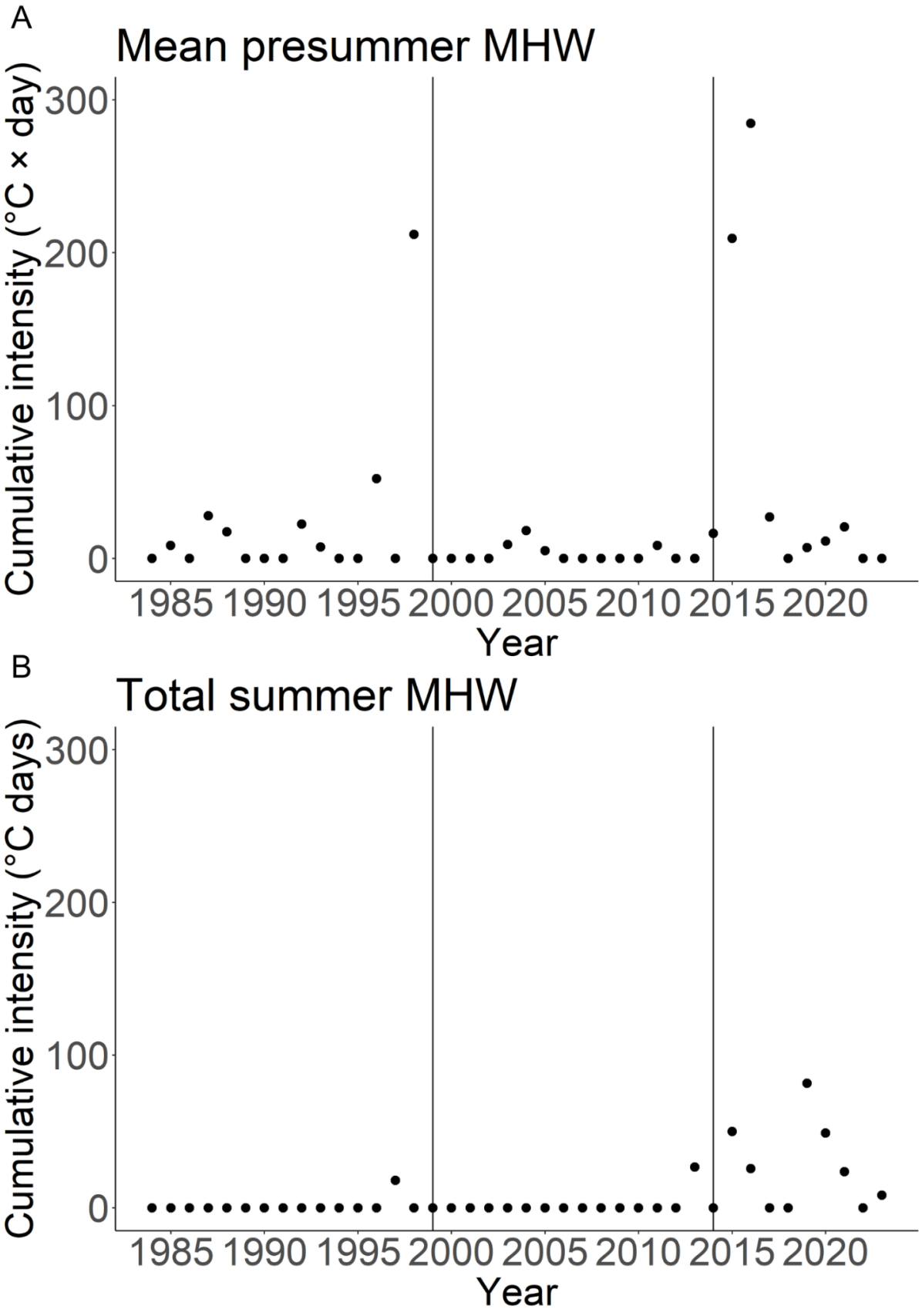
A
Mean presummer MHW
Cumulative intensity (°C × day)
300
200
100
0
1985 1990 1995 2000 2005 2010 2015 2020
Year
B
Total summer MHW
Cumulative intensity (°C days)
300
200
100
0
1985 1990 1995 2000 2005 2010 2015 2020
Year

Fig. B 2: A) Cumulative intensity of pre-summer MHWs (September of the previous year to June of the current year) from 1984 to 2023. B) Cumulative intensity of summer MHWs (July to August of the current year)